NASA CR-54692
TRW 4381-6017-R0000

RESEARCH ON ION BEAM DIAGNOSTICS

GPO PRICE $ _____

CFSTI PRICE(S) $ _____

Hard copy (HC) 3.00

Microfiche (MF) .75

ff 653 July 65

by

J. M. Sellen, Jr.
Robert F. Kemp

Prepared for: National Aeronautics
and Space Administration

Contract No. NAS3-6276

PHYSICAL ELECTRONICS LABORATORY
PHYSICAL RESEARCH CENTER

TRW SYSTEMS
AN OPERATING GROUP OF TRW INC.
ONE SPACE PARK • REDONDO BEACH, CALIFORNIA

NASA CR-54692
TRW 4381-6017-R0000

FINAL REPORT

RESEARCH ON ION BEAM DIAGNOSTICS

by

J. M. Sellen, Jr., and Robert F. Kemp

prepared for

NATIONAL AERONAUTICS AND SPACE ADMINISTRATION

February 10, 1966

CONTRACT NAS3-6276

Technical Management
NASA Lewis Research Center
Cleveland, Ohio 44135
Electric Propulsion Office
Sanford G. Jones

PHYSICAL ELECTRONICS LABORATORY
Physical Research Center

TRW Systems
One Space Park, Redondo Beach, California

TABLE OF CONTENTS

SECTION I.

INTRODUCTION

RESEARCH ON ION BEAM DIAGNOSTICS

by J. M. Sellen, Jr., and Robert F. Kemp

TRW Systems

I. INTRODUCTION

The program of research under Contract NAS3-6276, Research on Ion Beam Diagnostics, has been directed toward several problem areas. These have included the interactions of material surfaces with streaming plasmas, the acceleration of ions in a streaming plasma by an impulsive electric field, analytical and experimental studies of the properties of electron emissive probes, and the generation and conduction of neutralizing electrons from a discharge neutralizer to an ion thrust beam.

The results of these several programs are summarized in Section II, Program Review, and are detailed in the technical reports and published papers included in Section III. In addition, a manuscript detailing the performance of electron emissive E-field meters is included as an Appendix to this report. The work described in this Appendix has been conducted under a separate program, but is relevant to ion beam diagnostics research, and is included in this report for completeness.

SECTION II.

PROGRAM REVIEW

II. PROGRAM REVIEW

The first aspect of the program of research is reviewed in Section III.a, and considers the interaction of solar cell arrays in dilute streaming plasmas. The first configuration tested was that of a "bare" solar cell (i.e., without a protective cover glass). It was demonstrated that drainage currents from the dilute plasma to this solar array would impose severe penalties against the operation of the array, with power losses ranging to the level of 50% of the total available power for plasma conditions simulating the more dense portions of the space plasma and for maximum potentials in the solar array of the order of kilovolts. For plasma conditions simulating regions of the space plasma of lesser densities ($\sim 10^4$ ions/cm^3), operation of the bare array at high output potentials would become tolerable although, perhaps, a desirable operating condition would not yet be obtained. Considering the magnitudes of the space plasma density, the altitude regime below 10,000 kilometers would possess, in general, a plasma sufficiently dense to rule against the use of a high potential bare solar array. For an array with cover glasses, the current drains are substantially reduced. However, the extent of the plasma sheaths connecting the remaining exposed points of the solar array to the plasma ranges considerably beyond the physical size of these exposed points. In tests of modules of a solar cell array with these "connecting tabs" exposed and with an aerospace sealant placed over the tabs, a substantial reduction in the current drain from the plasma was noted for the "painted" module. This treatment would be the recommended procedure for an operating solar array to minimize current drains from the plasma. As a concluding aspect of this first study, the possible surge currents in a solar array powering an ion thruster system were considered for that failure mode in which neutralizer current is suddenly interrupted. Excessive currents in this failure mode would not occur unless the ion turnaround condition resulted in an arc between the ion source and the accelerating electrode. However, a sudden

restoration of the neutralizer capability could result in a damaging current surge if the emission limited neutralizer current is sufficiently large.

The second portion of the overall program of research is reviewed in Section III.B, Plasma Impellers-Thrust and Drag Devices Utilizing the Dilute Plasma of Space. Here, as in the preceding studies, described in Section III.A., the plasma wind tunnel was utilized to simulate the ordered plasma flow which would obtain between an orbiting spacecraft and the resident plasma in space. In the first configuration of the impeller which was examined, only steady state potentials were applied to the elements of the impeller. These steady state potentials reflected the plasma ions with comparatively small voltages. Employed on a space vehicle in a near earth orbit, a moderately sized impeller (of the order of 1 square meter) would provide sufficient drag force to produce angular accelerations in the milliradian/sec^2 to microradian/sec^2 range for a variety of spacecraft configurations. Such drag forces would certainly be capable of a variety of attitude control maneuvers. For the second configuration of the impeller the potentials applied to the elements of the impeller are time varying. Such time varying potentials may be utilized, under proper phasing conditions to provide either a thrust or a drag force. In the thrusting mode the ions entering the impeller are accelerated in the direction of their motion upon entry, while in the drag mode the ions are reflected. The thrust levels per square area of the impeller in this second condition of operation could, in principle, range up to two orders of magnitude above the steady-state potential operation as a simple plasma reflector. Experiments in the thrust mode of this pulsed impeller did demonstrate the acceleration, to substantial energies, of a fraction of ions entering the impeller. Overall thrust would appear to have been generated, although not, perhaps at the fullest levels indicated as possible for the calculated cases of operation. The efficient operation of such an impeller would require not only that thrust be created, but also that the input power to the impeller be transferred, in the main, to the ion flow, and, while ion acceleration was demonstrated, an efficient condition of acceleration was not attained.

The third portion of the overall program of research is presented in Section III.C., which treats the measurement of plasma potentials by electron emissive probes. While the emissive (or hot) probe was suggested by I. Langmuir in the same period in which the cold (conventional Langmuir) probe was first described, the intervening period of some four decades has seen almost a total absence of emphasis on the use of the hot probe. The general use of the cold probe may be prompted by the comparative ease of its fabrication, in that no heating circuit is required, and by the general desire to extract from the probe information on the particle temperatures and plasma densities. The hot probe does not appear to possess the capability for these determinations that are obtainable by the now well standardized cold probe techniques. However, the hot probe possesses marked advantages over the cold probe in its ability to determine the plasma potential and to detect shifts in the potential. The surface temperature necessary to create an emissive condition for the tungsten wire ($\sim$2500°K) insures that the wire surface is that of clean tungsten and thereby eliminates the gross uncertainties in plasma potential measurements which can be caused by contact potential effects on the surfaces of cold probes. The accuracy of potential measurements from the hot probe is, moreover, advanced by the very sharp break which occurs in the emissive characteristic as contrasted to the comparatively rounded "knee" in the conventional Langmuir probe trace. For this reason, plasma potential measurements with emissive probes may possess an accuracy of $\sim$.01 volt, provided the plasma to be diagnosed is, itself, constant in potential within this increment. The hot probes are also capable of detecting shifts in the plasma potential of this order of magnitude even if the frequency of such changes ranges into the megacycle region. In summary, the emissive probe possesses advantages in potential measurements which greatly broadened the capabilities of plasma diagnostics. The manuscript presented in Section III.C. details these capabilities from both an analytical and experimental point of view. This paper will be published in the April issue of the Review of Scientific Instruments and, it is believed, constitutes the first definitive publication on the emissive probe.

SECTION III.

TECHNICAL REPORTS AND PUBLISHED PAPERS

The concluding portion of the program of research is the investigation of cesium and mercury discharge neutralizers. This work is reviewed in Section III.D. The initial effort with the discharge neutralizer was directed toward a miniaturized electron bombardment configuration from which the electron component, rather than the ion component, was extracted. While this configuration provided electron currents in the ampere range, it did not provide an effective utilization of the gas introduced into the discharge region. Following the results of Ernstene with the cesium "plasma bridge" neutralizer, the orifice of the electron source was diminished and the inlet gas was changed to cesium from the utilized (for convenience) argon gas loading. This reconfigured discharge electron source allowed both the separate confirmation of the Ernstene results and the extension of the diagnostic treatment to include plasma potential measurements and electron temperature measurements. The floating emissive probe measurements indicated a plasma potential in the interior of the discharge neutralizer of $\sim$1 volt negative with respect to the plasma column exterior to the source. The electron temperatures measured in the exterior plasma column were $\sim$8000°K. Following this first portion of the neutralizer investigation, the gas loading was changed to mercury. Since mercury no longer yields the electron emissive surface conditions resulting from the cesium gas, an emissive coating on the neutralizer interior was required. An oxide coated nickel cathode was used in the first such mercury discharge neutralizer and did provide successful operation through a test of 100 hours in duration. The extraction of the electron current in this test was performed by a metal collecting plate. Operation of this device indicates that similar results to those obtained for the cesium discharge neutralizer may be expected for mercury, and that a potential for the requisite longevity also exists in the mercury device.

SECTION III.A.

OPERATION OF SOLAR CELL ARRAYS IN DILUTE STREAMING PLASMAS

OPERATION OF SOLAR CELL ARRAYS IN DILUTE STREAMING PLASMAS

by

J. M. Sellen, Jr. and Robert F. Kemp

The interaction between the solar panels of a spacecraft and the ambient space plasma is one of a general group of problems related to the interaction between material surfaces and streaming plasmas. Because the solar panel is not a "simple" surface, i.e., does not possess a single uniform characteristic conductivity or work function, but, rather, may be a mixture of conducting and non-conducting surfaces, the observed interaction between the plasma and a particular solar panel configuration cannot be generalized. There are, however, certain aspects of the interaction which may be discussed in general.

The primary concern in the plasma-solar panel interaction is the current flow from the plasma to the elements of the solar cell network and the effect which this particle flow has upon the spacecraft potential relative to the plasma. The first configuration to be considered will be that of "bare" solar cells, i.e., cells without protecting cover glasses. It will be assumed initially that the current flow from the plasma to the various portions of the solar array does not result in changes of the potential difference between the plasma and a particular cell in the array. If the cell is positive with respect to the space plasma, an electron current will flow from the plasma to the cell. If the thickness of the plasma sheath over the surface of the cell is small compared to the overall dimensions of the solar cell array, the magnitude of this current will be given by

$$j_e \simeq \frac{\rho_e v_e}{4},$$

where ρ_e is electron charge density and v_e is rms electron thermal velocity. For peak plasma densities of ~2×10^6 electrons/cm^3 and $v_e = 3 \times 10^7$ cm/sec (2500°K electrons), the resulting current would be

$$j_e \approx 2.4\ \mu A/cm^2.$$

The electrons which flow from the plasma to the cell are accelerated to an energy eV_c where V_c is the potential of the cell. In the eventual return of the electrons to the plasma, to be discussed later, this electron kinetic energy at collection is non-recoverable, and an energy expenditure of eV_c per electron is imposed. From j_e and this accelerating potential, the power loss due to the current flow becomes

$$2.4 \times 10^{-6} \ (V_c) \ \text{watts/cm}^2$$

Now, for $V_c = 10^3$ volts and a total cell area of 10^3 cm^3 ($\sim$1 sq. ft.), the total power loss is $\sim$2.4 watts. For solar cells providing 10 watts/ft^2, this power drain represents a loss of $\sim$25 percent of the available power. A solar cell array extending to 2500 volts (for example, to provide a direct power lead to the ion source electrode of an ion thrustor) would suffer a loss of $\sim$63 percent of the generated power due to this current from the plasma to the solar array.

There are several methods by which this power drain could be lessened. The first of these is to operate the solar array at smaller potential differences from the plasma and to provide the requisite power conditioning if higher bus voltages were required for an ion thrustor. For example, at $V_c = 100$ volts, the power drain would be $\sim$.24 watts/cm^2, and the loss would be $\sim$2.5 percent of the available power. A second method would be to operate the solar cell so that it is negative with respect to the space plasma. The current carriers now collected would be ions and the resulting current density would be reduced by an order of magnitude from the electron collection current. Since the ion thermal speed is small compared to the vehicle velocity, the relevant streaming velocity is

$$j_+ \approx \rho_+ \, v_{veh}$$

For $v_{veh} = 10^6$ cm/sec and $n_+ = 2 \times 10^6$ ions/cm^3, $j_+ \approx .32$ μamps/cm^2. For $V_c = -10^3$ volts the power drain due to collected ion currents would be $\sim$.3 watts/ft^2, and the power loss is $\sim$3 percent of the available cell output. This approach would require a voltage inverting system if the eventual

power requirement must be delivered at large positive potentials. Of further concern is the fact that the current carriers reaching the solar cell surfaces are high energy ions which may cause sputtering damage.

The next feature to be treated in the discussion is the density of the space plasma. The calculated power drains discussed thus far have utilized an ambient plasma density of $\sim 2 \times 10^6$ ions/cm^3. While such densities are attained in the ionosphere, they are limited to daytime conditions and occur only through a limited range in altitude. At altitudes of 1000 kilometers or so a more representative value of this density would be in the range of $\sim 10^5$ ions/cm^3. Under the expressions previously utilized for power drains, the reduction in ρ_+ and ρ_e by an order of magnitude would reduce the corresponding power losses by an order of magnitude. The simple planar Langmuir probe collection theory, utilized in the current drain equations, may not, however, remain applicable as the ambient plasma becomes more and more dilute. The existence of large potential differences across the solar cell-to-plasma sheath and the reduction of the plasma density act together to increase the effective area of collection of current carriers from the plasma. This increase in the collection area removes the normal saturation features of the planar Langmuir probe and leads to currents which exceed those derived from planar Langmuir probe theory. The extent to which the actual power drains now exceed those calculated from ρ_+, v_+, v_e, etc. by the earlier expressions is complicated, depending upon the potential differences between the plasma and the solar cell, the dimensions of the solar array, the plasma density and ion and electron temperatures, the spacecraft velocity and the orientation of the solar array in the plasma flow. Since so many parameters are involved, no attempt will be made here to derive estimates of the power drains as functions of the several variables, and the discussion will merely point out that the power drains indicated from the planar Langmuir probe theory represent only lower bounds to the losses. In summary, while the reduction of ρ_+ and ρ_e tends to lower the power losses, the reductions will not follow the diminution in ρ exactly. An increase in effective collecting areas of charge carriers from the plasma at lower plasma densities will tend to produce non-negligible power losses in the density range of 10^5 ions and electrons/cm^3.

For the altitude ranges in which plasma densities become of the order of 10^4 ions and electrons/cm^3 or less, the power losses, even at large cell potentials and with bare cells, are not likely to be of importance. Thus, a solar array at altitudes of several thousand kilometers will no longer have significant power drains because of particle collection from the plasma.

A final consideration in the calculation of current flow from the plasma to the solar array is that of a protective covering over the surfaces of the cells. The resulting increase in the weight of the solar array will not be discussed here, since these factors of the technology are still in the process of change. It will be assumed that the voltage imposed across the protective coating by the solar cell potential relative to the plasma is not sufficient to cause breakdown. In this condition the outer surface of the protective coating would acquire a surface charge from the plasma, but there would be no steady state current flow and no power loss. The cover glasses over the cell surfaces would act as a "dielectric" in a "parallel plate capacitor" in which one electrode is the solar cell and the other "electrode" is the plasma. This is illustrated in Fig. 1.

The fact that current flow through the cover glasses is not permitted does not mean that particle currents will not flow between the plasma and the solar cell array for a conventional solar panel construction. The mere covering of the solar cell surfaces still leaves uncovered conducting portions of the solar cell network, principally in the interconnecting tabs from cell to cell. Because of the low plasma density and the large potential difference between the connecting tab and the plasma, the effective area of particle collection may exceed many times the exposed area of the connecting tabs. For this reason, the presence of exposed areas of the solar cell array which represent only a few percent of the total cell area can still result in particle collection currents of the level calculated earlier. This condition is illustrated in Fig. 2.

The effectiveness of the particle collection by these exposed tabs was illustrated by the plasma-solar cell interaction for panels utilized on the OGO spacecraft. Fig. 3 illustrates the solar cell module and various

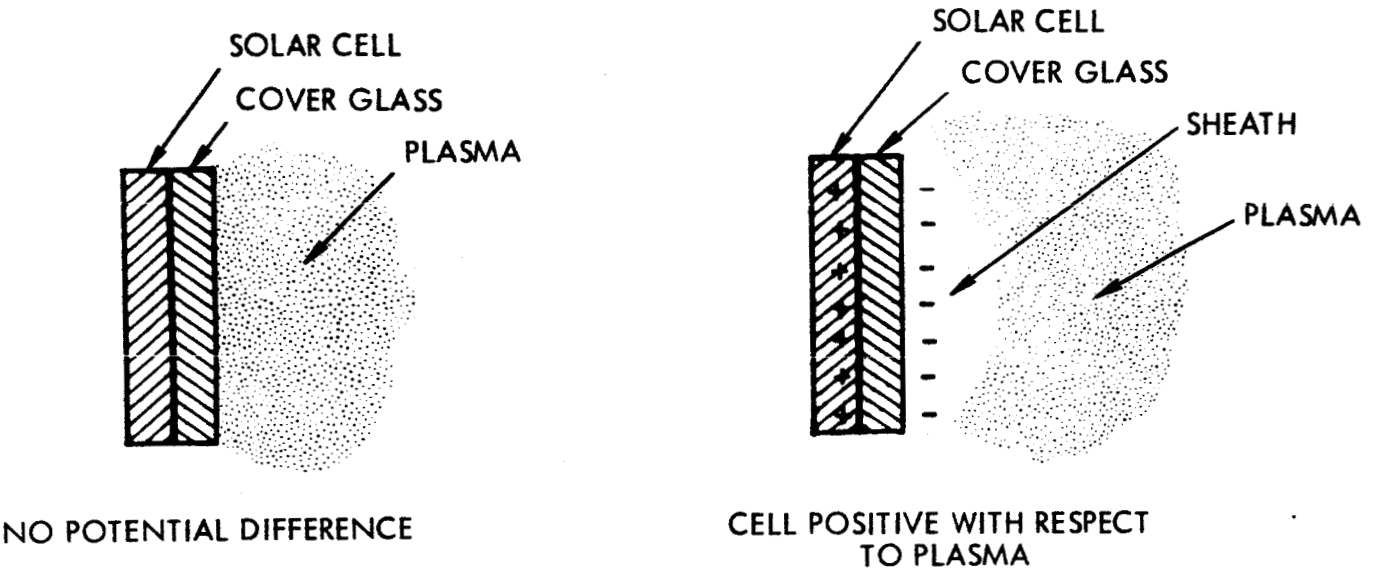

Figure 1. Sketch Shows How A Capacitor Is Formed By A Solar Cell With Cover Glass In A Plasma

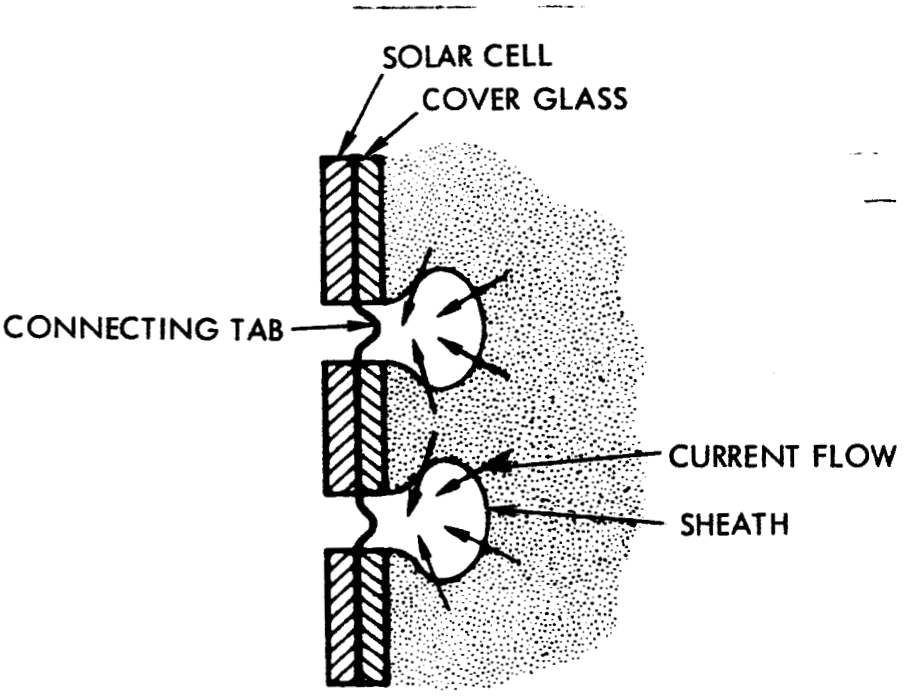

Figure 2. Sheaths Over Exposed Connecting Tabs In A Solar Cell Array May Have Much Larger Electron Collecting Area Than The Tabs

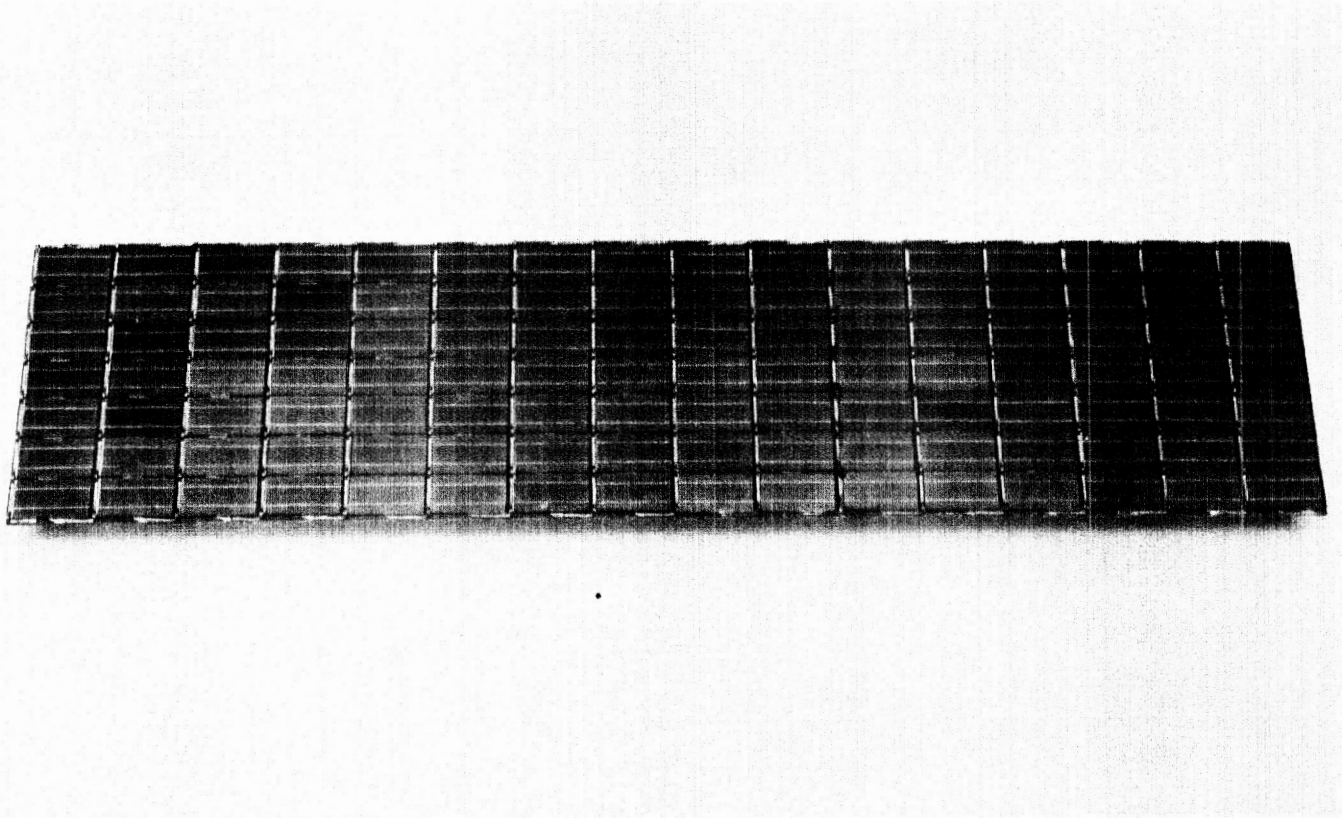

Figure 3. Photograph Of A Solar Cell Array Used On The OGO Satellite

components of the array. When this module was placed in the streaming plasma flow of a plasma wind tunnel the current-voltage characteristic illustrated by the solid curve in Fig. 4 was obtained. After the connecting tabs were painted with an aerospace sealant (Dow-Corning 170), the current collection was reduced to the dashed curve in Fig. 4. The influence of this solar cell collection current upon the spacecraft potential will be discussed in a later paragraph.

A "bare" solar cell panel, supplied by NASA/LeRC, was also placed in the plasma wind tunnel. Portions of current-voltage collection curves obtained in this plasma flow are given in Fig. 5. Elevation of the cell potential above several hundred volts produced prohibitive current drains from the plasma streams ending in complete disruption of the plasma flow. The experiments demonstrated, at least qualitatively, that the current drains from the plasma to a bare solar cell array would result in losses of the greater part of the available power from the solar array.

The discussion to this point has considered that the solar cell potential relative to the plasma is not affected by the flow of particles from the plasma to the cell. Since the spacecraft is an electrically isolated body, the collection of a particle current of one polarity must be accompanied by the release of a particle current, similar both in polarity and magnitude, or by the collection of another current of opposite polarity. For an "active" spacecraft such as one bearing an ion engine, the release of particle currents which may balance this current collection by the solar array is possible. An illustration of such a possible process is given in Fig. 6. It should be noted, however, that the release of an extra current of electrons, as in Fig. 6, can only be accomplished by a variation of the spacecraft potential relative to the plasma away from that value which would exist if no current drain to the solar array existed. Although such potential shifts may not necessarily need to be large, their occurrence could lead to difficulties if the spacecraft had a scientific payload. For this reason, minimization of current drains to the solar array is desirable, even if the power drains associated with this particle flow are no longer of significant magnitude to affect the overall electrical efficiency of the thrustor.

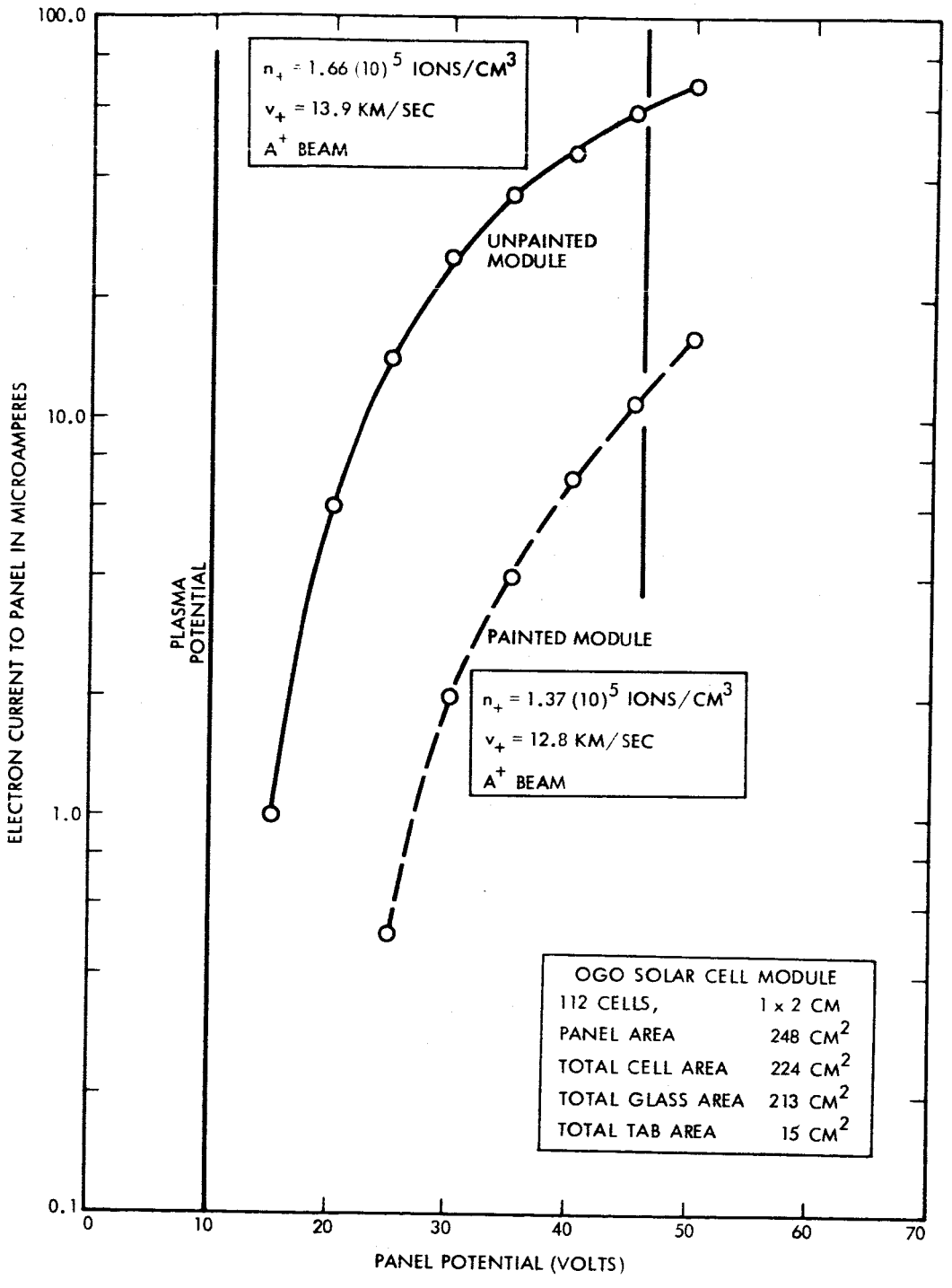

Figure 4. Current-Voltage Characteristics Of A Solar Cell Panel With Painted And Unpainted Interconnecting Tabs

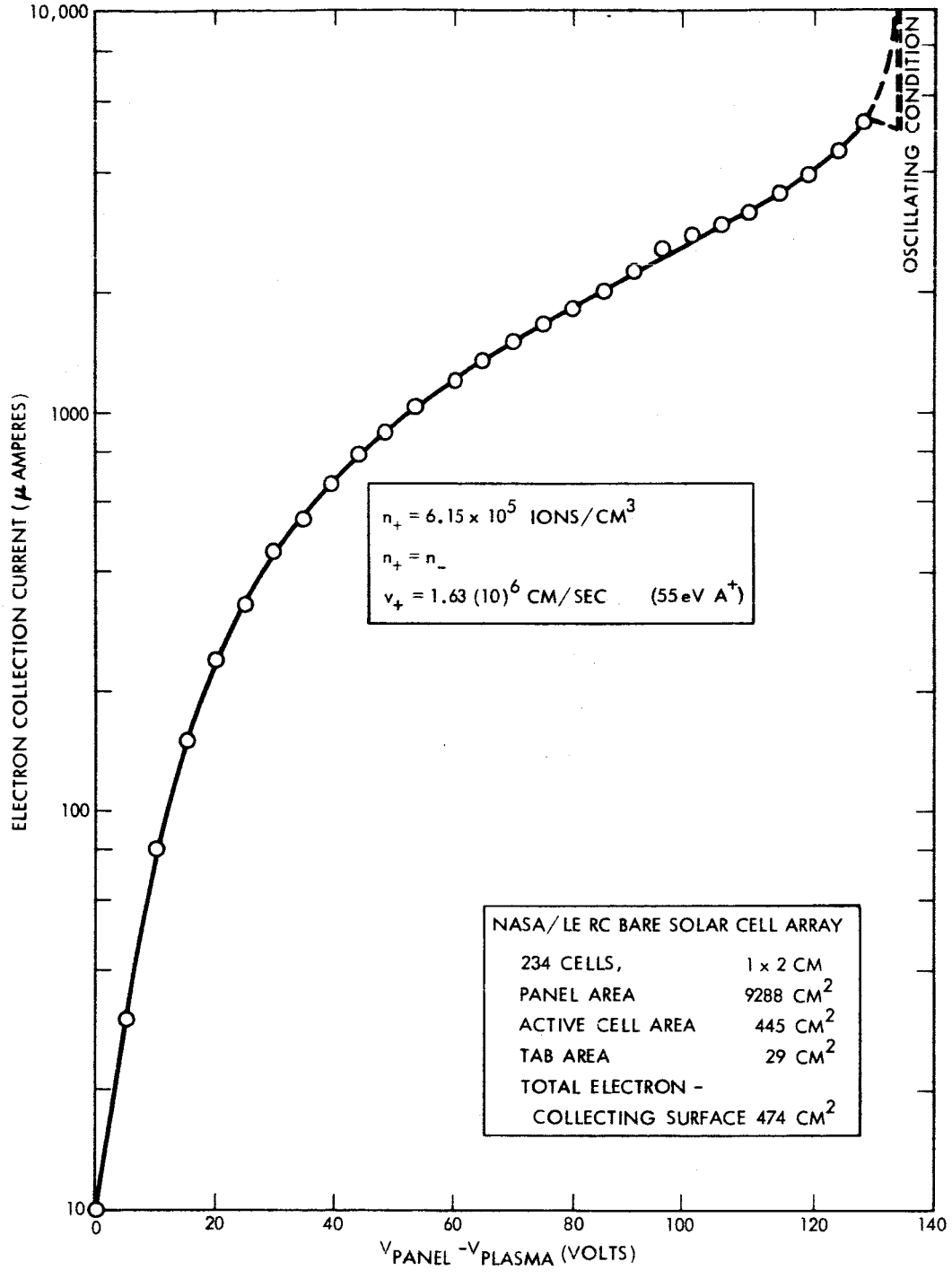

Figure 5. Current-Voltage Characteristic Of A Solar Cell Panel Without Cover Glasses

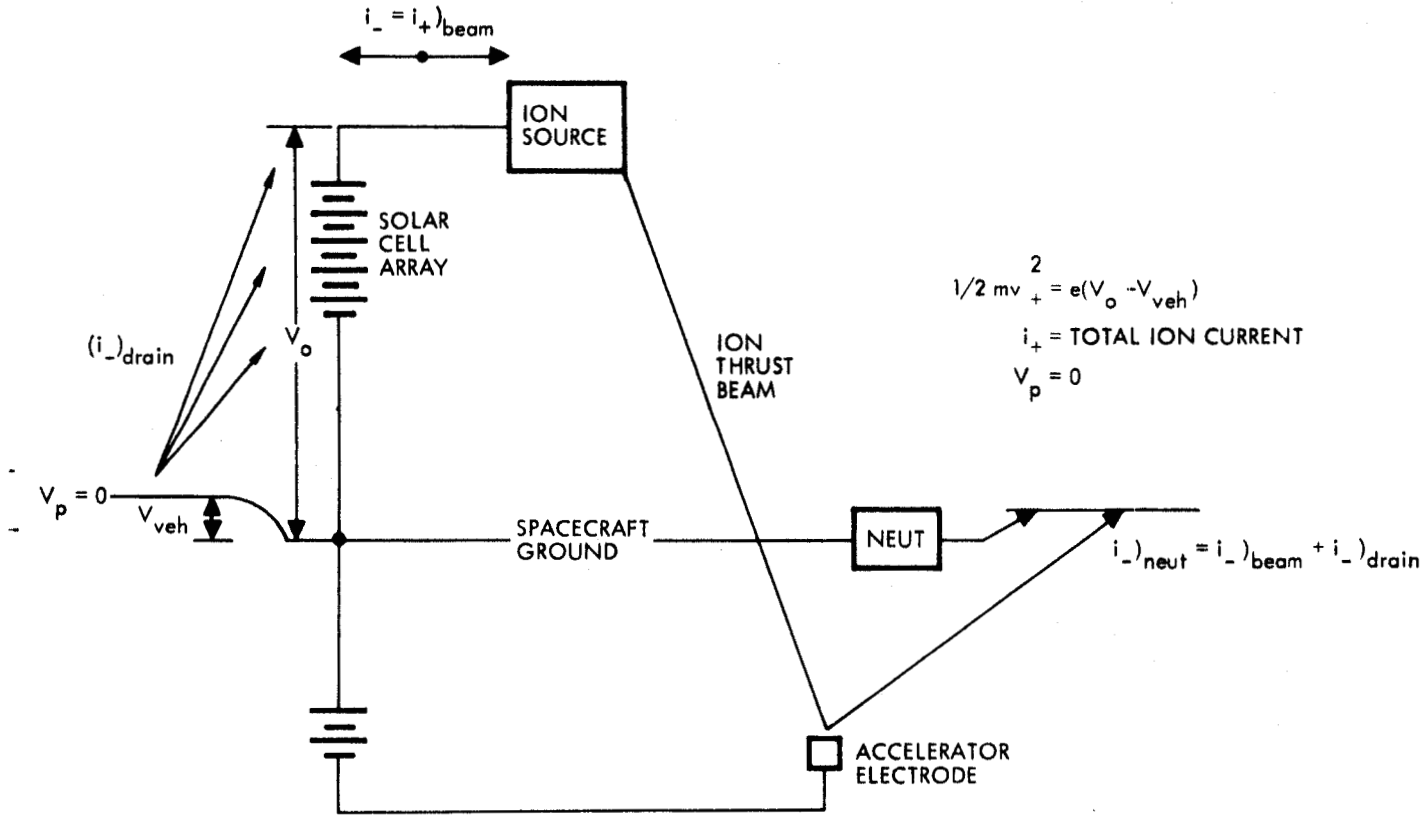

Figure 6. Potential Diagram Of Spacecraft Showing How An Additional Current From The Neutralizer May Balance Electron Current Collected By A Solar Cell Panel

For a "passive" spacecraft which cannot discharge particle currents, the collection of a current by the solar cells can cause a major drift in the spacecraft potential relative to the plasma. This process is illustrated in Fig. 7. In the experience gained with the OGO-spacecraft, the collection of electrons by the exposed connecting tabs of the solar cells (a +36 volt network, the negative end of which is connected to the spacecraft) caused the craft to attain an equilibrium potential of $\sim$-15 volts. The connecting tabs of the solar cells of a second OGO spacecraft were treated with the aerospace sealant previously described. For this spacecraft, the potential difference relative to the plasma was $\sim$ -2 volts, demonstrating the extent to which the sealant had reduced the particle drain to the solar array.

A final consideration in this discussion of the solar cell-plasma interaction is the possibility of current surges in the solar cell circuitry from the operation of the thrustor. For example, the abrupt interruption of the neutralizer current through some failure in the neutralizer causes the vehicle to charge to a negative potential relative to the plasma. The rate of change of the vehicle potential is given by

$$\frac{dV_{veh}}{dt} = -\frac{I_+}{C_{v-p}}$$

where I_+ is the total ion current expelled by the thrustors and C_{v-p} is the total vehicle-to-plasma capacitance. Since the bulk of the vehicle to plasma capacitance will be, in all likelihood, in the solar array-to-plasma capacitance, most of the current flow into the solar cell acts to discharge this capacitance and to recharge the array to negative potentials. The available current with which this discharge may take place is, as given in Fig. 8a, the I_e ($=I_+$) from the ion source. As may be noted this is the usual current flow through the array and there are no particular problems of an unusually large current surge. After a brief interval the vehicle attains a steady state negative potential in which most of the ion current is returned to the accelerator electrode. Unless an arc occurs in the engine, the current flow through the solar cells remains at I_e ($=I_+$). This is illustrated in Fig. 8b. If the neutralizer should abruptly resume operation, then the

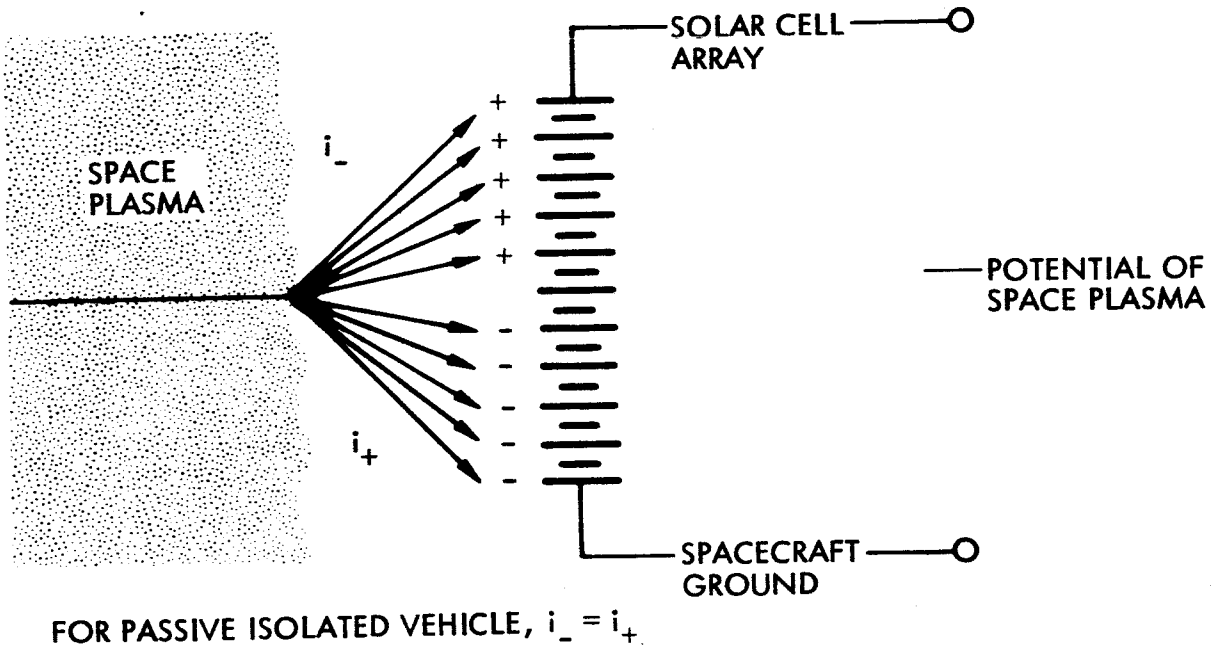

Figure 7. Diagram For Passive Spacecraft Showing Potential Equilibrium Such That Net Current Collected By Solar Cell Panels Equals Zero

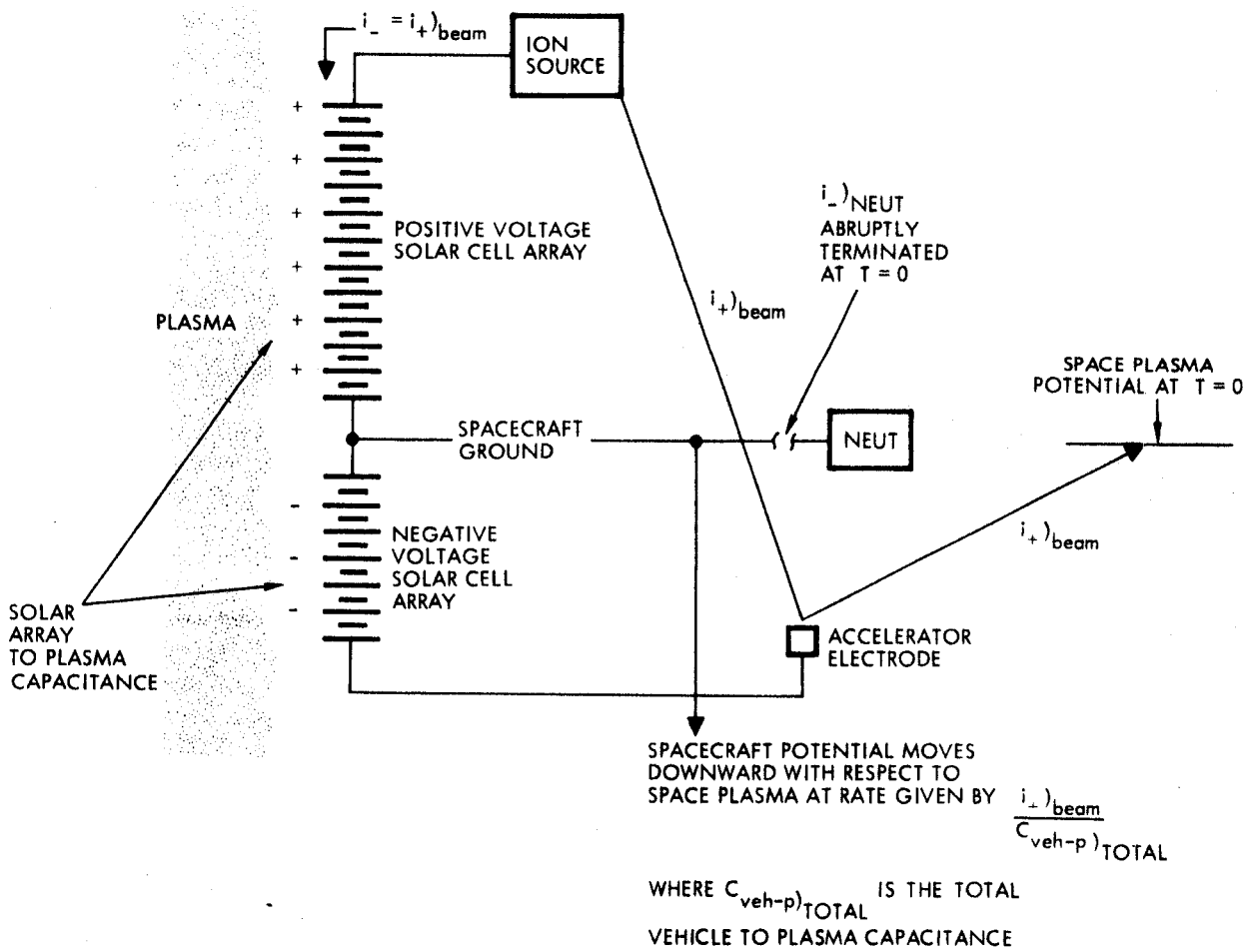

Figure 8a. Diagram Showing Currents And Direction Of Changes In Potential Following Interruption Of Neutralizing Current

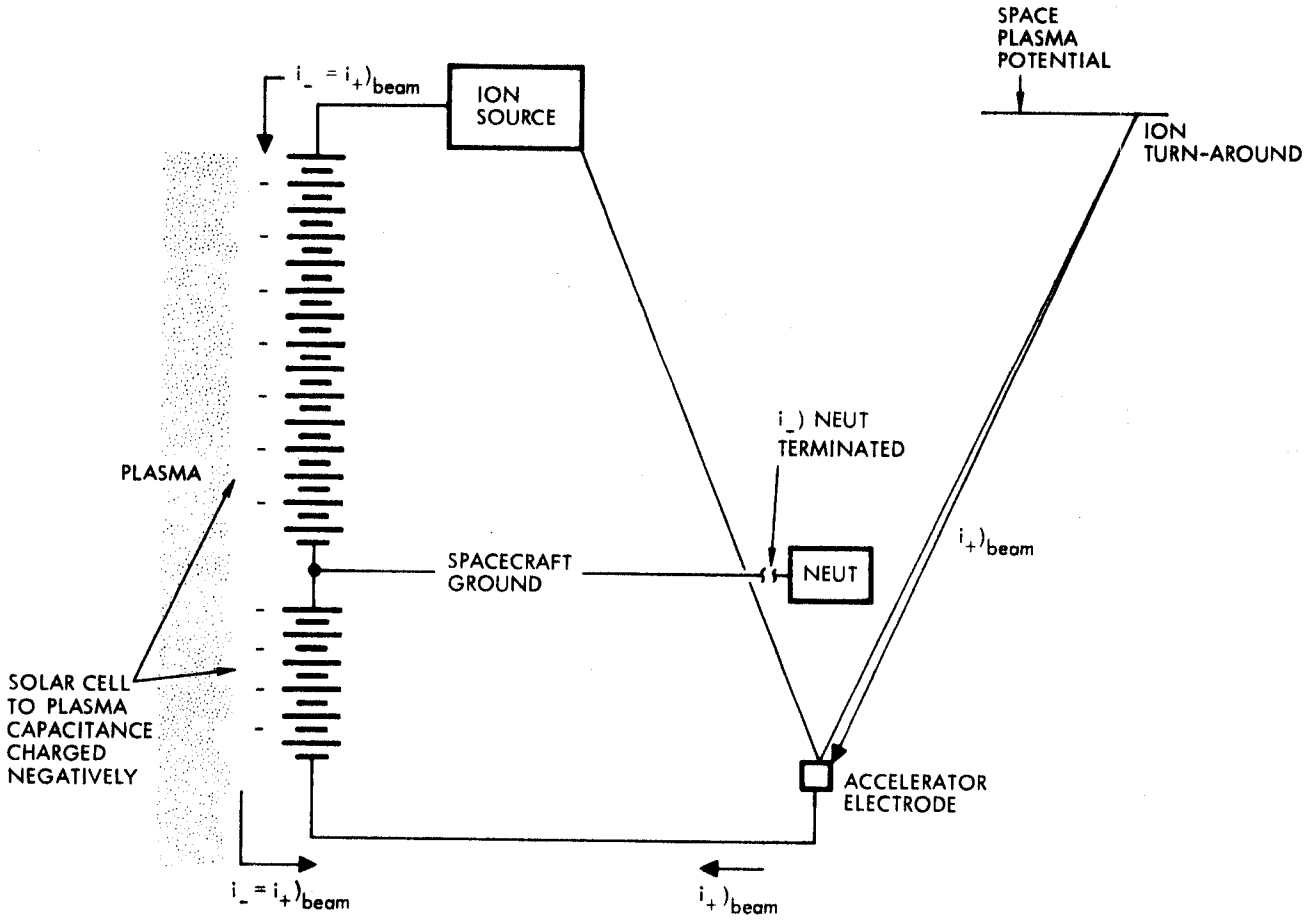

Figure 8b. Diagram Showing Steady-State Condition Without Neutralizer Current

negative charge on the solar cells will be discharged into the plasma through the neutralizer. If this emission capability is large (many times I_+) then a high current surge in the solar cell circuitry could result. This is illustrated in Figure 8c. The major hazard in current surges due to the solar cell-plasma capacitance would appear during this "restorative" phase of neutralizer operation if the neutralizer were in intermittent operation. The solar cell array should certainly be capable of sustaining current surges equal to the peak emission capability of the neutralizer.

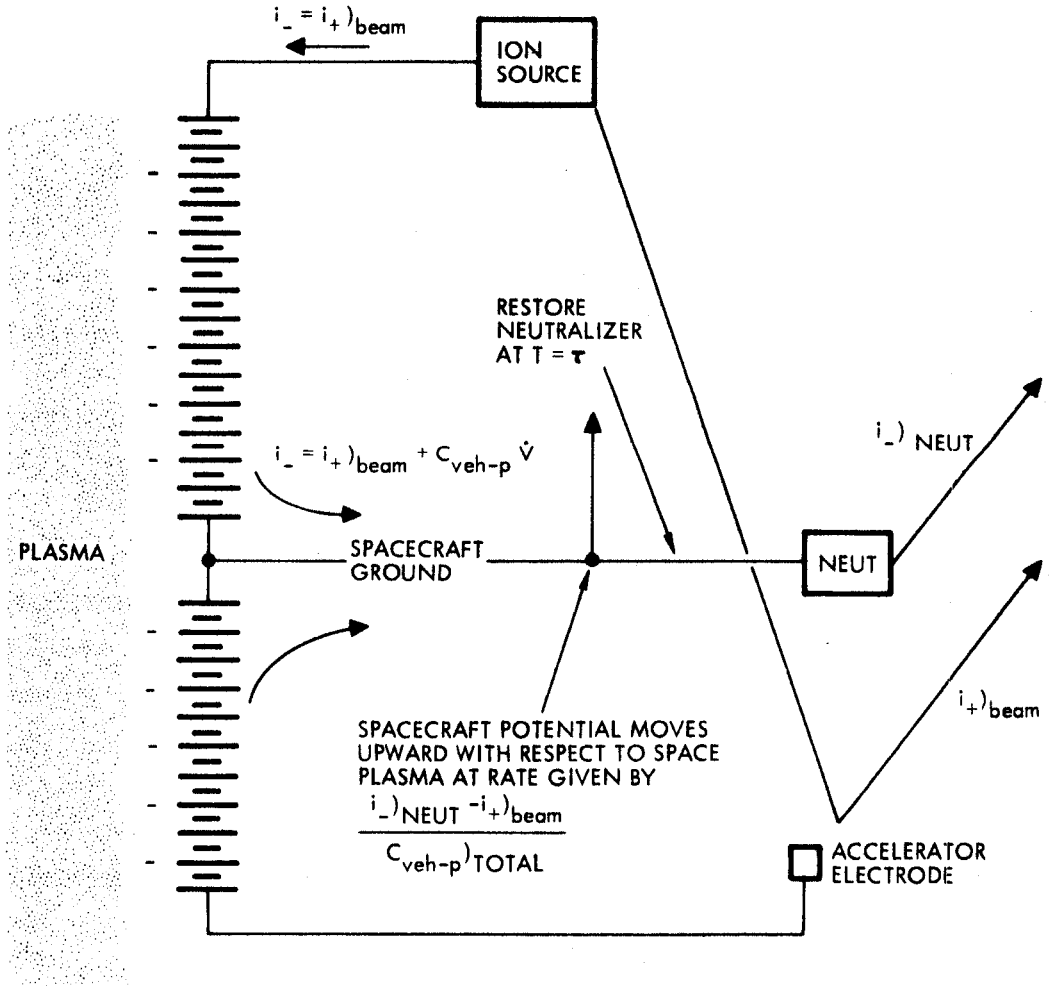

Figure 8c. Diagram Showing Currents And Direction Of Changes In Potential Following Restoration Of Neutralizer Current. Current In Solar Cell Panel Is Limited To The Emission Capability Of The Neutralizer.

SECTION III.B.

PLASMA IMPELLERS - THRUST AND DRAG DEVICES UTILIZING THE DILUTE RESIDENT PLASMA IN SPACE

PLASMA IMPELLERS - THRUST AND DRAG DEVICES UTILIZING THE DILUTE RESIDENT PLASMA IN SPACE

by

David F. Hall, R. F. Kemp, and J. M. Sellen, Jr.

I. INTRODUCTION

The dilute resident plasma in space attains peak densities in excess of 10^6 ions/cm^3 in the F_2 layer. Since the vehicle velocity is, in general, much greater than the ion thermal velocity, the ion motion, relative to the vehicle, is essentially at the vehicle velocity. Ions posses, therefore, an apparent ordered motion relative to a vehicle orbiting in this region. The plasma impellers to be described produce a momentum interchange with this ordered plasma flow to provide either a thrust or drag.

To investigate the interaction of the plasma with an impeller, a plasma wind tunnel has been utilized. An electron bombardment engine has been used to produce plasma streams of nitrogen, helium, argon, and neon. The densities, ionic species and abundances, and velocity dispersions have been determined for each of these plasma flows. These streams have then been impacted against a stationary impeller to simulate the interaction which would occur between a moving impeller and a stationary plasma.

The first impeller configuration tested is that of a steady state electrostatic "mirror" which reflects the plasma flow. Reflection of the plasma flow is determined by an array of Faraday cups mounted in the vacuum testing chamber. This reflection of the plasma stream, for plasma densities and streaming velocities simulating vehicle motion through the F_2 layer, produces a momentum interchange of ~1 dyne/meter^2. At a moment arm of several meters such pressures could produce angular accelerations of milliradians per sec^2 to microradians per sec^2, the latter figure pertaining to a larger vehicle with a moment of inertia

of the order of 10^8 gram cm^2. Re-orientation times for attitude corrections of .1 radians range from 10^2 to 10^3 seconds, depending upon the vehicle moment of inertia.

Additional drag forces and possible thrust forces should be obtained by the application of time-varying electric fields within the impeller. In the thrust mode, these time-varying fields act to accelerate the ions so that they acquire an additional velocity in the original direction of (relative) motion. In the drag mode the ions are reflected and acquire an increase in the magnitude of their average velocity relative to the impeller. Calculations indicate that thrust levels of $\sim$10 dynes per $meter^2$ may be obtained by the use of time-varying electric fields in the impeller.

II. DRAG DEVICE

A. Theory

A spacecraft orbiting the earth in the ionosphere has a velocity of $\sim$8 km/sec, whereas the thermal velocity of the ionic species occurring throughout and below the F_2 layer (altitude < 1200 km) is less than 1.5 km/sec. Therefore an observer on a spacecraft in this region sees an almost completely ordered flow of ions passing him at a velocity of $\sim$8 km/sec. The basic concept of an electrostatic drag device is to place an ion reflection element in this stream and transfer momentum from the spacecraft to the ions, thereby decelerating the spacecraft.

The ionic species of the ionosphere are shown in Table I, along with other pertinent information[1,2]. The listed values of ion concentration n represent the approximate maxima that occur for geomagnetic latitudes near 35°. Temperatures used to calculate average ion thermal velocity $V_{+,th}$ are those of the neutrals in the region. The values given for v_s, the spacecraft velocity, are for circular orbits; higher velocities can be attained in elliptical orbits and space probe trajectories; lower velocities occur at apogee for probe shots that return to the earth. Values of the average electron thermal velocity exceed 100 km/sec and therefore appear quite random to all orbiting spacecraft.

Table I. Typical Values of Ionosphere Variables Important to Simulation

Altitude (Km)	Designation	Constituents	n_{max} (ions/cm^3)	$v_{+,th}$ (Km/sec)	v_s (Km/sec)
60-85	D	NO^+(?)	1×10^3	0.4	7.9
85-140	E	O_2^+,NO^+	2×10^5	0.4	7.9
140-200	F_1	NO^+,O_2^+,O^+	4×10^5	0.9	7.8
200-1200	F_2	O^+,N^+	2×10^6	1.4	7.5
1200-3400	Heliosphere	He^+	1×10^4	3.7	7.3-6.4
3400-	Protonosphere	H^+	1×10^3	5.6	6.4-

To minimize weight, an ion reflector should consist of a grid of fine wires. From the values given in Table I, 100 percent reflection should occur with a minimum space potential between grid wires of approximately +10 V with respect to the ionospheric plasma. Compromises between grid mesh size, weight, and the potential applied to the wires in order to attain this minimum must be made. It will also be necessary to shield this positive grid from the ionospheric electrons; otherwise, increased power would be needed for their collection and more potential would have to be applied to compensate for their space charge. Basic shielding would consist of two negative grids parallel to and on either side of the positive element.

B. Experimental Configuration

The concept of an ion-reflecting drag device was demonstrated in the laboratory by using the "plasma wind tunnel,"[3,4] in which spacecraft motion through the ionosphere is simulated by directing a streaming plasma at a stationary object within a vacuum chamber. The usual plasma

Table I. Typical Values of Ionosphere Variables Important to Simulation

Altitude (Km)	Designation	Constituents	n_{max} (ions/cm^3)	$v_{+,th}$ (Km/sec)	v_s (Km/sec)
60-85	D	NO^+(?)	1×10^3	0.4	7.9
85-140	E	O_2^+,NO^+	2×10^5	0.4	7.9
140-200	F_1	NO^+,O_2^+,O^+	4×10^5	0.9	7.8
200-1200	F_2	O^+,N^+	2×10^6	1.4	7.5
1200-3400	Heliosphere	He^+	1×10^4	3.7	7.3-6.4
3400-	Protonosphere	H^+	1×10^3	5.6	6.4-

To minimize weight, an ion reflector should consist of a grid of fine wires. From the values given in Table I, 100 percent reflection should occur with a minimum space potential between grid wires of approximately +10 V with respect to the ionospheric plasma. Compromises between grid mesh size, weight, and the potential applied to the wires in order to attain this minimum must be made. It will also be necessary to shield this positive grid from the ionospheric electrons; otherwise, increased power would be needed for their collection and more potential would have to be applied to compensate for their space charge. Basic shielding would consist of two negative grids parallel to and on either side of the positive element.

B. Experimental Configuration

The concept of an ion-reflecting drag device was demonstrated in the laboratory by using the "plasma wind tunnel,"[3,4] in which spacecraft motion through the ionosphere is simulated by directing a streaming plasma at a stationary object within a vacuum chamber. The usual plasma

source and downstream Faraday cups (j_+ boxes) were augmented by an array of seven j_+ boxes on a boom above the plasma source, as shown in Fig. 1, and in the photograph, Fig. 2.

The final experimental version of the electrostatic mirror is shown in Fig. 2. Some of its design was dictated by its intended use as a thrust device, which is described in later sections. The grids were each 12 inches in diameter and were wound of 0.005-inch-diameter nickel wire on 1/4-inch spacing. The interplane spacings are 8 inches. As shown in the figure, a circumferential shield surrounds the grids, and between each pair of grids are three guard rings to reduce edge effects.

This mirror was capable of totally reflecting the plasma incident upon it. However, with the plasma densities used ($\sim 10^6$ ions/cm^3 before entering the mirror), oscillatory behavior was observed, which was taken as evidence that space charge was playing an important role. The period of these oscillations was approximately equal to the time between ion entrance and ion exit from the device. It is felt that the oscillations resulted from a variation of the plane of reflection with time, an effect previously observed in another context.[5] In an earlier compressed version of the mirror, with 1 inch between grid planes, oscillatory behavior was not observed. The oscillatory features associated with ion turn-around in space charge clouds would not be expected in this compressed geometry.

III. THRUST DEVICE

A. Theory of Operation

To produce thrust on a spacecraft traversing the ionosphere without making use of onboard propellant, it is necessary to increase the kinetic energy of the ions streaming past it by supplying energy from an onboard power source. The electric impeller, operating in the mode experimentally investigated, generates cycles each consisting of the following sequence of events. First, the ions are allowed to flow part of the way into an acceleration space; next, this group of ions is

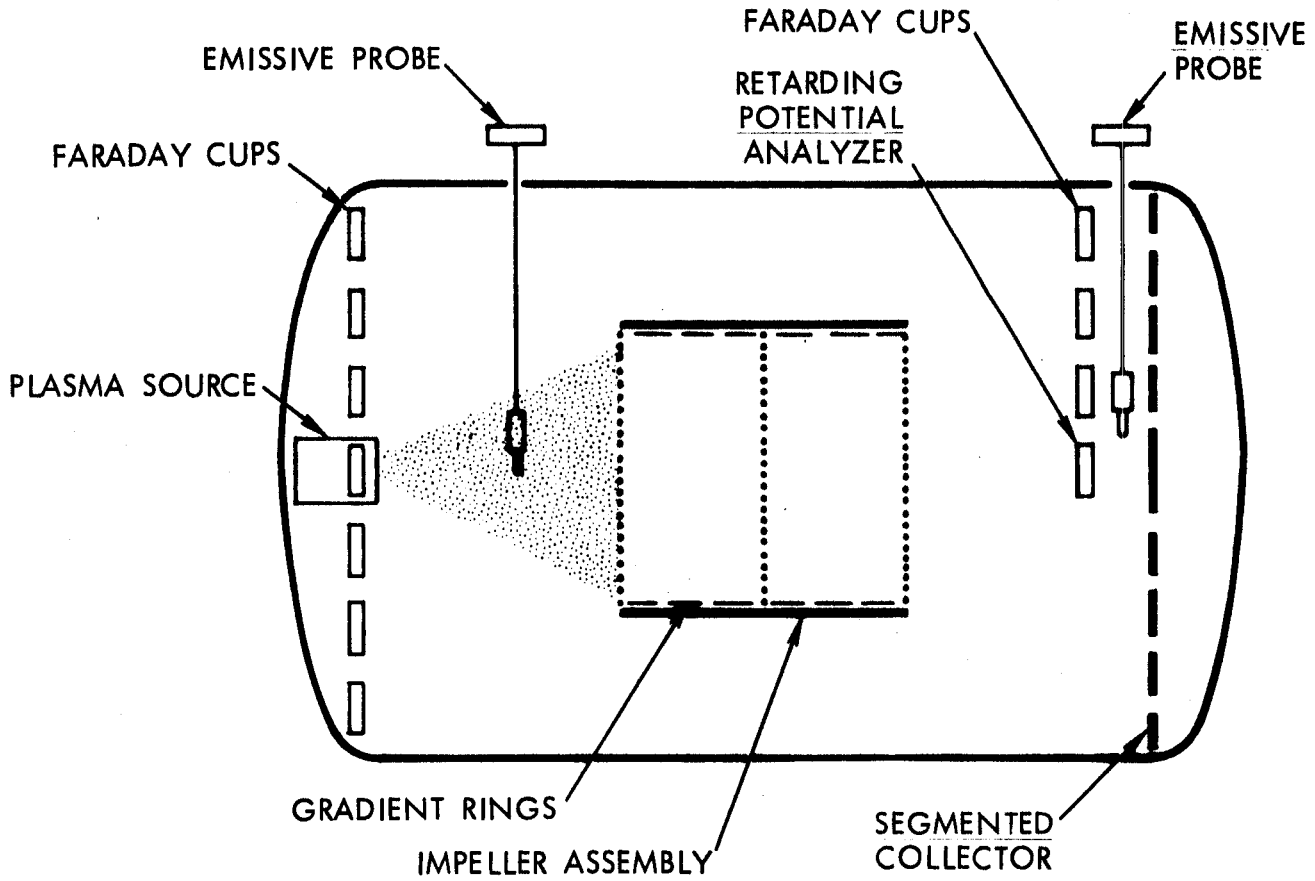

Figure 1. Plasma Wind Tunnel Facility Used in Plasma Impeller Studies.

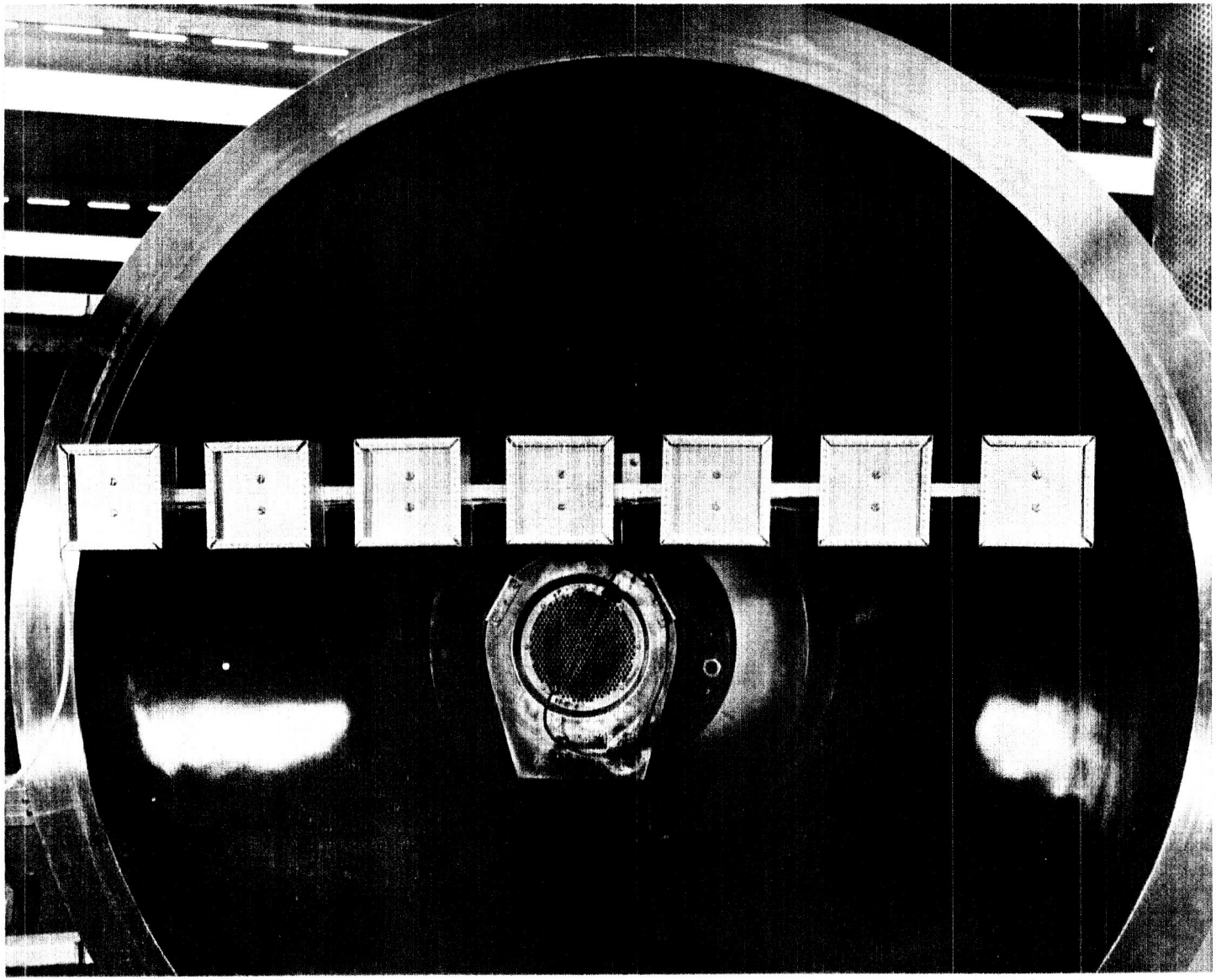

Figure 2. Photograph Of Seven Faraday Cups Mounted Above The Plasma Source Used To Detect Ions Reflected By The Electrostatic Mirror

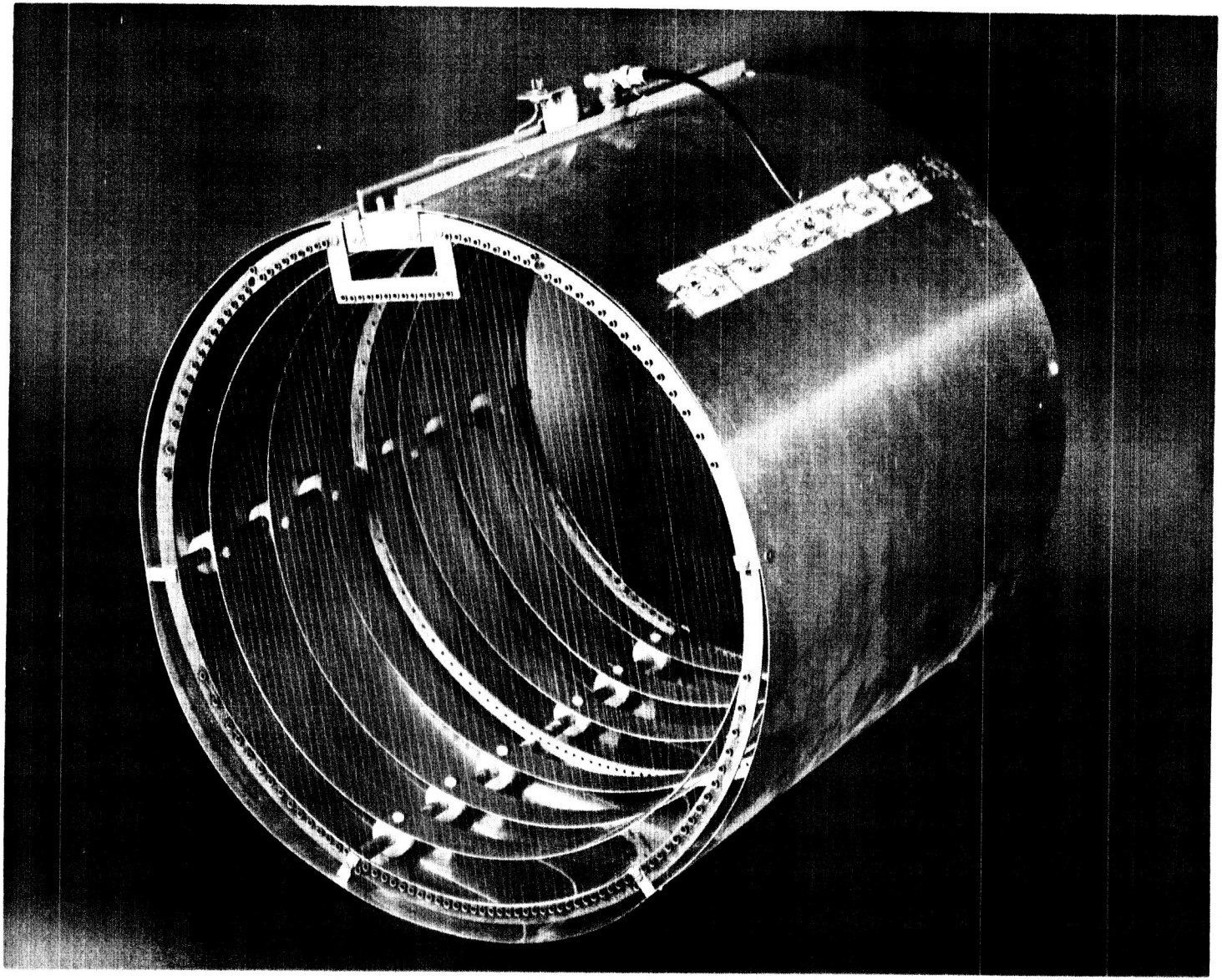

Figure 3. Photograph Of Final Version Of Electrostatic Mirror Which Was Also Used As An Impeller By Pulsing Its Grid Potentials

strongly accelerated by an applied electric field, during which time a negligibly small number of new ions flow into the acceleration region; finally, when the accelerated ions reach the field-imposing grid, the grid potential is quickly reduced to zero and the accelerated ions pass out of the device without deceleration. Meanwhile, a new group of ions has entered the acceleration region to start the next cycle.

In a device of the sort shown in Fig. 2 this operational description implies the application of a periodic-waveform potential to the center grid. In a practical application, a compromise immediately arises. A rectangular waveform is most advantageous for the operation of the device as described, but a rectangular waveform offers no possibility of recovering the energy used to charge the capacitance of the system. From this energy viewpoint, a resonant circuit and a sinusoidal waveform are desired. The attitude taken in the experimental work to be described was that effort in the first step in the development of such a thrustor should be concentrated on demonstrating that the device will produce thrust under the most ideal conditions obtainable. If thrust could be demonstrated, then attention might be directed to the power efficiency of the device. Accordingly, the work described will always involve the use of a rectangular waveform.

The basic plan of the experiment was to direct the streaming plasma at the impeller, as in experiments with the electrostatic mirror, and make observations downstream from the device. With the impeller at its floating potential, the current density and energy distribution of the ions were measured with a retarding potential analyzer. Then the outer grids of the impeller were biased to reject electrons, and a high-output pulse generator was connected to the middle grid. Again the ion current density and its energy distribution were measured. In all experiments two effects were noted when the impeller was pulsed: the downstream current density was reduced, and the energy distribution was broadened.

The low axial transmission of earlier versions of the impeller without guard rings between grids was at least partly due to the defocusing

of the ion stream by the curved equipotential surfaces within the device. The addition of these rings and their associated frequency-compensated potential dividers substantially increased the axial transmission to ~2/3. Further increase in this figure might have resulted from an investigation of those ion trajectories that form an angle with the axis and the use of more rings with smaller potential steps between them, but inasmuch as the transmission of the device is partly dependent on the particular waveform applied to the center grid attention was concentrated instead on what was happening to the on-axis group that was transmitted.

The observed broadening of the energy distribution did not, by itself, demonstrate a net thrust because some ions were decelerated, reducing the effect of those that were accelerated. The equation used to average these effects is based on measured energy distribution, which, in turn, is derived from retarding potential analyzer data. The retarding potential analyzer collects all ions having kinetic energies per charge greater than the potential applied to its collector. Therefore, the first derivative of its collected current with respect to applied potential, $\Delta I/\Delta V$, yields the energy distribution of the beam. Assuming that all ions enter the impeller with kinetic energy eV_o and that all particles are transmitted through the impeller, one computes the net thrust implied by a given measured energy distribution as

$$F_{net} = \left(2\,\frac{m}{e}\right)^{1/2} \int_o^\infty \left(V^{1/2} - V_o^{1/2}\right) \frac{\Delta I}{\Delta V^{1/2}}\, dV^{1/2} .$$

B. Experimental Considerations

The experimental demonstration of the impeller was beset by a number of experimental complications that are worthy of discussion, especially if further work on the device is undertaken in the future. The fact is that although some encouraging results were finally obtained, the concept never received a test under favorable conditions.

Perhaps the most serious limitation on providing a fair test was the inability to obtain a pulser with the desired characteristics. With the beams available, an ideal pulser for the impeller design used would produce a rectangular pulse train at 100 kHz, with pulse duration of 1.0 μsec and amplitude of -1.0 kV. Furthermore, it should be capable of supplying this pulse train to a load impedance of approximately 2 megohms in parallel with 50 pf., and it should be sufficiently shielded so that rf radiation does not disturb the diagnostic instruments used in the experiment.

With the time and funds available it was not possible to obtain a pulser with all of these characteristics. One unit employed was sufficiently shielded but would not operate at repetition rates exceeding 30 kHz, whereas another unit was capable of 100 kHz repetition rates but emitted enough rf to cast doubt on the instrument readings despite careful shielding of these circuits. The basic design of the latter unit is shown in Fig. 3, because it is felt that careful attention to shielding of this instrument might produce a satisfactory pulser.

Another experimental complication encountered was that even with the pulser off, the ions measured downstream fell into two energy groups...an essentially monoenergetic group with an energy corresponding closely to the acceleration potentials applied to the ion source, and a much broader group with energies between 0 eV and the potential applied the neutralizer filament. Experiments supported the hypothesis that the low-energy ions originated from charge exchange collisions of the primary ion beam with ambient neutral atoms within the chamber; for instance, this population grew as the pressure in the chamber was increased from the typical 5×10^{-5} torr to 10×10^{-5} torr. The energy spread observed in the charge-exchange group must then be largely due to a distribution in the direction of ion velocities with respect to the retarding potential analyzer. (The analyzer only measures the energy component normal to its collector.)

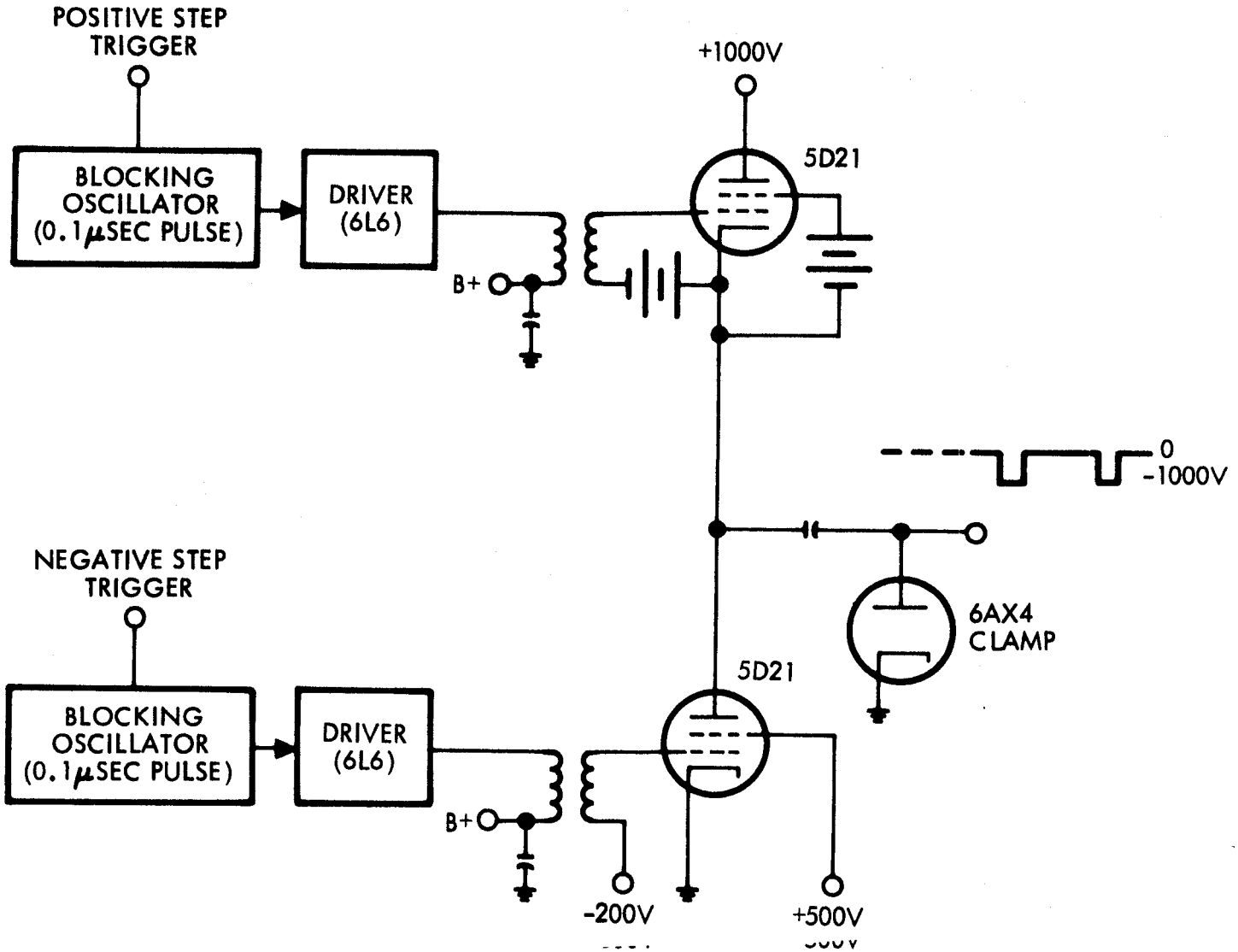

Figure 4. Schematic Diagram Of Most Successful Pulser Used, Careful Attention To R,F, Shielding Probably Would Have Made It Satisfactory For The Experiment.

While the population of this group did not change significantly when the pulser was applied, suggesting that some of these ions are formed in the region between the impeller and the analyzer and/or that their directions are sufficiently random that the impeller has no net affect on them, their presence is undesirable for two reasons. First, one can never be certain when the pulser is on whether some of the last ions observed originated from the charge exchange group, or conversely, some of the primary ions have been decelerated into this low-energy range. Second, the presence of an essentially resident colony of ions within the impeller itself can only serve to "load" it and decrease its effectiveness.

The reason for the rather high pressure in the chamber is that a high gas pressure is required within the ion source (a modified version of the SERT I type Kaufman electric rocket designed to use mercury and much larger extraction potentials) to maintain a gas discharge. To reduce the gas pressure into the chamber, a new ion source would have to be designed or a differential pumping scheme employed. (In the current configuration, a 3000 ℓ/sec diffusion pump is attached to the center of the cylindrical 4 x 8 foot chamber.) Another approach to reducing the charge exchange population is to position an electrostatic reflector, adjusted to reflect low-energy ions while transmitting the primary ions, between the ion source and the impeller. Because both the primary ion and neutral gas densities are highest in the immediate vicinity of the source, the downstream charge exchange population can be substantially reduced by this technique. However, a disadvantage of this approach is that the grid wires of the reflector become scattering centers for the primary ions and introduce a distribution in transverse velocity component. Indeed, in other experiments[4] such a grid was successfully employed to achieve this very effect. Since the construction of such a reflector is not time consuming, whereas reducing the gas pressure would have represented a major effort, it was decided to construct a reflector to experimentally determine its effectiveness despite this disadvantage. A three-grid reflector was built that is similar to the impeller but has smaller dimensions. Each grid is 30 x 30 inches and consists of crossed wires with 1/4 inch spacing. The grid planes are 1 inch apart. Figure 4 is a photograph of the completed reflector. With this reflector in operation it was possible

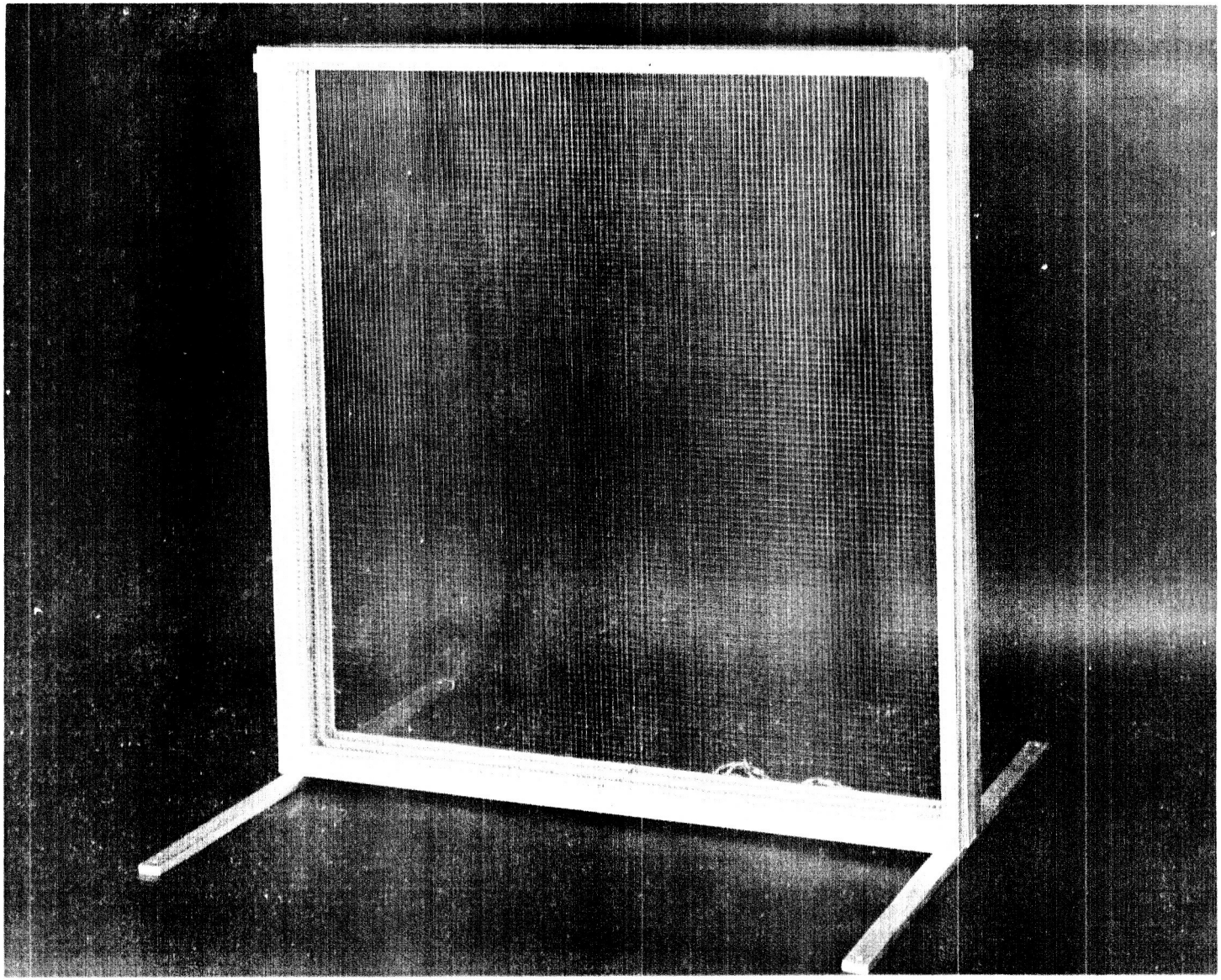

Figure 5. Photograph Of The 30" x 30" 3-Grid Reflector Used To Reduce The Number Of Low Energy Ions Reaching The Impeller

to decrease the size of the charge exchange group arriving at the analyzer from ∿50 percent to between 10 and 20 percent.

Another experimental problem encountered was that immediately following a change in the potential applied to the analyzer plate, the current collected by the plate would change with time. We suspected that an insulating film was forming on the collector and charging up during the period of observed change in collected current. Therefore, a switching circuit was built to hold the analyzer collector and guard ring at a large negative potential just before a measurement was taken. The energetic ions striking these electrodes sputtered and warmed them, with the result that these surfaces remained "clean" over a period long enough to allow a measurement to be made.

Finally, it was often observed that when the ion retarding potential on the analyzer collector was increased past the point of ostensibly zero collected current, a negative current was collected. Such a negative current would arise from electron collection. Some of these electrons could have originated as secondaries from ion collisions with the electron suppression grid in front of the analyzer collector, but at least some of them were very energetic and must have originated as secondaries from the approximately -500 volt accelerator grid on the ion source. The negative current was observed to respond to changes in this potential. With a single electron suppression grid in front of the analyzer it was not possible to make its potential sufficiently negative to reflect these very energetic electrons without significantly modifying the trajectories of the ∿50 volt ions in the vicinity of the analyzer. A two-grid system would have allowed the use of a highly negative electron suppressor at the cost of increased secondary production at the grid itself. However, by careful adjustment of the various experimental parameters this negative current was reduced to an acceptable value, especially since one could expect it to be virtually constant during a retarding potential run, whereas changes in collected current yield the energy distribution sought.

C. Experimental Results

In Fig. 5 is shown two energy distributions of a 49-V N_2 beam, taken with the impeller on and off. These data were taken before the charge exchange ion reflector was available and the charge exchange group represents about 45 percent of the total current arriving at the analyzer with the impeller off and about 52 percent when it is on. Note that when the impeller was turned on the total beam current dropped to 64 percent of the initial value.

However, application of Eq. (1) under the assumption that the initial condition was that of a monoenergic beam of 49 volts still indicates net thrust was obtained. This assumption is clearly pessimistic since it implies that all those observed ions with less than 49 volts had been decelerated producing drag. In fact a large fraction below 49 volts were present as low energy charge exchange ions and were not decelerated. Therefore, the net thrust must be larger than that calculated under the stated assumption.

The conditions of the experiment were as follows. The beam consisted of nitrogen ions, and the center grid of the impeller was at -30 V for 8.8 μs and -650 V for 4.4 μs during each repetition.

In summary, despite numerous experimental difficulties, these experiments repeatedly demonstrated the ability to substantially accelerate some of the ions incident on the impeller. In addition, some data obtained suggested that net thrust had been achieved.

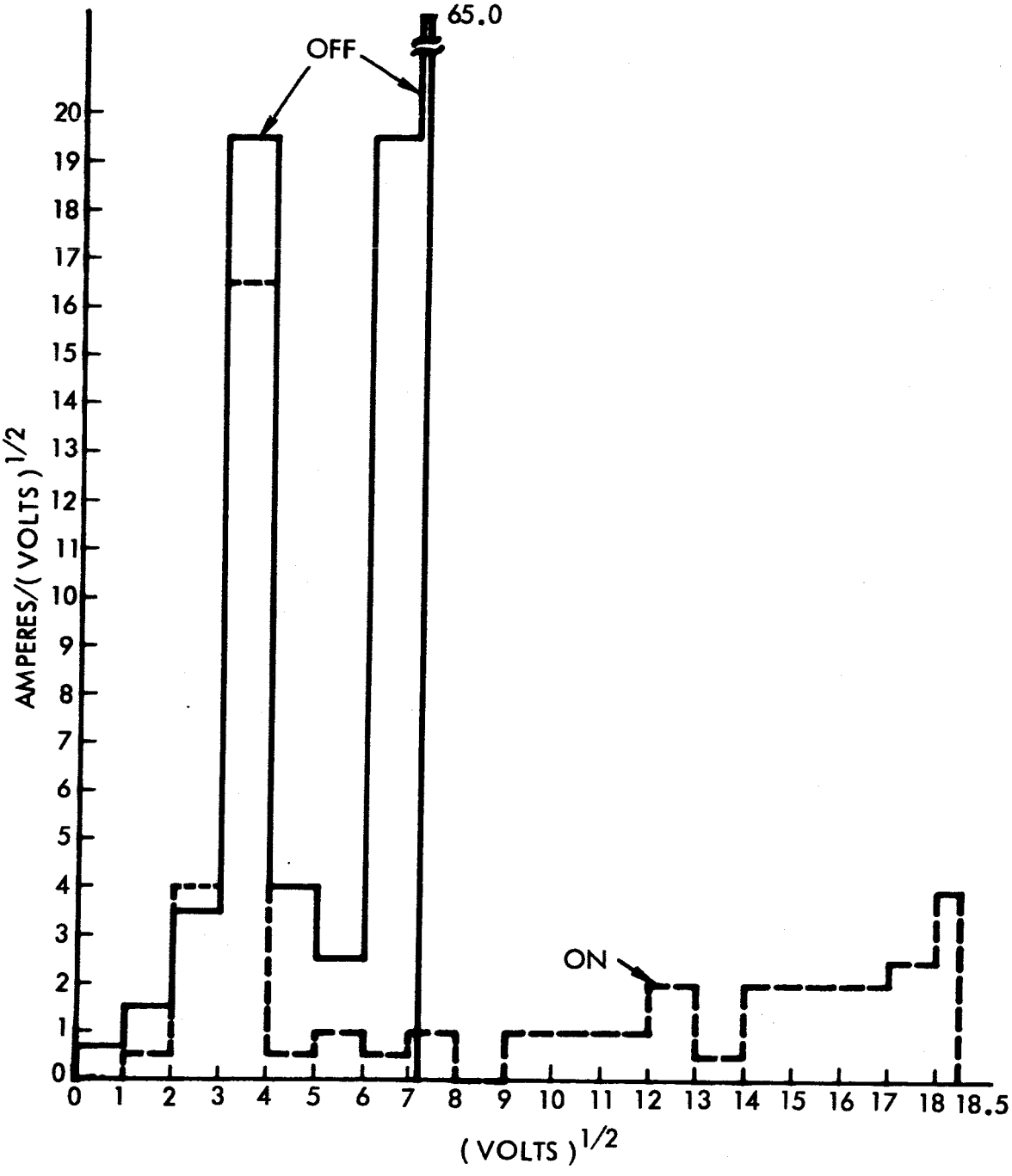

Figure 6. Energy Spectrum At Analyzer With Impeller Off (Solid Line) And With Impeller In Operation (Broken Line)

REFERENCES

1. Hanson, W. B., "Structure of the Ionosphere," Satellite Environment Handbook, edited by F. S. Johnson (Stanford University Press, Stanford, Calif., 1961), pp 27-46

2. Hanson, W. B. "Upper-Atmosphere He Ions," J. Geophys. Res. 67, 183-188 (1962)

3, Hall, D. F., Kemp, R. F., and Sellen, J. M., Jr., "Plasma-Vehicle Interaction in a Plasma Stream," AIAA J. 2, 1032-1039 (1964)

4. Hall, D. F., Kemp, R. F., and Sellen, J. M., Jr., "Generation and Characteristics of Plamsa Wind-Tunnel Streams," AIAA J. 3, 1490-1497 (1965)

5. Sellen, J. M., Jr., and Shelton, H., "Transient and Steady State Behavior in Cesium Ion Beams," RW-RL-186, ARS Preprint 1379-60, November 1960

SECTION III.C.

PLASMA POTENTIAL MEASUREMENTS BY ELECTRON EMISSIVE PROBES

Reprinted from THE REVIEW OF SCIENTIFIC INSTRUMENTS, Vol. 37, No. 4, 455–461, April, 1966
Printed in U. S. A.

Plasma Potential Measurements by Electron Emissive Probes

ROBERT F. KEMP AND J. M. SELLEN, JR.
Physical Research Division, TRW Systems, Redondo Beach, California 90278
(Received 29 October 1965)

Several methods of using hot wire, electron emissive probes for potential measurements in quiescent plasmas are described. A plot of the probe emission characteristic gives a precise dc determination; the floating probe rapidly follows potential fluctuations of several volts magnitude; the cutoff slope detects small signals up to tens of megacycles per second. Calculations are discussed which describe the potential distributions around an emissive wire immersed in plasma, with and without the formation of a virtual cathode. Sheath dimensions are ~10 wire diameters at 10^{10} ions/cm^3; orders of magnitude larger at 10^6 ions/cm^3. Emission levels appropriate to given plasma densities are shown. The range of application has a low density limit of ~10^4 ions/cm^3 because of minimum useful emitted current, and a high density limit of ~10^{12} ions/cm^3 because of electron collection from the plasma.

I. INTRODUCTION

WHEN a small electron emissive filament is immersed in a plasma, a diode is formed in which the plasma itself acts as the "plate." The nature of this diode is more involved than that of a conventional vacuum tube because the filament is surrounded by charged particles of both polarities. Consequently, the "plate" not only acts to collect or repel electrons emitted by the filament, but can also supply currents of positive or negative particles to the filament. Furthermore, the geometry of this diode is not fixed, inasmuch as it is dependent not only on the filament configuration, but also on the charged particle distribution in the surrounding space.

The dependence of the emitted electron current on the plasma to filament potential difference can provide an accurate method of determining the space potential within the plasma. Figure 1 is a schematic of an emissive probe and associated circuitry which can be used for such plasma

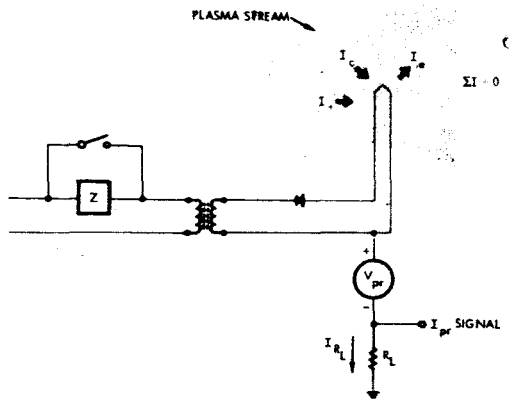

FIG. 1. Emissive probe circuit. Equilibrium exists between collected ion current I_+, collected and emitted electron currents I_e and I_e, and current in the load resistor I_{R_L}.

measurements. The figure shows that in the filament-plasma diode several currents exist simultaneously, each with its own functional dependence on probe potential.

Two means for measuring plasma potential were described by Langmuir in 1923.[1] One used an emissive probe, and the other was the familiar electron-collection (Langmuir probe) method. Figure 1 shows that either method can be used with the same filament.[2] Langmuir's technique for detecting emitted current at a given probe potential was to increase the filament temperature from a warm, nonemissive state, to a hot, emissive condition.

Langmuir later published a set of electron collection and emission curves for planar, cylindrical, and spherical concentric electrodes,[3] from which Fig. 2 was derived. These curves were calculated from Maxwell-Boltzmann statistics, conservation of energy and angular momentum considerations, and the assumption of negligible space charge in the sheath. In Fig. 2 the units of current are arbitrary, $\xi=\pm eV/kT$ where e is electronic charge, V is the potential difference between electrodes, k is Boltzmann's constant, and T is the absolute temperature. The slopes of the lines in the retarding potential regions of the curves are equal to $1/T_e$, where T_e is electron temperature (°K). Although these curves were calculated from "vacuum" trajectories of emitted particles and fixed geometry, they are nevertheless illustrative of the "volt-ampere" characteristics obtained with the hot wire probe. Specifically, the internal collector curves are typical of Langmuir probe curves, and the internal emitter curves represent emissive probe characteristics.

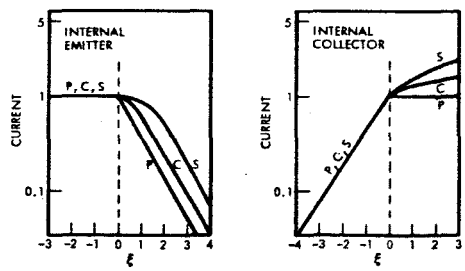

FIG. 2. Electron emission and collection curves for diodes of planar P, cylindrical C, or spherical S fixed geometry (from Langmuir[3]). Units of current are arbitrary; the variable $\xi=eV/kT$ is proportional to the potential difference between electrodes. Calculations for these curves assume no space charge, hence rounding is due solely to trajectory effects.

The curves of Fig. 2 also indicate qualitative changes seen in probe characteristics that are due to plasma density variations. In relatively dense plasmas, sheath dimensions are small compared to wire radii, and the geometry is characteristically planar. At very low densities, sheath thicknesses may be orders of magnitude larger, so that the sheath boundary resembles a sphere centered on the filament.

Within a wide range of plasma characteristics, the hot wire probe using the basic circuit of Fig. 1 has a number of uses as a diagnostic tool for measuring plasma potential and electron temperature. Although the experimental context of Fig. 1 is the diagnosis of synthesized plasma streams,[4,5] the method is equally applicable to plasmas that possess no gross over-all motion relative to the probe. The following sections present refinements of technique and modes of application of the emissive probe. Also discussed are the results of calculations which aid in understanding the effects of plasma density on probe operation.

II. PRECISE MEASUREMENT OF PLASMA POTENTIAL WITH EMISSIVE PROBE

Typical probes for the uses mentioned above have been constructed as shown in Fig. 3. The emissive filament is a small "hairpin" loop of 0.0025 to 0.005 cm diam tungsten wire. It is supported and electrically fed by two larger nickel wires, which are mounted within a two hole ceramic insulator. For electrical and mechanical shielding, the assembly is encased in a 0.3 cm diam, thin walled, stainless steel jacket in such a way that only the heated tip of the tungsten filament is exposed to the ion stream.

As shown in Fig. 1, the filament temperature is shifted by a shorting switch across a series impedance in the filament transformer primary. Measurements of emitted current are made during those portions of the power waveform when heating current is blocked by the diode in the secondary circuit. At these times, the filament is a unipotential

[1] I. Langmuir, J. Franklin Inst. 196, 571 (1923). Also in *The Collected Works of Irving Langmuir*, edited by C. Guy Suits (Pergamon Press, Inc., New York, 1961), Vol. 5, pp. 1–10.

[2] Although the Langmuir probe measurement is traditionally made with the probe cold, an advantage of using a hot but not emissive wire is that it maintains a clean (constant work function) surface.

[3] I. Langmuir and K. T. Compton, Rev. Mod. Phys. 3, 191 (1931). Also in *The Collected Works of Irving Langmuir*, edited by C. Guy Suits (Pergamon Press, Inc., New York, 1961), Vol. 4, pp. 326–393.

[4] J. M. Sellen, Jr., W. Bernstein, and R. F. Kemp, Rev. Sci. Instr. 36, 316 (1965).

[5] R. F. Kemp, J. M. Sellen, Jr., and E. V. Pawlik, NASA TN D-1733 (1963).

surface, and no correction need be made for longitudinal potential drop. The value of the emitted current is measured by observing the potential developed across the small load resistor by means of a sensitive oscilloscope. The probe potential is adjusted (usually in increments of 0.1 V) by means of a stepping switch, which is either connected to a string of stable batteries, or controls a floating power supply having a low stray capacitance to ground.

When these precautions are taken, and if the plasma is of sufficiently high density and is quiescent and stable for the several minutes required to record a number of emission values, a semilog plot of these values is asymptotic to two straight lines (emission limited below the plasma potential, Maxwell-Boltzmann cutoff above). The intersection of these lines often indicates the plasma potential unambiguously within 0.01 to 0.03 V.

III. FLOATING EMISSIVE PROBE

If the load resistor (Fig. 1) is large ($\geq 10^6\ \Omega$) (and the floating bias supply is removed from the circuit) the probe potential assumes an equilibrium value related to the following considerations: With the probe nonemissive, the first equilibrium potential is reached when the ion current balances the load-resistor and Langmuir probe currents. In streaming plasma beams the intercepted ion current is equal to the ion current density times the projected area of the wire and is small; hence, the probe potential with the wire cold is below that of the plasma. As the wire is heated and becomes emissive, a range of equilibrium values is reached near the plasma potential, as indicated by the plateau above the knee in the curve of Fig. 4. When the emissive probe is thus used in a "floating" mode, R_L can be the input resistance of an oscilloscope or part of the attenuator input to a telemetering amplifier. Within its accuracy, the floating probe indicates plasma potential directly, without step by step measurements or data reduction operations.

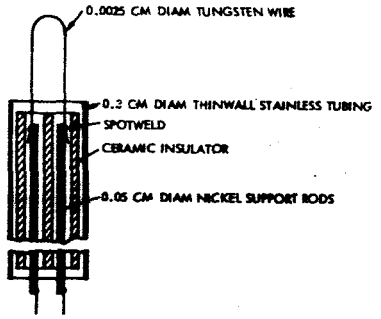

FIG. 3. Construction details of the "hairpin" emissive probe.

As a consequence of its direct readout, the floating probe is capable of following changes in plasma potentials at frequencies extending into the low rf range. The limitation on frequency response is the stray capacitance that must be charged by the emitted and collected currents. In Fig. 5(a) is an equivalent circuit for the floating emissive probe. It shows the stray capacitances connected to the plasma potential through the coupling impedance R_d of the probe. This is a dynamic resistance, the value of which is found from the rate of change in load resistor current with respect to probe voltage at the operating point. The value of R_d depends also on filament temperature (emission capability) and in the vicinity of the plasma potential is given approximately by

$$R_d \approx kT/2eI_0 \quad (\Omega), \tag{1}$$

where I_0 is the emission limited current in amperes, e is electronic charge (C), k is Boltzmann's constant (J/°K), and T is the temperature (°K) of the wire or of the plasma electrons. The factor of 2 in the denominator follows from the assumption of equal contributions from emitted and collected electrons. For $T_e = T_w = 2500$°K, $R_d \approx 0.1/I_0(\Omega)$. Thus, if $I_0 = 1$ mA, $R_d \approx 100\ \Omega$; if $I_0 = 1\ \mu$A, $R_d \approx 100$ kΩ; etc. Consequently, the floating probe exhibits a higher frequency response limit [$=1/(2\pi R_d C_s)$] in a relatively dense plasma (relatively higher emission possibility) than in a dilute one.

A practical floating emissive probe instrument having wide frequency response can be made using the circuit of Fig. 5(b). Here the capacitance seen by the floating probe is no longer the capacitance to ground, but to a shield,

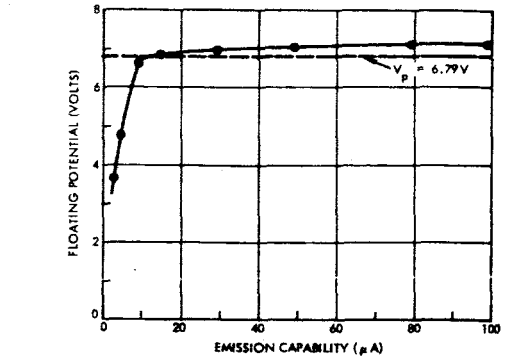

FIG. 4. Emissive probe floating potential vs emission limited current. At each of several filament temperatures the value of R_L was shifted from $10^8\ \Omega$ (current measurement) to $10^6\ \Omega$ (potential measurement). The medium was a cesium plasma of 7×10^5 cm/sec streaming velocity and about 1×10^9 ions/cm^3 density at the probe position. The plasma potential V_p of 6.79 V was determined from the cutoff characteristic of the same probe as described in Sec. II.

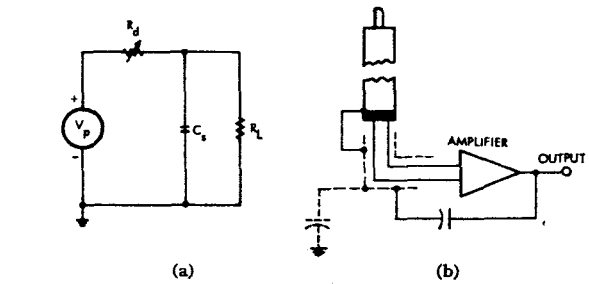

FIG. 5. Floating emissive probe circuits. (a) Small signal equivalent circuit. If R_L is large, the upper cutoff frequency is $1/(2\pi R_d C_s)$. (b) Driven shield circuit for floating emissive probe instrument.

the potential of which is driven by the amplifier. The low impedance output of the amplifier is used to drive the capacitance to ground, which in a laboratory instrument, may include that of a significant length of cable.

Because it provides a direct indication and is simple to instrument, the floating emissive probe can be a very useful potential indicating device.

IV. EMISSIVE PROBE INDICATION OF SMALL POTENTIAL FLUCTUATIONS

When the plasma potential undergoes small amplitude fluctuations about a constant mean value, the emissive probe provides a convenient means of indicating the fluctuations. In this application, the circuit of Fig. 1 is used with a small value of R_L and a value of probe bias slightly higher than the plasma potential. This biases the probe at the point near the upper end of the Boltzmann line where the rate of change of emitted current with plasma potential is greatest. The resultant fluctuations in the voltage drop across R_L are readily observed with an oscilloscope. The magnitude of the plasma potential excursions may be calculated from a knowledge of the slope of the Boltzmann line (i.e., from the emissive probe characteristic at the given filament temperature). In this measurement, the relative importance of the changes in collected electron current may be minimized by increasing the filament temperature so that the emission limited current is several times the Langmuir probe current at the bias potential.

This method has the advantage over the floating probe method that the measuring amplifier input is near ground potential but is at the same time directly coupled to the signal source. Furthermore, the impedance between the filament and ground is low; consequently, the frequency response is good. Small plasma potential fluctuations at frequencies of several megacycles per second have been readily detected by this technique.

V. CALCULATIONS OF EMISSIVE WIRE SHEATH POTENTIALS

When used with quiescent plasmas in which the ion densities are from 10^7 to 10^{10} ions/cm^3, the emissive probes have characteristics that show on a semilog plot as straight lines and a fairly sharp knee. At lower densities, the knee extends over a wider range of potentials and the cutoff slope is indicative of a higher temperature than that of the wire. This effect is shown in Fig. 6. The low density curves resemble the cylindrical and spherical curves of Fig. 2(a). In order to gain further understanding of the operation of the emissive probe, and in particular to seek a mechanism for the difficulties that arise at low density, a series of calculations was undertaken to describe the electric potential distribution in the sheath surrounding an emissive wire in a plasma.

The calculations relate the factors of electron temperature and density within the plasma, wire temperature (electron emissivity), and the potential difference between

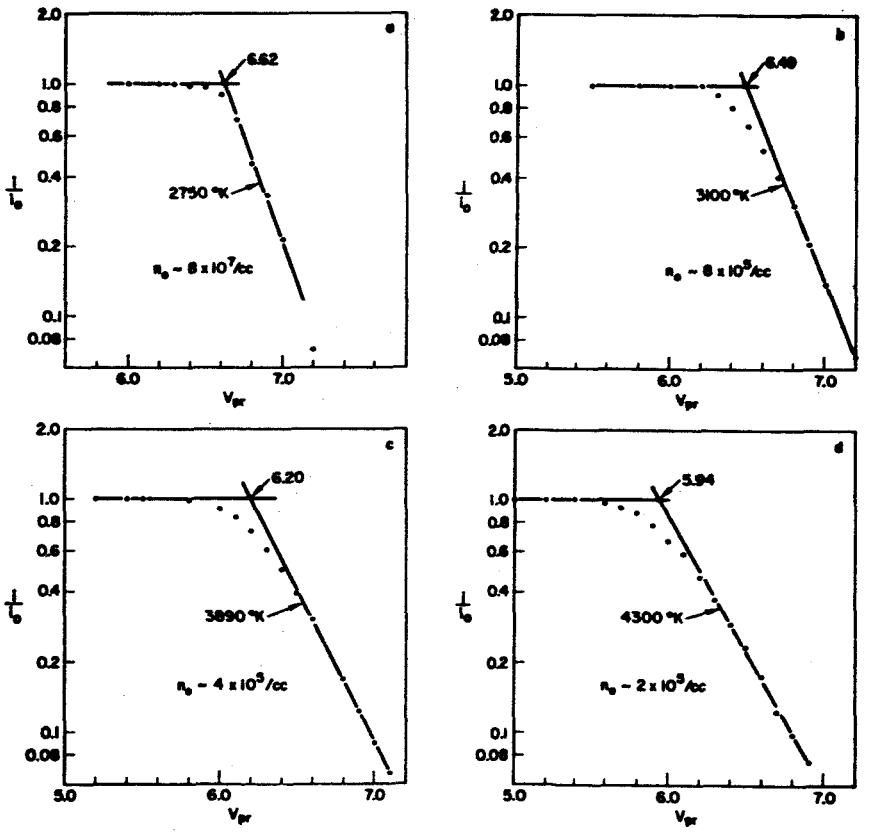

FIG. 6. Examples of emissive probe characteristics which show increased rounding of the knee of the curve as the plasma density is reduced. Not only density, but also plasma bias potential was allowed to vary during this series of measurements.

the wire and the plasma. The method used was the machine solution, by iterative process, of Eq. (2), a normalized Poisson equation in cylindrical coordinates,

$$\frac{d^2\xi}{d\theta^2}+\frac{d\xi}{\theta d\theta}=-C\left\{1-\exp[-B(\xi_p-\xi)]-\frac{A}{\theta(2\xi+1)^{\frac{1}{2}}}\right\}. \quad (2)$$

Here $\xi(=eV/kT_w)$ is the normalized potential relative to the surface of the emitting wire; ξ_p is the normalized plasma potential; $\theta(=r/r_0)$ is the radial distance relative to wire radius; $A(=\rho_{-0w}/\rho_0)$ is the space charge density of emitted electrons at the wire surface relative to ion charge density; $B(=T_w/T_e)$ is the wire temperature relative to electron temperature in plasma; and $C(=e\rho_0 r_0^2/kT_w\epsilon_0)$ is a constant resulting from the normalization of the equation, where e is the electronic charge and ϵ_0 is the permittivity of free space. The assumption implicit in maintaining ion charge density ρ_0 $(=en_0$, where n_0 is the number density) constant is that in streaming plasmas the kinetic energy of the ions is so great that ion trajectories are not significantly affected by small potential fluctuations in the vicinity of the wire; hence, the ion space charge density does not vary within the wire sheath. Emitted electrons have been assigned an injection energy in the radial direction of $kT_w/2$; azimuthal velocity has been neglected. This is a justifiable assumption for the calculations described in Sec. V(A) inasmuch as electron velocities outside the wire are always $\geq$ the emission velocity. Boltzmann statistics are assumed for plasma electrons, however.

A. Space Charge Limited Emission

The first set of cases sought values of emitted current for a given wire radius and a given plasma density that cause the wire to operate space charge limited, but without the formation of a virtual cathode. Hence, the boundary conditions were

$$\theta=1\begin{cases}\xi=0\\ d\xi/d\theta=0\end{cases}\qquad \lim_{\theta\to\infty}\xi=\xi_p.$$

TABLE I. Sheath dimensions around emissive wire, zero surface electric field, $T_e=T_w=2500°K$, and $r_0=0.00125$ cm.

n_0 ions/cm³	ξ_p	Values of θ for which $\xi=0.2\xi_p$	$\xi=0.5\xi_p$	$\xi=0.8\xi_p$
10^6	5	98	311	736
	3	95	295	715
	1	97	300	760
10^7	5	39	101	236
10^8	5	12.5	34	77
10^9	5	5.5	12.6	26
	3	5.4	12.4	27
	1	5.5	12.6	29
10^{10}	5	2.8	5.4	9.8
	3	2.8	5.3	9.9
	1	2.9	5.5	11

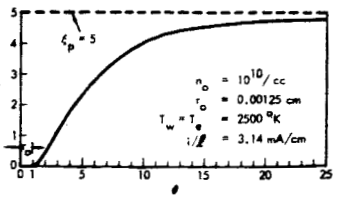

FIG. 7. A solution curve for Eq. (2) which describes the radial distribution of potential in the vicinity of a space charge limited emissive wire.

A typical solution curve for one calculation is shown in Fig. 7. For each such curve, the value of A found by the computer is one point of the function $A(\xi_p,C)$ which satisfies the given boundary conditions. These results are displayed in Fig. 8. Here they have been rescaled to values of microamperes per centimeter length of emissive wire, with wire radius and plasma number density as parameters.

Integration of the equation proceeded from the point $\theta=1$ sufficiently far in the direction of increasing θ to assure that each solution was asymptotic to the plasma potential. The resulting curves display the configuration of the sheath surrounding the wire for the several cases calculated. The computer listings were examined for approximate values of normalized radius at which the space potential equals a given proportional value of the surrounding plasma potential. These are given in Table I for several values of ion number density and plasma potential. The significant indication here is that the extent and shape of the sheath are primarily dependent on plasma density, and do not vary with ξ_p (which is dependent on wire emissivity according to Fig. 8).

B. Virtual Source Formation

In a second set of calculations, the starting values for Eq. (2) were the end values from the solutions to a related set of boundary value problems; this time, the value of A was specified in advance, and appropriate values of ξ_p were sought. The starting solutions describe the potential field surrounding a wire that is emitting more current than can escape into the surrounding region, and around which the excess electron space charge forms a virtual cathode.

The equation used for the region between the wire sur-

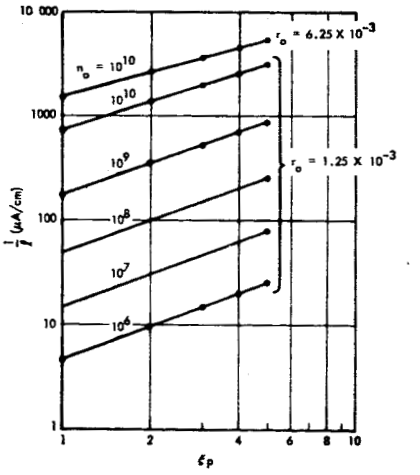

FIG. 8. Calculated electron emissivity of wires of radius r_0 (cm), operating space charge limited in a plasma of density $n_0(cm^{-3})$ without virtual source (surface electric field is zero). For $T_w=2500°K$, $\xi_p=V_p/(kT_w/e)=V_p/0.215$ V.

face and the point of potential minimum (virtual source position) is

$$\frac{d^2\xi}{d\theta^2}=\frac{1}{\theta}\left\{-\frac{d\xi}{d\theta}+De^{\xi}[1+\mathrm{erf}(\xi-\xi_{\max})^{\frac{1}{2}}]\right\}-C \qquad (3)$$

Here $D=(er_0 i_{tr}\gamma/\epsilon_0 kLT)(m/8\pi kT)^{\frac{1}{2}}$; i_{tr} is the electron current per unit length of wire transmitted by the virtual cathode; γ is the ratio of emitted to transmitted current; m is the electron mass; L is the wire length (emissive region); and

$$\mathrm{erf}(x)=\int_0^x e^{-\eta^2}d\eta.$$

The constant C, defined in connection with Eq. (2), again represents the ion charge density. Note, also, that the relationship between the magnitude of the potential minimum at the virtual cathode, $\xi_{\max}$, and the transmitted current factor is

$$\gamma=e^{-\xi_{\max}}.$$

For this equation, it was necessary to give the emitted electrons a Maxwell-Boltzmann velocity distribution; again, only radial velocities have been accounted for. The contribution to the space charge of plasma electrons within the virtual source region has been neglected. This is justified by the fact that $A\gg 1$.

Starting at the wire surface ($\theta=1$), values were sought for the initial potential slope such that each potential would go through a specified minimum value. The values of θ at which these minima occurred and the corresponding values of transmitted current were the starting values for Eq. (2) for the region exterior to the virtual source. In the exterior region, the iterative process sought for appropriate values of ξ_p. Figure 9 shows the results of piecing together the resulting curves.

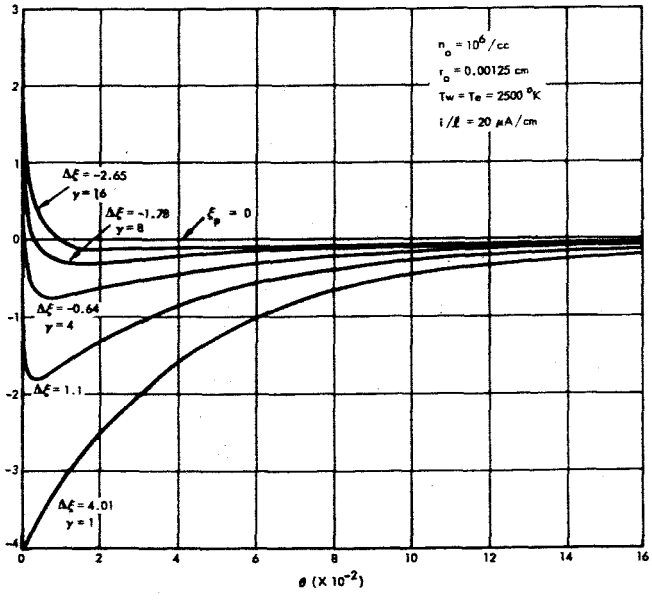

FIG. 9. Calculated radial potential distributions for emissive wires at different potentials, but constant emissivity. The fraction of emitted current which is transmitted to the plasma is $1/\gamma$; for $\gamma=1$, no virtual source is formed. In the limit of large γ the value of the potential difference between the filament and the plasma is $\Delta\xi=-\ln\gamma$.

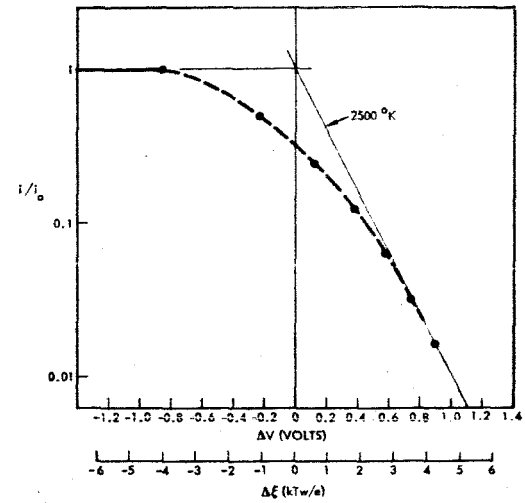

FIG. 10. Emitted current vs calculated potential difference between plasma and wire (from Fig. 9) plotted as an emissive probe characteristic. Space charge rounding of the knee of the curve occurs at this emissive level.

In Fig. 10 the values of transmitted current from Fig. 9 are plotted against the potential difference between the plasma and the probe $\Delta\xi$ as an emissive probe characteristic. At this emissive level and plasma density, the effect of electron space charge is to begin to repel some of the emitted current back to the filament when the filament is 0.86 V ($4.01\ kT_w/e$) below the plasma potential. At lower emission levels or greater densities the point of departure from the emission limited value would move closer to the intersection with the Boltzmann line. The exact value at which space charge rounding begins can be found from Fig. 8, within the ranges plotted. One would usually operate the probe with a value of i/l such that rounding would occur at $\Delta\xi\gtrsim 1$.

VI. EMISSIVE PROBE CHARACTERISTICS AT LOW PLASMA DENSITY

Comparison of the indicated sheath size for a plasma density of 10^6 ions/cm^3 (Table I) with the dimensions of a typical hairpin filament probe as shown in Fig. 3 shows that the assumption of cylindrical symmetry implicit in the calculations for Fig. 9 is not applicable to the hairpin probe at low plasma densities. In fact, as mentioned previously, the small hairpin probe shows premature rounding and poor cutoff slope in this situation even for appropriately reduced values of i/l. Since no part of the small filament is separated by more than about 100 wire radii from an adjacent wire, each side of the filament operates in the sheath of the other side. The resulting additional space charge can contribute to the premature rounding of the cutoff characteristic of the hairpin probe in low plasma densities.

In order to determine experimentally the extent of the

improvement that could be obtained by opening the loop of the hairpin probe, a special linear emissive probe was constructed. The design of this probe is shown in Fig. 11. The curves of Fig. 12 compare the cutoff characteristics of the linear probe and a hairpin probe in the same plasma at a density of 2×10^6 ions/cm^3. The linear probe curve compares favorably with those of hairpin probes at densities two orders of magnitude higher. Not only is the knee sharper, but the Boltzmann line is straight and indicates a temperature not greatly different from the ~2500°K wire temperature. The combination of excessive rounding and abnormally high temperature cutoff of the hairpin probe lead to an erroneously low indication of plasma potential in this instance.

The calculations have brought to light two mechanisms for rounding of the knee of the emissive probe curves, but there is nothing in the formulation of the equations to account for the observed variations in the cutoff slope. One possible cause of the high effective cutoff temperature is the contribution of the azimuthal velocity component of the emitted electrons, and in particular, the possibility of variations in angular momentum at distant positions within the extended sheaths which occur at low densities. Noncentral forces or microscatterings would, for the most part, tend to change electron trajectories so that electron dwell time in the sheath region is prolonged. Opportunities for further, and perhaps, nonconservative interactions between the electron and the plasma are thus increased, with the possible result of an enhanced current of electrons escaping from the wire.

VII. RANGE OF APPLICATIONS

The lower limit in plasma density for the use of the emissive probe occurs because of space charge rounding of the probe characteristic. From Fig. 8 and the conditions that apply there, the lower limit in plasma density is ~10^5 ions/cm^3 for an accuracy in potential measurement of ~0.01 V. This plasma density would permit a wire emission of ~2 μA/cm, and the signal from this current would be at a usable level. For general applications, emission levels below 1 μA/cm are not readily useful. This limitation would then yield an accuracy level of ~0.1 V at plasma densities of 10^4 ions/cm^3 and ~1 V at 10^3 ions/cm^3.

The upper limit in plasma density for the application of

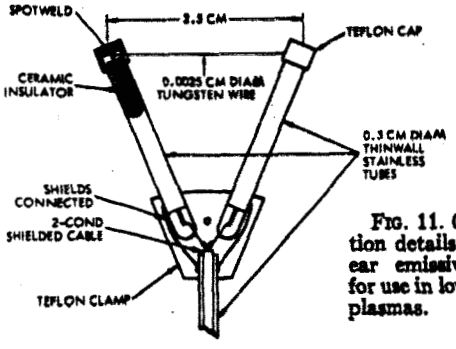

FIG. 11. Construction details of a linear emissive probe for use in low density plasmas.

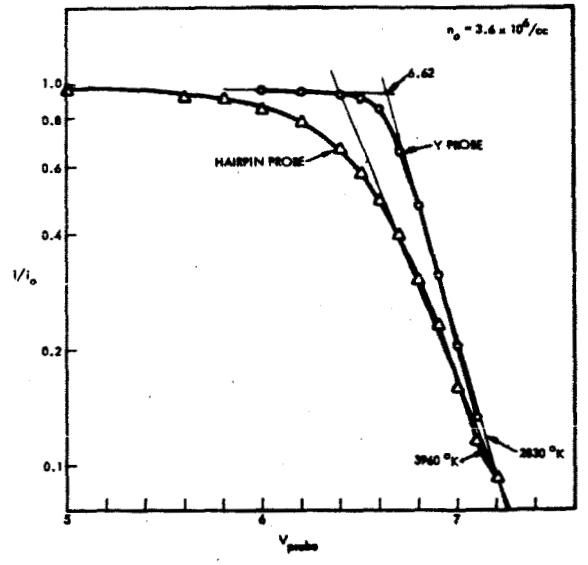

FIG. 12. Comparison of the cutoff characteristics of a "hairpin" probe and the linear probe in the same low density plasma.

the probe occurs because of the magnitude of the collected electron (Langmuir probe) signal. For plasma electron temperatures of 2500°K, this electron collection signal is ~10 mA/cm (for a 0.025 mm wire) at a plasma density of 10^{12} ions/cm^3. The emitted current of electrons must equal or exceed this collected electron signal if an accurate probe measurement is to be obtained, and wire temperatures of ~3000°K would be required to provide 10 mA/cm emitted current from these wires. This wire temperature and the indicated behavior in space charge rounding in Fig. 8 would indicate an upper limit of 10^{12} ions/cm^3 for the accurate application of the probe. In summary, then, potential measurements with an accuracy of ~0.01 V may be obtained in the density range from 10^5 to 10^{12} ions/cm^3 with diminishing accuracy in the regions above and below this central range.

The application of the probe, for a rectified ac heating current, is in general restricted to plasmas in which only weak magnetic fields are present because the $\mathbf{j}\times\mathbf{B}$ forces due to the heating current and the field cause wire breakage at the higher field values. For strong magnetic fields (~5 kG), direct current has been used for the probe heating, and successful probe operation has been achieved, although the accuracy of the probe is diminished (to ~0.1 V) because of the potential increment along the wire.

A final possible limitation in probe application may occur if the combined effects of plasma density and plasma temperature yield power inputs to the probe wire such that a warm nonemissive condition cannot be realized. In general, however, the density limitations previously described impose the major restrictions to probe applications.

ACKNOWLEDGMENT

Work supported by NASA, Lewis Research Center, under Contracts NAS 3-4114 and NAS 3-6276.

SECTION III.D.

INVESTIGATIONS OF CESIUM AND MERCURY DISCHARGE NEUTRALIZERS

INVESTIGATIONS OF CESIUM AND MERCURY DISCHARGE NEUTRALIZERS

by

Robert F. Kemp and J. M. Sellen, Jr.

I. INTRODUCTION

At the time work was initiated on Contract NAS3-6276, there remained unsolved a basic problem in electric propulsion relating to the lifetime of the neutralizer required for space-charge and current neutralization of the thrust beam of an ion engine. The problem is that of maintaining adequate electrical coupling between the electron emitter and the thrust beam, and at the same time shielding the emitter from sputtering erosion by the high energy ions. Developments in the electron-bombardment mercury thruster, and in both the bombardment and contact-ionization types of cesium thrusters, had led to designs which had demonstrated useful lifetimes of all components except the neutralizer. By the conclusion of NAS3-6276, a solution to this problem seems to be at hand, not only for the cesium thrusters, but also for the mercury thruster. The device which provides both adequate coupling to the thrust beam and shielding of the electron emitter is a small hollow cathode internally supplied with a suitable gas which operates as a neutralizer by forming a thermionic arc with the thrust beam plasma as anode. A successful version of a cesium discharge neutralizer was described in a paper by Ernstene, et al.,[1] at the AIAA Second Annual Meeting, 26-29 July 1965. This report discusses that device and the steps in the development, from that concept, of a mercury discharge neutralizer for the Kaufman electron bombardment thruster.

II. "ON-RAMP" NEUTRALIZER

Early in the program, it was proposed that a small electron-bombardment plasma source be used as a neutralizer. The low-energy ions from such a source would neutralize the electron space charge around the filament and provide coupling to the ion thrust beam to be neutralized. It was envisioned that the electron emitter would be similar to that used as the cathode of the electron bombardment thruster, and would have similar longevity.

Several small devices of this type were built which incorporated ribbon filaments, electromagnet windings, and relatively large orifices. Discharges were obtained with them using nitrogen or argon gas as the discharge medium and metal plates as anodes. For all of these, however, the vapor feed rate was inordinately high, as were, also, the minimum vacuum system pressures in which they could be operated. Plans for further development of the "on-ramp" neutralizer called for decreasing the orifice diameter to improve the differential pumping, and for continued operation with argon or nitrogen, inasmuch as these gases are simpler to handle than mercury. These plans were set aside at the time Ref. 1 appeared in favor of an investigation of the configuration which it described. Whether or not the original approach would have eventually led to the present configuration of the mercury discharge neutralizer, it is clear that our experience with the cesium discharge bypassed several steps leading to that goal.

III. INVESTIGATION OF THE "PLASMA-BRIDGE" NEUTRALIZER

According to the description of the "Plasma-Bridge" neutralizer given in Ref. 1, a cesium discharge is enclosed within a metal chamber, the temperature of which is held at about 900°K. Electrons are conducted from the internal plasma through a .005" diameter orifice in the discharge chamber and to the thrust beam plasma by a plasma "bridge" in which slow ions neutralize the electron space charge. Operating characteristics for the device are reported as follows:

"590 mA electron current
5.5 volts beam potential
10.3 watt cathode power
590°C cathode temperature
6.7 watt cesium vaporizer power
35 mA/watt efficiency"

The reported cesium consumption rate is one cesium atom per 100 electrons generated.

Some interesting calculations can be made with respect to the plasma column which extends through the small orifice in the discharge chamber. The current of electrons in this plasma column is given by

$$i_e = n_e e \langle v_e \rangle A_b \qquad \text{(amperes)}$$

where n_e is the plasma density in electrons/cm^3, e is the electron charge, $\langle v_e \rangle$ is the average over the electron velocity distribution for motion along the axis of the plasma column, and A_b is the cross sectional area of the column. Under the assumption that the electron velocity distribution is somewhat random, that is, includes motion both outward and inward along the column axis as well as transverse to the axis, the component average $\langle v_e \rangle$ must be less than $\sqrt{\langle v_e \rangle^2}$. For the stated conditions in reference 1, i.e., electrons with an average kinetic energy of a few electron volts, this average velocity would be

$$\langle v_e \rangle \lesssim 10^8 \qquad \text{cm/sec,}$$

hence, a lower bound on n_e would be

$$n_e \gtrsim \frac{i_e}{10^8 A_b e} \qquad \text{electrons/cm}^3$$

For 600 mA of electron current and $A_b = 1.26(10)^{-4}$ cm^2, the current density is about 4750 A/cm^2, and hence the required electron density is in excess of 3×10^{14} electrons/cm^3.

From the quoted value of cesium consumption, the following calculation can be made. Inasmuch as diffusion of neutrals through the orifice is unidirectional, and with the mean free path assumed long compared to

orifice dimensions, the current equivalent of neutral cesium is given by

$$i_n = n_n \frac{ev_n}{4} A_b$$

where n_n is the neutral particle density in atoms/cm^3, v_n is the rms neutral particle velocity, and A_b is the area of the orifice. At a temperature of 900°K, v_n is ~4 x 10^4 cm/sec. Hence, for a cesium efflux of 0.01 atoms/electron

$$n_n = \frac{6 \times 10^{-3}}{1.601(10)^{-19}(10)^4(1.26)(10)^{-4}}$$

$$= 3 \times 10^{16} \text{ atoms/cm}^3.$$

Accordingly, the neutral density would be 100 times greater than the electron concentration arrived at from the earlier calculation, and many orders of magnitude in excess of that predicted from the known ionization cross section and previously calculated electron densities, assuming the electron kinetic energy to be as high as the estimate given above. Thus, an apparent discrepancy existed between numbers calculated from known data and readily made assumptions.

In addition to the questions concerning densities, a number of other questions concerning the cesium discharge neutralizer came to mind:

1. Does all the electron current come through the orifice in the discharge chamber, or is some of it emitted by the (presumably cesium coated) front surface of the device?

2. How much does the thrust beam potential in the injection region differ from the reported floating collector potential?

3. What is the initiating mechanism for the discharge, and how long a time is required for the discharge to strike, or restart if momentarily interrupted?

4. How seriously is the discharge affected by magnetic fields such as those associated with electron-bombardment thrusters?

And, finally,

5. Could a similar device be built which would operate with mercury, and, even if so, how different would the two types be?

Several configurations of the cesium discharge neutralizer were built, having chamber diameters from 1/16 in. to 1 in. and orifice diameters from .005 in. to .020 in. Details of the configuration seemed to be relatively unimportant, inasmuch as hollow cathode arcs were obtained between each cathode and a metal-plate anode at approximately the same values of discharge chamber temperature, and internal vapor pressure (as indicated by the vaporizer temperature). Three modes of operation were quickly identified. First, with the chamber at operating temperature, but the vaporizer slightly below its operating point, a very small electron current (less than 1 mA) can be drawn to the collector plate. With the vaporizer at a minimum operating temperature, a noisy type of arc is observed which is accompanied by the appearance of a luminous cone extending more than an inch from the chamber orifice. At higher vaporizer temperatures, the discharge switches to a quieter type of arc (voltage and current signals noise free) with the light emission limited to a bright bluish spot at the orifice. During some of these runs, plasma potentials were monitored with a floating emissive probe and found to be consistently below 10 volts. In one instance, in a discharge from a .005" diameter orifice carrying 400 mA, the measured electron temperature was about 8000°K and the plasma potential was 7 volts. Electron currents over 1.25 A were easily obtained with a .005" diameter orifice and with a vaporizer temperature of ~275°C (corresponding to ~1 torr Cs vapor pressure and $\sim 10^{16}$ density in the 600°C discharge chamber).

In other experiments, the discharge plasma was subjected to both transverse and parallel magnetic fields. Parallel fields up to approximately 15 gauss intensity caused a slight confining effect on a neutralizer beam several inches long, and a 20 percent reduction in current, but did not significantly affect the plasma potential. Transverse field intensities of about 25 gauss were sufficient over this path length to interrupt the

electron flow and quench the discharge. Pulsing of the anode voltage demonstrated that discharges form in less than 100 μsec, and that striking time and anode voltage overshoot are dependent on anode spacing.

Two experiments are worth mentioning in particular: In one, the neutralizer was operated continuously until an initial vaporizer charge of 1.2 grams of cesium had been expelled. Results from this run were:

$I_{electrons}$ = 620 mA

Total electron charge = 23.84 Ampere hours

Cesium equivalent = 0.24 Ampere hours

Cesium consumption = 99.3 electrons/Cs atom.

For the other experiment, a special cathode was built which incorporated an emissive probe in the interior of the discharge. This cathode was operated at about 500 mA electron current and the floating potential of the internal probe is compared to that of a similar probe mounted between the cathode and the metal anode. In this experiment as in the others, the wall of the cathode chamber is at the zero-reference potential. With the discharge off, the internal probe potential is also zero. With the arc operating, and the internal probe cold, its potential is about 1.5 to 2 volts; at its operating temperature, the internal probe floating potential is about 7 to 8 volts--approximately 1 volt lower than the potential of the external probe. Inasmuch as this difference in potential is less than the uncertainty associated with floating probe measurements, it can only be taken as an approximate value.

The results of observations of the cesium discharge neutralizer to this point can be briefly summarized as follows: When the arc is operating in its "quiet" mode, a plasma exists in the interior of the chamber, and the space potential within this plasma is about 1 volt below that of the coupling plasma between the cathode and the metal anode. All measurements tend to confirm the fact that the electron current which this device delivers does indeed emerge from the small hole. Observed current densities up to 10,000 A/cm^2 are comparable in magnitude with those reported for the cathode spots in mercury pool rectifiers. Vaporizer temperature measurements imply cesium vapor pressures in the discharge chamber of about 1 torr, hence, neutral density in the chamber of about $1 \times 10^{16}/cm^3$, in good agreement with

the number inferred from efflux measurements. Cesium coverage of the internal walls of the chamber at this density and temperature results in a low work function surface easily capable of emitting the observed electron currents. Electron temperature in the coupling plasma suggests that the average electron velocity may correspond to about 0.8 eV kinetic energy, much less than originally suggested. As electron temperature T_e is reduced, v_e decreases as $T_e^{1/2}$; consequently, the lower bound on n_e from earlier estimates must be raised, and, in the range of interest of T_e, the ratio of ions to neutrals r_i decreases rapidly.[2] Very likely a consistent solution can be found in the neighborhood of the following set of values:

$$n_e = n_+ = n_{neut} \tilde{=} 10^{16} \text{ cm}^{-3}$$

Hence, $r_i \tilde{=} 0.5$, which is appropriate for $T_e = 2000°K$. The Langmuir probe measurement of $T_e = 8000°K$ was not made within the orifice, but at a point just outside where, conceivably, the electrons could have received additional acceleration. Although it does not confirm the 2000°K value, it is not inconsistent with it.

The observations at TRW Systems had essentially duplicated the performance reported in Ref. 1 (except for thermal efficiency, on which no effort was expended), and, by means of the emissive probe and Langmuir probe measurements and pulsed operation had added a measure of insight into the workings of the device. Effort then turned to the substitution of mercury for cesium as the discharge medium.

IV. EXPERIMENTS WITH HOLLOW-CATHODE MERCURY ARCS

Several differences exist between cesium and mercury which are of importance to the problem of making a discharge neutralizer which works with mercury instead of cesium. The most significant of these is also basic to the reason for using a mercury neutralizer instead of cesium with a mercury thruster, i.e., the ability of cesium to coat metallic surfaces and to lower their surface work function. It is felt that if cesium vapor were to be

deposited on the accelerator grid surfaces of a mercury thruster, it could lead to localized sources of "drain" currents. Inasmuch as mercury does not wet a great many of the materials which might be used in a neutralizer discharge chamber, and its work function is high (4.5 V vs 1.8 V for Cs), vapor coating of the discharge chamber interior cannot be relied upon to provide an electron-emitting surface. Rather, a special low-work function surface must be provided which has the capability of surviving many hours in a mercury arc plasma. Another difference between the two gases is that of ionization potential. Again, that of mercury is higher (10.39 V vs 3.87 V for Cs); this raises the question of relative difficulty in initiating and maintaining a discharge under conditions suitable for a neutralizer.

A. Early Experiments

A hollow cathode was built in which the vapor delivery tube was electrically insulated from the discharge chamber walls. The chamber itself was made of stainless steel, and was lined with a nickel sleeve which had been internally coated with a standard emission carbonate. A five mil hole in the end of the chamber was placed close to a collector plate. After the cathode surface had been activated, argon was admitted to the device, and a discharge was formed between the cylindrical cathode and the vapor feed tube, which acted as an internal anode. Whether or not this internal arc was operating, no current was drawn to the external collector.

Another similar device was made, again with a stainless steel chamber. This time, however, the inside of the chamber was nickel plated, and coated with emission oxide over the entire inside, including the region around the orifice. After activation, a small electron current could be drawn through the orifice to an external anode placed a few thousandths of an inch away. When mercury vapor was introduced at about 200 torr pressure, an arc formed between the cathode and the external anode. The arc was localized to the orifice, and after a few minutes had enlarged it to about 1/8 inch diameter. This probably was a "cold-cathode" type of arc, although the internal oxide coating may have helped to initiate it.

A similar type of arc was operated with a cathode made of molybdenum. The internal diameter of this cathode was about 1/8 inch--sufficient to fit over the delivery tube to which it was brazed. This also had a five mil hole in the end. No special coating was applied. Stable operation of an arc between this cathode and an external anode was obtained with the tip at about 1200°C, vaporizer at about 300°C, and anode to cathode potential of about 170 volts. The internal mercury vapor pressure was about 1/3 atm. for this arc, also. Once the arc had formed, heating of the cathode by ion bombardment was more than sufficient to maintain its temperature.

From these results, it was clear that "cold-cathode" arcs could be operated with vapor-feed hollow cathodes at elevated internal mercury pressure. But such arcs are destructive to non-refractory metals. It also seems clear that the presence in the interior of the cathode of a low work function surface is not effective unless that surface extends up to and, ideally, through the small orifice.

B. An Oxide-Coated Mercury Discharge Neutralizer

One device which operates in a satisfactory manner is a hollow cathode made of solid nickel and coated internally with an emission carbonate. This coating is then reduced to the oxide and activated in vacuum at a temperature of about 1100°C. Then, upon the admission of mercury vapor at a pressure of approx. 20 torr, an arc can be formed between the cathode and an external anode, with an anode to cathode potential drop of about 10 volts, or higher depending on the anode to cathode spacing. From a few preliminary measurements of this dependence, it appears that for mercury the change in anode potential for a given change in anode spacing may be 10 to 15 times that for cesium.

Construction details and a photograph of the present configuration of the mercury discharge neutralizer are shown in Figs. 1 and 2. The photograph, Fig. 2 shows the device without the heat shielding in place.

Two interesting runs which were made with this type of cathode gave results which give some promise of longevity for the hollow-cathode mercury neutralizer. One was a continuous run of 138.5 hours at an electron

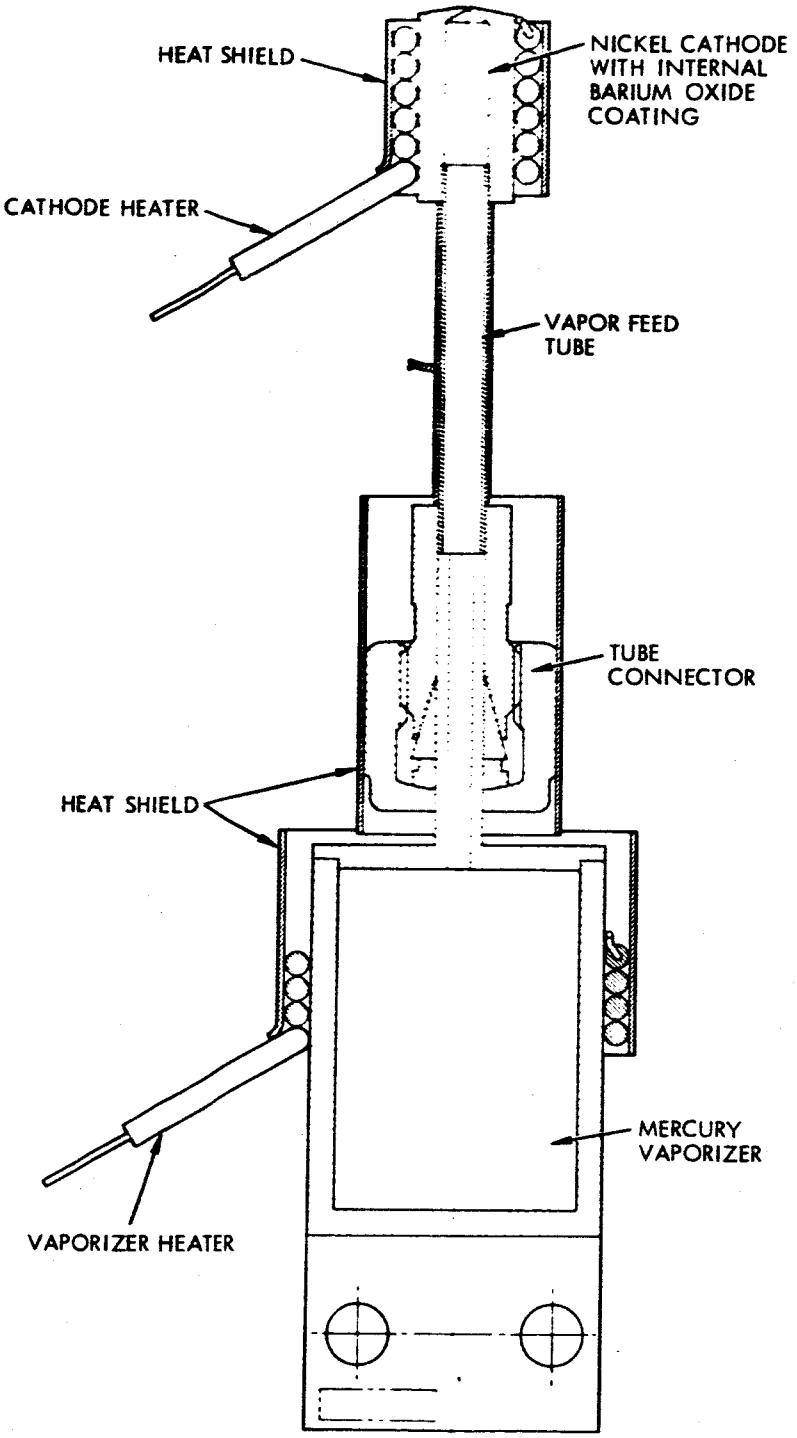

Figure 1. Construction Details Of The Mercury Discharge Neutralizer.

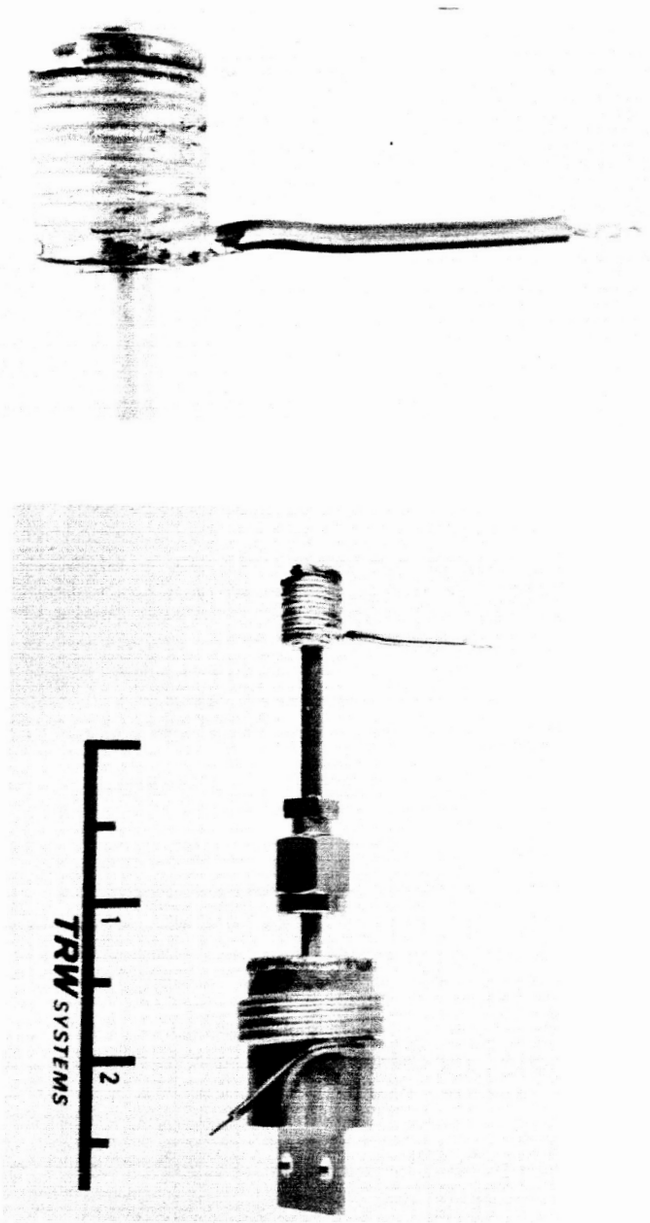

Figure 2. Photographs Of The Mercury Discharge Neutralizer Without Heat Shielding In Place

current of about 600 mA. No damage to the cathode was indicated by deterioration in the operating point of the arc. The other experiment involved measuring the space potential in the interior of the discharge chamber with a floating electron-emissive probe, as had been done earlier with the cesium device. The results of this experiment are given in Fig. 3 which is a plot of the internal plasma potential vs. emitted electron current over the range of zero to 1 ampere. The plot indicates that the internal potential, which represents the "cathode fall" over the low-work-function surface, manages to adjust itself to that value required to deliver the electron current called for by conditions in the space outside the chamber between the cathode and anode. This function (Fig. 3) was quite independent of either anode spacing or anode potential, per se; hence, this experiment indicates that over the range zero to 1 ampere, ion energies arriving at the electron emitting surface will be well below the threshold for damage to that surface.

V. CONCLUSIONS

Studies have been made of the cesium "plasma bridge" neutralizer described in Ref. 1. Reported results have essentially been duplicated or exceeded, and some further insight into the operation of the device has been gained. Comparison of cesium with mercury indicates the conditions under which a similar mercury device can be made to operate.

A hollow-cathode device has been built and operated in a thermionic mercury arc which, according to experimental evidence, has the potential for long life as a neutralizer for the mercury electron-bombardment thruster. Future work with the device will be required to demonstrate this potential longevity, as well as to demonstrate actual compatibility with an operating ion thruster.

One possible drawback to the present configuration is the difficulty that might be experienced in either activating an oxide cathode after the launching of the thruster into space, or the protection of a previously activated one from exposure to air prior to launch. This difficulty might

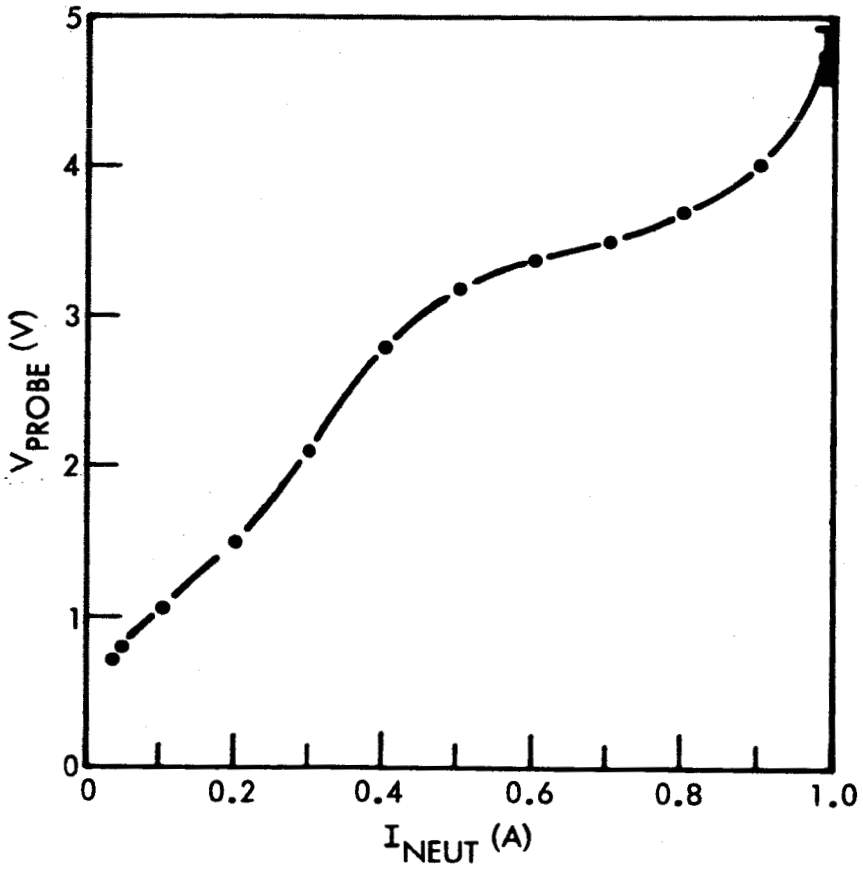

Figure 3. Floating Potential Of The Internal Electron-Emissive Probe As A Function Of Current Being Drawn From The Neutralizer

be overcome by the use of a barium-impregnated "dispenser" cathode, and this should be investigated.

It also seems likely that, given the high-density, low-energy plasma which the discharge neutralizer forms between itself and the thrust beam, this would be a fortuitous location for an electron emissive probe. The floating potential of a probe in the neutralizer plasma would be an approximate indication of the thrust beam plasma potential, and, hence of neutralizer effectiveness. An investigation should be made of the accuracy with which the thrust beam potential could be indicated by comparison of neutralizer current and neutralizer plasma potential.

REFERENCES

1. Ernstene, M. P, Forrester, A. T., James, E. L., Purmal, G. W., and Worlock, R. M., "Surface Ionization Engine Development," AIAA Preprint No. 65-375 (July, 1965).

2. Thompson, W. B., An Introduction to Plasma Physics, London, Pergamon Press (1962), p. 21.

SECTION IV.

APPENDIX

FIELD STRENGTH MEASUREMENTS BY EMISSIVE E-METERS

FIELD STRENGTH MEASUREMENTS BY EMISSIVE E-METERS

by

ROBERT K. COLE and J. M. SELLEN, JR.
TRW, Inc.
Redondo Beach, California

AIAA Paper
No. 66-74

AIAA
3rd Aerospace Sciences Meeting
NEW YORK, NEW YORK/JANUARY 24-26, 1966

FIELD STRENGTH MEASUREMENTS BY EMISSIVE E-METERS*

by
Robert K. Cole** and J. M. Sellen, Jr.***

I. INTRODUCTION

It is not only desirable but often essential to know the electric field strength on the surface of a spacecraft. If the vehicle contains onboard instrumentation for measurements on the charged particles in space, both the directionality and the energy of these particles may be influenced by the surface electric field. If the spacecraft is propelled by an electric propulsion unit, this surface electric field, and, hence, the potential of the vehicle relative to its surrounding environment, may be sensitively influenced by the effectiveness of the thrust beam neutralization. Conversely, the measurement of the surface electric field may be utilized as a diagnostic measure of the performance of the thrustor neutralization.

The purpose of an electric field meter (E-meter) is to determine the electric field at a point on the surface of a spacecraft. From this measured field strength and a previous calibration of the spacecraft-E-meter system, the potential of the vehicle relative to its surroundings is inferred. Two basically different E-meters have been employed to determine this surface field. Both meters make use of the effect of electric fields upon charges. The first, and perhaps, most familiar type of E-meter is the "field-mill" or "rotating vane" E-meter.[1] In this instrument a conducting surface is periodically

*This work supported under Contract AF 33(615)-3195

**Assistant Professor, University of Southern California, Los Angeles, California

***Member Technical Staff, TRW Systems, Redondo Beach, California

exposed to and shielded from the electric field, usually by means of a second, rotating, conductor. The alternating electric field on the static conductor causes the plate to alternately charge and discharge. The resulting induced currents are measured and the electric field on the surface of the spacecraft is determined through a comparatively simple functional relationship of the current to the electric field strength.

A second type of E-meter is the emissive E-meter which employs a current of free electrons. The trajectories of these electrons are affected by the electric field. This results in a functional relationship between the electric field and the distribution of the current to the collecting elements. The electron current may be a carefully collimated beam of monoenergetic electrons from an electron gun and optical system or it may be the rather diffuse electron current emitted by a heated surface. In general, the source of the electrons is negative with respect to the collecting surfaces. This E-meter may then be described as a triode with the electric field serving the function of a control grid.

E-meters of this emissive type, which employed a heated barium impregnated porous tungsten cylinder for the cathode and a flat annular anode[2] were successfully used in the Ion Engine Ballistic Flight Tests of the Air Force Project 661A Series in 1964.[3,4]

Following this first series of tests the emissive E-meter was redesigned. The porous tungsten "button" cathode was replaced by a heated tungsten whose emission properties are less subject to the deleterious effects of the pre-launch and launch environments.

A variety of emissive E-meter configurations have been investigated in order to study the following instrumental properties: (1) the sensitivity of the E-meter to a wide range of

magnitudes of electric fields; (2) the reliability and reproducibility of the response to electric fields; (3) the sensitivity to environmental conditions such as outgassing of the vehicle, ultraviolet radiation, plasmas, contact potential effects, and magnetic fields; (4) the power demands; and (5) the response to rapid changes in electric fields.

II. GENERAL DISCUSSION OF THERMIONIC EMISSIVE E-METERS

The emissive E-meters described in this paper employ what may be described as an unfocused electron beam which consists of electrons traversing a wide variety of trajectories. The electron current is produced by an extended filament (with one exception) which is heated to a temperature sufficiently high so that electrons are freely emitted from its surface. The filament is self-biased in part by means of the heating voltage. An additional potential difference is usually applied between the filament or cathode and the collecting surfaces or anodes. Several collecting plates are placed in a symmetrical manner about the cathode with the cathode along the symmetry plane.

Several geometrical arrangements of the collecting plates were studied and are described in detail in the next section. In addition, meters having a cathode that consists of only a bare filament, a filament partially enclosed by a hood, and a filament-hood-grid structure were examined. The filaments were either 0.002 inch tungsten or 0.002 inch tungsten-26% rhenium, and were approximately one inch in length. One meter has a filament in the form of a small loop. The filament is positioned close to the inner collecting surfaces (1/8 inch above the inner plates in the plane collector meter). Tungsten was selected for the filament since the electron emission from a heated tungsten surface is less subject to deterioration than the more complex, low work function surfaces. The 0.002 inch

tungsten wire is a compromise between low power consumption and high strength. Since a tungsten wire embrittles upon heating, the filament of a calibrated meter with a tungsten filament would have to be replaced before the vehicle launch. Tungsten-26% rhenium filaments do not become brittle and their use eliminates the need of filament replacement after initial calibration. However, a tungsten-26% rhenium filament requires somewhat more power than a pure tungsten filament.

A schematic diagram of typical electron trajectories for an E-meter with a bare filament and plane collecting surfaces is shown in Fig. 1. The cathode is held negative with respect to the collecting plates which are at the same potential as the surface of the vehicle. The center or inner collecting plates intercept more current per unit area than the outer plates. When the vehicle is negative with respect to its surroundings, the cathode emission is increased and the average currents collected by the anodes are decreased. This results from a net shift outward of the electron trajectories. When the vehicle is positive the cathode emission is decreased. The electron trajectories now tend to crowd inward with an overall increase in the total plate current, at least up to a point. Thus, the electric field near the surface of the vehicle exerts a control on the electron paths to the collecting surfaces. There exists a functional relationship between the current to any collecting plate and the average electric field that exists in the region traversed by the electrons. However, the current to a plate or to a pair of symmetrically positioned surfaces may be double valued so that the electric field cannot be unambiguously determined at all times from measurements of the current to one plate or to a pair of plates. In order to determine the electric field in these cases it is necessary to measure two currents. Either the filament emission current and one collecting surface current may be measured or the currents

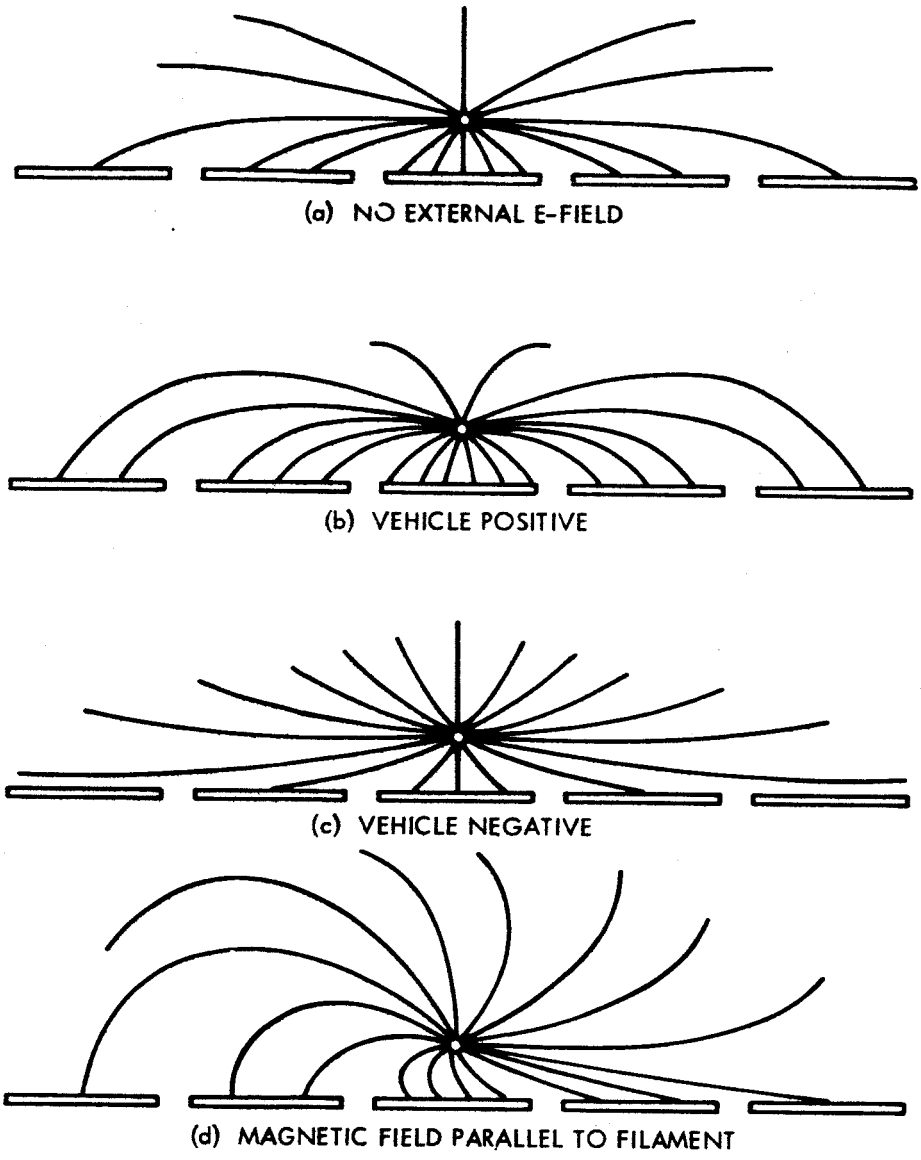

Figure 1. Schematic Diagram Of Electron Trajectories In An Emissive E-meter. The Potential Of The Vehicle Is Referred To Infinity

to two or more sets of these sensing elements determined. The current to the collector just below the filament is the least sensitive to the influence of an electric field and provides a measure of the emission stability of the filament.

The sensitivity of the meter depends on how readily the electrons are bent by the electric field. Since the radius of curvature of the electrons in an electric field is proportional to the electron energy, low energy electrons will make a more sensitive instrument, that is, a meter that will respond to small electric fields. However, low energy electrons are also easily bent by a magnetic field and this effect could impair the performance of the meter. Another consideration entering into the choice of the electron energy is the heating voltage drop along the filament. This is approximately 4 volts for a one inch long, 0.002 inch diameter tungsten filament, and leads to a distribution of electron energies along the filament. The electron acceleration voltage should be large compared to this voltage increment in order to make an instrument of uniform response along the length of the filament and to reduce the effects of a change in the heating voltage in the response of the meter. These considerations lead to a choice of the electron accelerating voltage in the region of 10 to 20 volts. For electrons of this energy the radius of curvature produced by a 1 gauss magnetic field (a vehicle in polar orbit might encounter magnetic fields from 0.2 to 0.75 gauss) approximately equals the radius of curvature produced by an electric field of 1 volt/cm. For higher energy electrons the E-meter becomes relatively more sensitive to magnetic fields since the radius of curvature of an electron in a magnetic field is proportional to the square root of the electron's energy while in an electric field it is proportional to the energy.

Figure 1 illustrates the effect of a magnetic field parallel to the filament (greatly exaggerated). All electron orbits are deflected in a similar way with approximately the same number of trajectories bent onto the left plate as are bent away from the corresponding right hand plate. The effect of a magnetic field parallel to the filament is reduced by the symmetry properties of the meter if the currents collected by plates symmetrically placed with respect to the filament are added. Magnetic fields perpendicular to the filament exert a smaller influence on the electron paths. Tests were performed with magnetic fields both parallel to the filament and in the plane perpendicular to the filament. These tests indicate that a meter with symmetrically positioned plane collecting surfaces is insensitive to magnetic fields of up to 2 gauss. That is, the change in the current to a symmetric pair of collecting plates caused by the 2 gauss field is less than the current change produced by a 0.2 volt/cm change in E.

Two modifications of the exposed filament plane collector geometry were examined. By placing the collecting surface in a shallow vee or on the inside surface of a semi-cylinder, the total charge collected by these surfaces can be enhanced. The filament is also protected by the collecting surfaces. On the other hand, the response to electric fields should be slightly reduced since the field must now penetrate into the cavity and act on slightly shorter electron paths from the filament to the collectors. The "vee" E-meter is less sensitive to small electric fields than the "plane" E-meter but offers a more extended response to larger electric fields. If the filament is on the apex of a convex surface such as an isosceles prism with the collecting surfaces forming the sides, the electron trajectories are on the average longer and, consequently are deflected more by an electric field. However, the current density to the collecting surfaces is less. This meter is more

sensitive to small electric fields and responds to a shorter range of electric field strengths.

By placing a conducting hood over the filament, the filament may be shielded from the influence of external electric fields. The cathode current is then relatively independent of the electric field and may be used as a monitor of the filament emission characteristics. By normalizing the currents to the collecting surfaces by means of the shielded cathode emission, the effects of fluctuations of the cathode emission on the meter performance can be taken into account. However, now the filament emission can no longer serve as a measure of large electric field strengths as it does for the unshielded meter.

The hood is simply a metal foil shaped to be the upper surface of a cylinder whose axis is the cathode (See Fig. 7). The sides of the cylinder are open to permit the partially collimated electron beam to escape. Additional grid structures can also be added to enhance the current and obtain greater control of the energies and trajectories of the electrons. The simplest grid consists of a wire mesh placed over the open sides of the cylinder. The combination of a hood and grid effectively shields the filament and provides a simple control of the electron energy.

The filament is held in place by means of a locating screw and spring assembly. The spring provides the necessary tension to keep the hot filament tight and aligned. On the early models tested a simple bent wire provided the spring tension. One end of the filament was welded onto this bent wire and the other was welded to a fixed support. In order to facilitate filament replacement and to permit the accurate positioning of a filament, a small clamp has been designed. The filament is now positioned by means of a groove or a locating pin and can be replaced to within 0.005" of its former position. The necessary tension

is obtained from a small coil spring inside the holder assembly.

III. DESCRIPTION OF E-METER GEOMETRIES INVESTIGATED

One of the simpler electric field meters consists of a plane array of collecting plates and a thin filament supported above and parallel to the plane of the collectors. The collecting plates are symmetrically positioned about the filament. Figure 2 illustrates a representative model. The overall size of the meter illustrated is approximately 2 inches by 4 inches. Typical plate dimensions are 1 inch by 1/4 inch for the inner plates (plates close to the filament) and 1 inch by 1/2 inch for the outer plates. The filament is 0.002 inch diameter tungsten wire, one inch long, and is positioned 1/8 inch above the collector plane.

In order to investigate the effect of collector geometry on the sensitivity of the meter several modifications of the plane collector geometry were studied. One modification is shown in Fig. 3. In this meter the inner collecting surfaces have been raised to form an inverted vee with the filament above the apex.

Figure 4 illustrates the opposite modification. All but the two outer collector plates have been depressed to form a wide vee. A slightly different version, shown in Fig. 5, mounts the collecting plates on a semicylinder with the filament on the axis of the cylinder.

An E-meter possessing azimuthal symmetry is illustrated in Fig. 6. The inner collecting surfaces form a shallow cone. The outer collector is flat and may represent the surface of the vehicle. The filament is a small loop of tungsten wire.

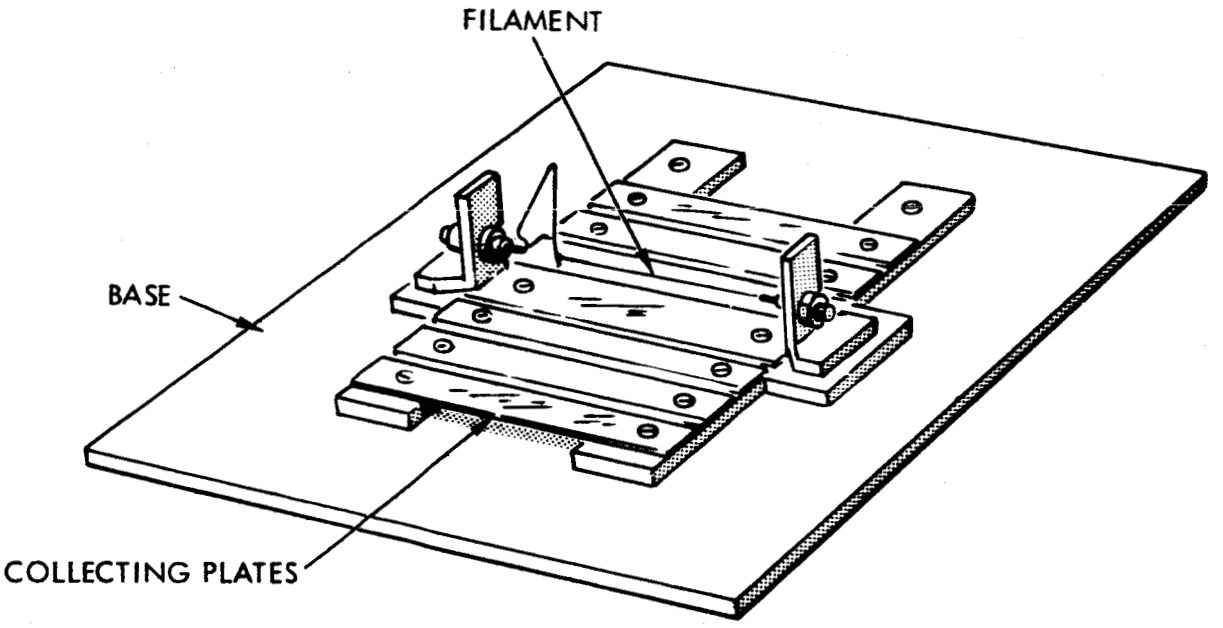

Figure 2. Plane Collecting Plate E-meter

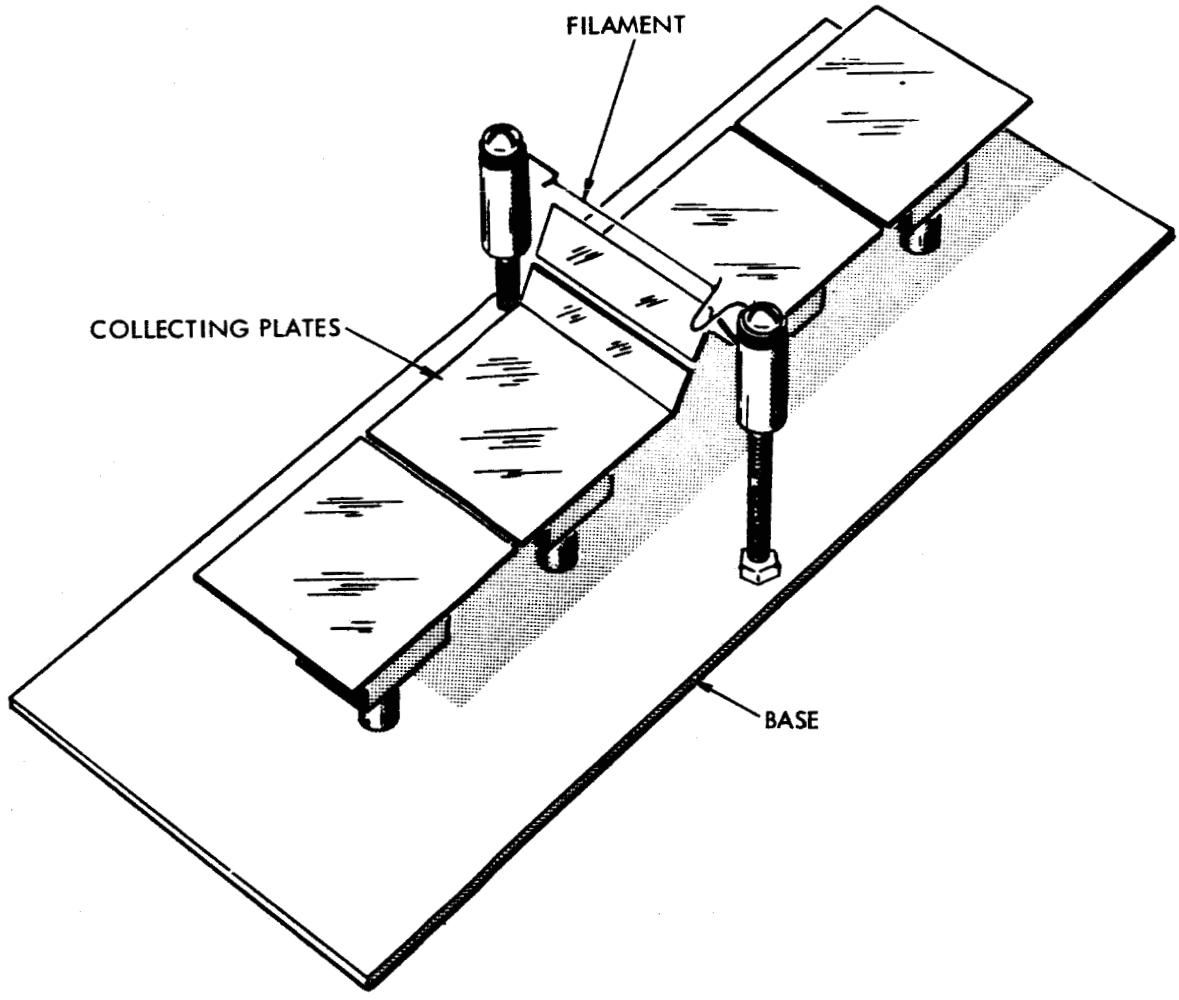

Figure 3. Inverted Vee Collecting Plate E-meter

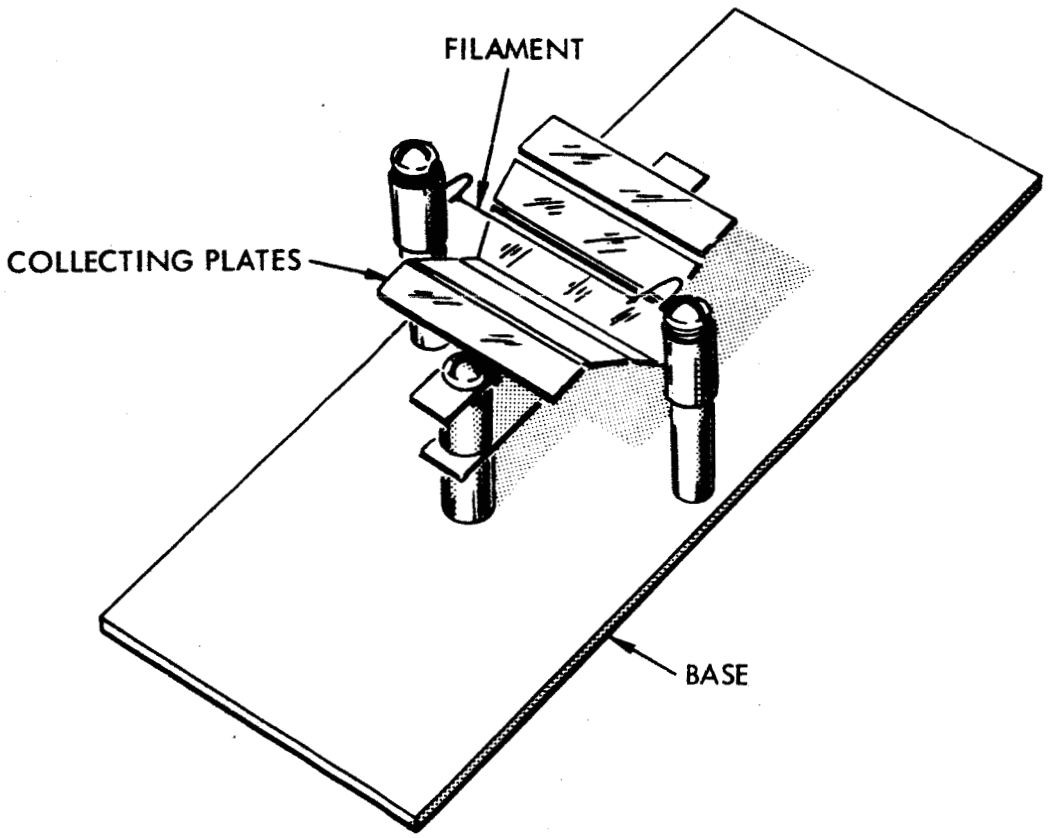

Figure 4. Vee Collecting Plate E-meter

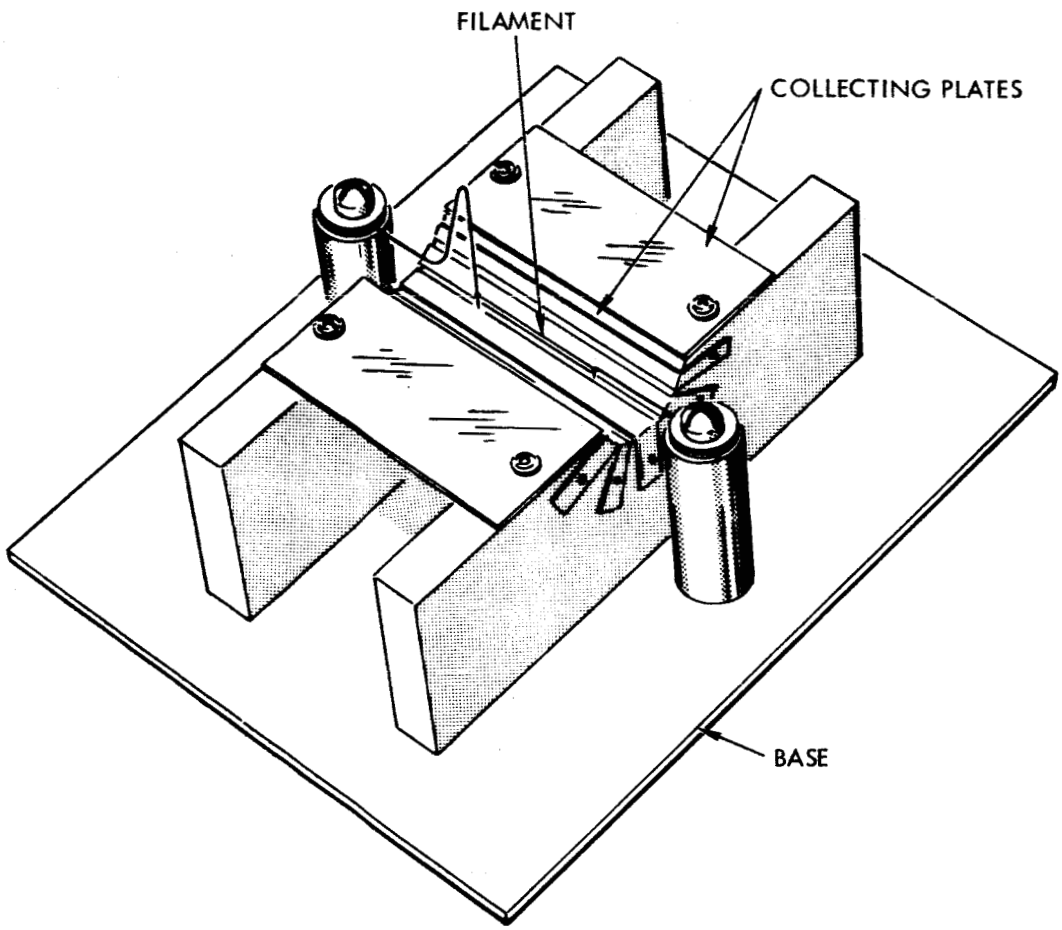

Figure 5. Cylindrical Collecting Surface E-meter

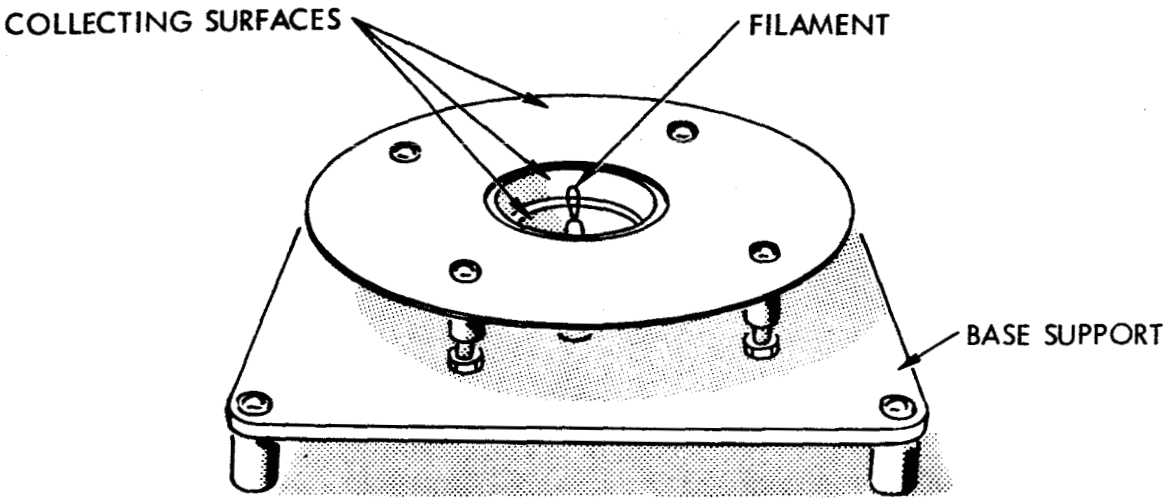

Figure 6. Azimuthally Symmetric E-meter With Conical Collecting Surfaces

Figure 7 shows a plane collector meter with the filament hooded. The overall dimensions are approximately 6 inches by 2 inches with the outer plates one inch square.

IV. CALIBRATION AND TESTING PROCEDURES

All E-meters were calibrated in a cylindrical vacuum tank approximately 20 inches long and 18 inches in diameter, operating at $<5 \times 10^{-6}$ torr. The meter was placed on the horizontal aluminum base plate of the vacuum tank. A large flat upper plate was supported above the meter. This plate was parallel to the base plate and could be raised or lowered to change the distance between the plate and the E-meter. A uniform electric field was produced by applying a potential difference between the base plate and the movable upper plate. With the potential of the upper plate positive with respect to the base plate, an electric field is produced with the E vector pointing into the base plate. This field is considered to be a positive electric field in this paper.

Representative response curves of E-meters are shown in Figs. 8 through 14. Figures 8 and 9 show the response of the plane collecting plate E-meter of Fig. 2. The tungsten filament heating current was 0.60 amperes. The filament power was approximately 3 watts. The collecting plates were 10 volts positive with respect to base plate and the cathode. Figure 8 shows the ratio of the current to the two intermediate pairs of collecting plates I_o divided by the cathode current I_E plotted as a function of the electric field strength. The response of the current to these plates is double valued and from this response, there are, in general, two possible values of E. The measurement of the cathode current, in turn, selects the appropriate field value including the sign. Figure 9 shows the E-field

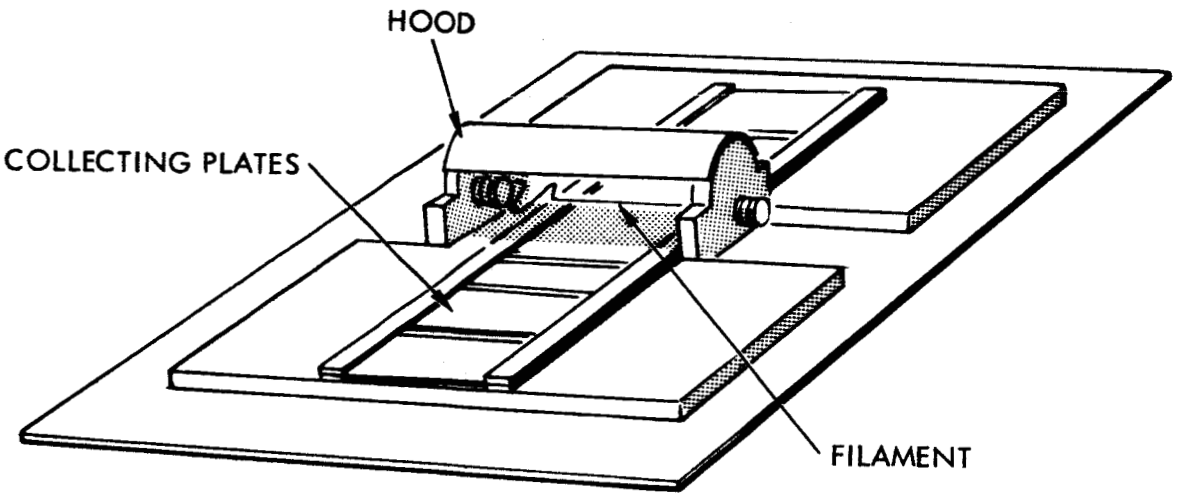

Figure 7. Plane Collecting Plate Hooded-Filament E-meter

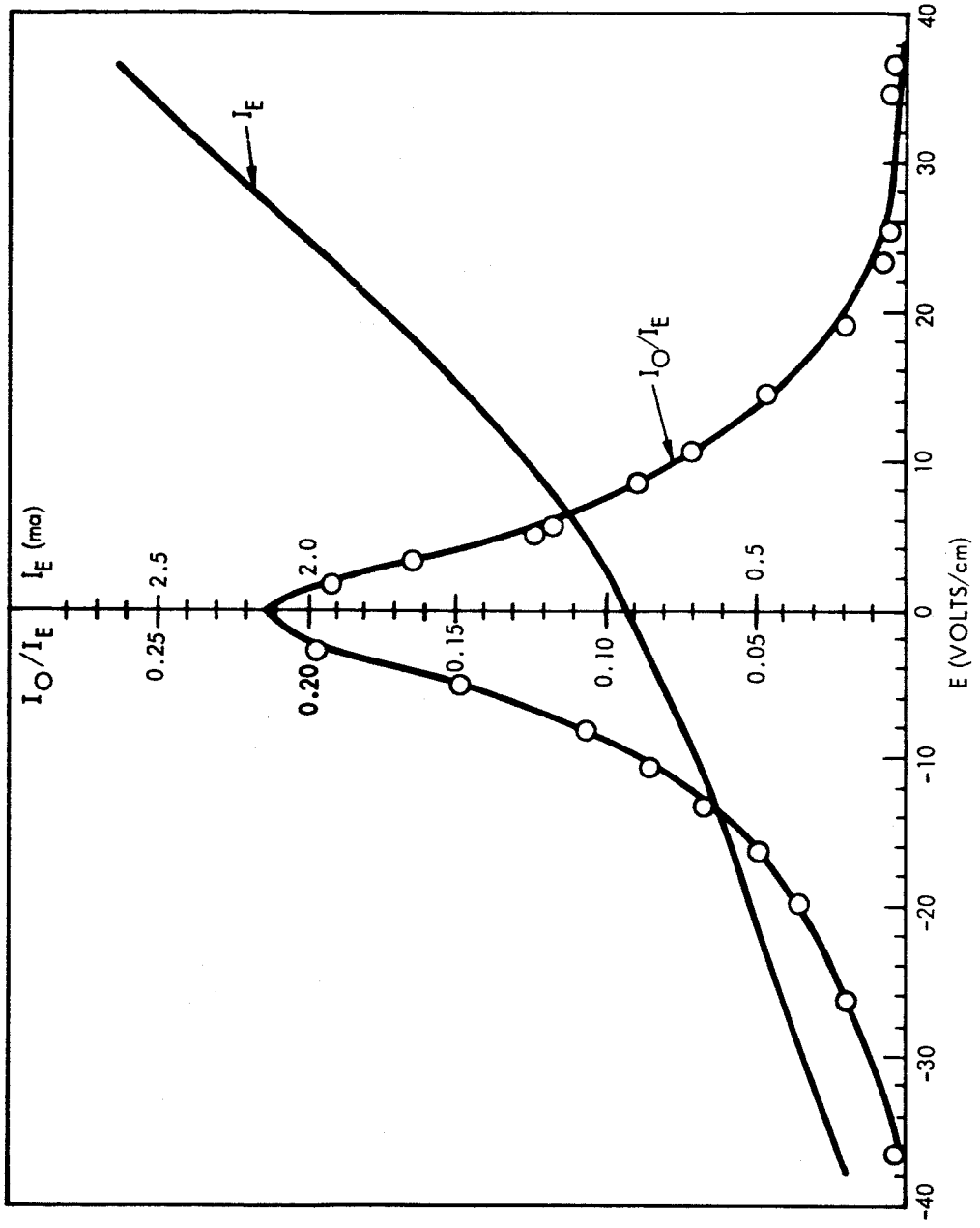

Figure 8. Response Of A Plane Collecting Plate Emissive E-meter To Electric Fields. The Positive Direction Of The Electric Field Is Into The Vehicle. I_E Is The Cathode Emission Current. I_o Is The Current To The Outer Pair Of Collecting Plates

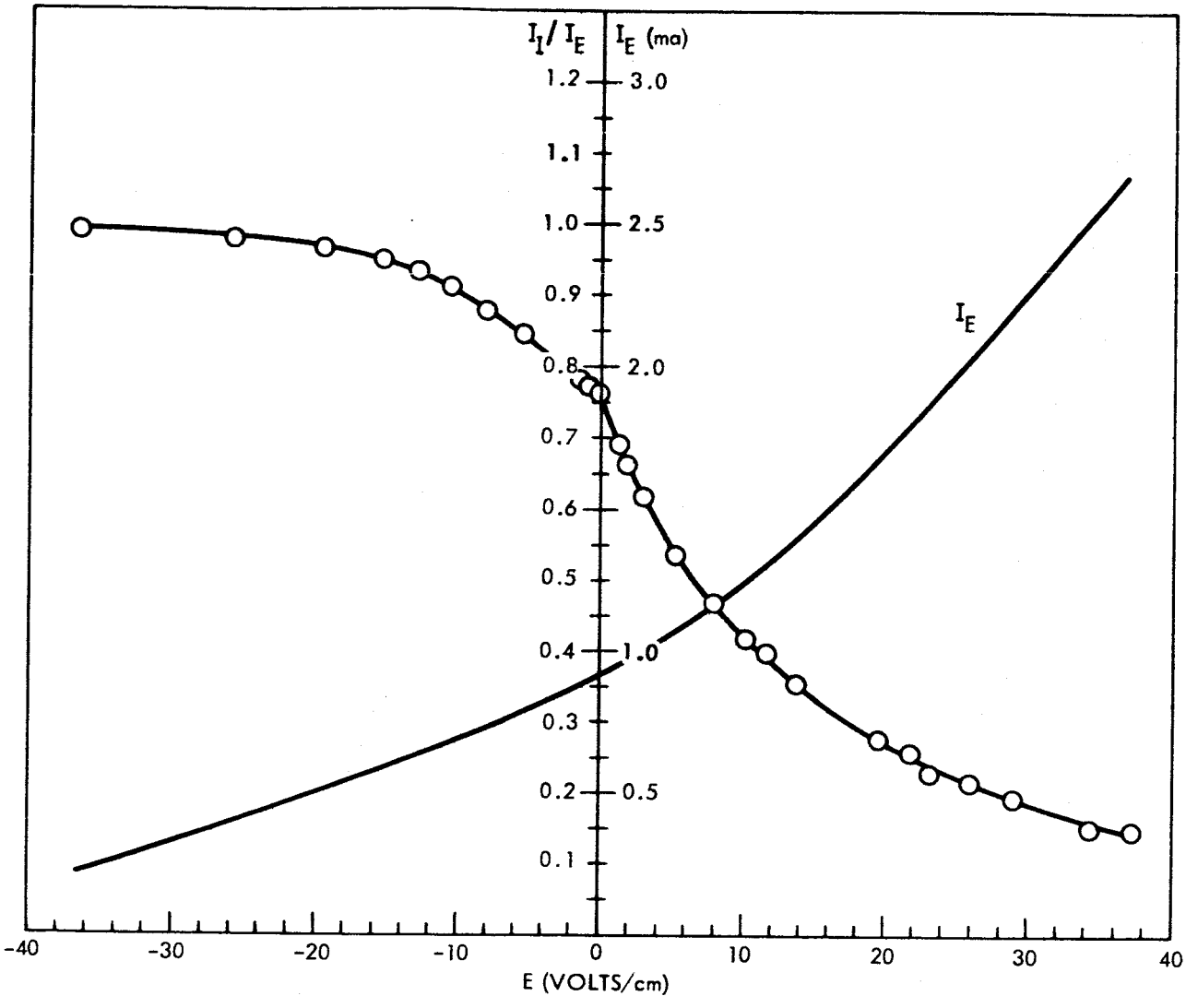

Figure 9. Response Of A Plane Collecting Plate E-meter To Electric Fields. I_I Is The Current To The Inner Pair Of Collecting Plates. I_E Is The Cathode Current.

dependence of the current to the inner pair of collecting plates. The current to the inner pair of plates is less sensitive to changes in the electric field and constitutes the high field or low sensitivity range. A measurement of the current to the inner collecting plates gives both the magnitude and the sign of the electric field.

The current collected by any symmetrical pair of plates proved to be sensitive to the height of the filament above the collecting plates. The modified filament holder discussed in Section II permitted the repeated replacement of a filament with negligible change in meter response. The collected currents are also sensitive to the potentials of the plates. A comparison of the currents to the inner and outer plates can reduce the uncertainty reflected in plate bias shifts. However, it is advisable to carefully stabilize the bias supply to better than $\pm$ 1/2 volt. The response of the meter is relatively insensitive to filament power fluctuations since the filament is operated under space charge limited conditions.

The functional dependence of the current to the outer pair of collecting plates of the inverted vee meter (Fig. 3) is given in Fig. 10. The tungsten filament heating current is 0.60 amps and the power dissipation is approximately 3 watts. The collector plates are 10 volts positive with respect to base plate and the filament. With zero electric field the average collector current density is about 0.03 mA/cm^2. The comments concerning the filament position and collector plate bias made for the plane collecting plate meter also apply here. The plate currents are much more sensitive to small electric fields than the corresponding currents of the plane E-meter (See Fig. 8).

Figures 11 and 12 illustrate the functional relationship of electric fields to the currents at the outer and inner pairs of collecting plates of a plane collecting plate E-meter which has

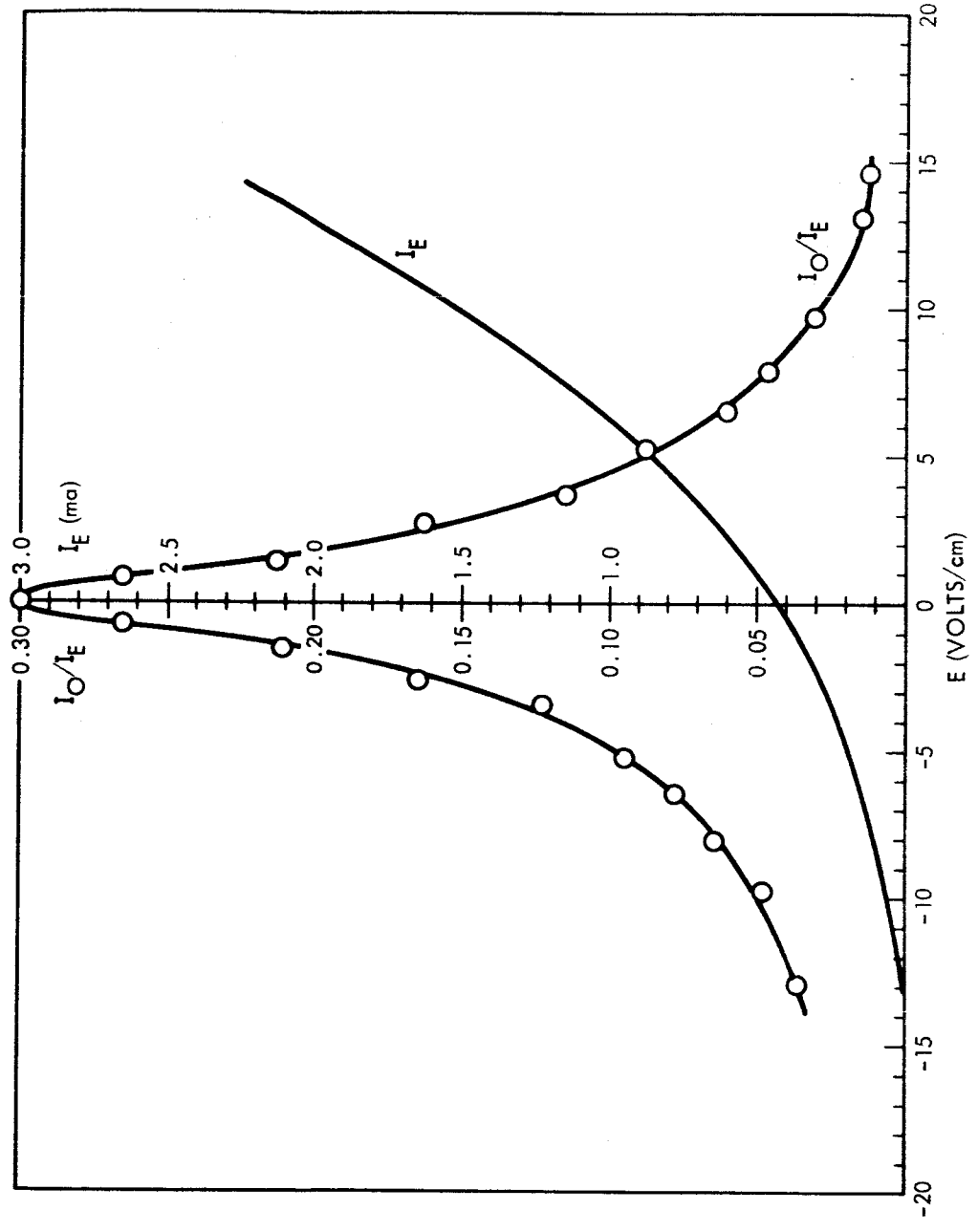

Figure 10. Response Of The Inverted Vee Collecting Plate Emissive E-meter To Electric Fields. The Ratio Of The Outer Collecting Plates Current To The Cathode Emission (I_O/I_E) Is Given As A Function Of The Electric Field

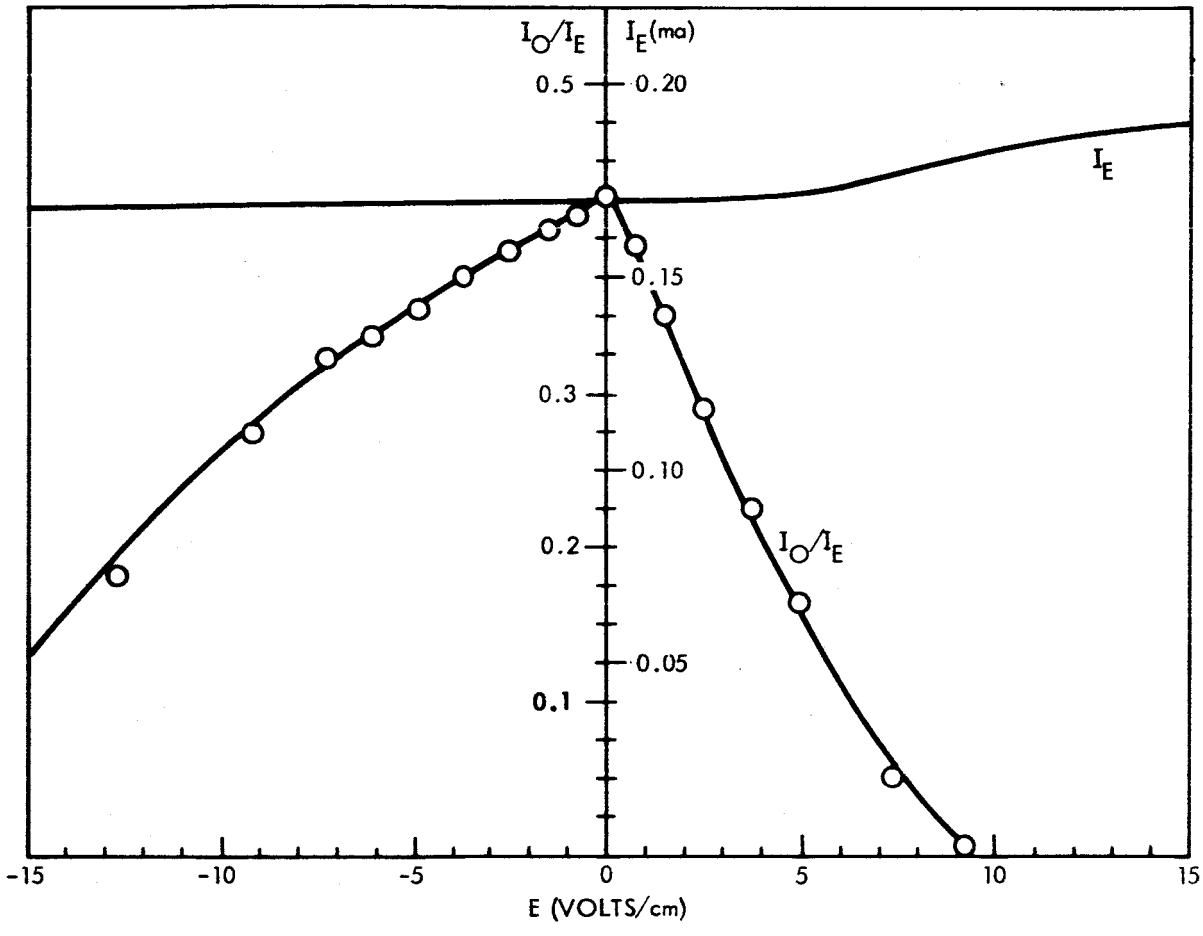

Figure 11. Response Of The Plane Collecting Plate Hooded Filament E-meter To Electric Fields. The Ratio Of The Outer Collecting Plate Current To The Cathode Emission (I_o/I_E) Is Given As A Function Of The Electric Field. The Collecting Plates Are Positive With Respect To The Vehicle

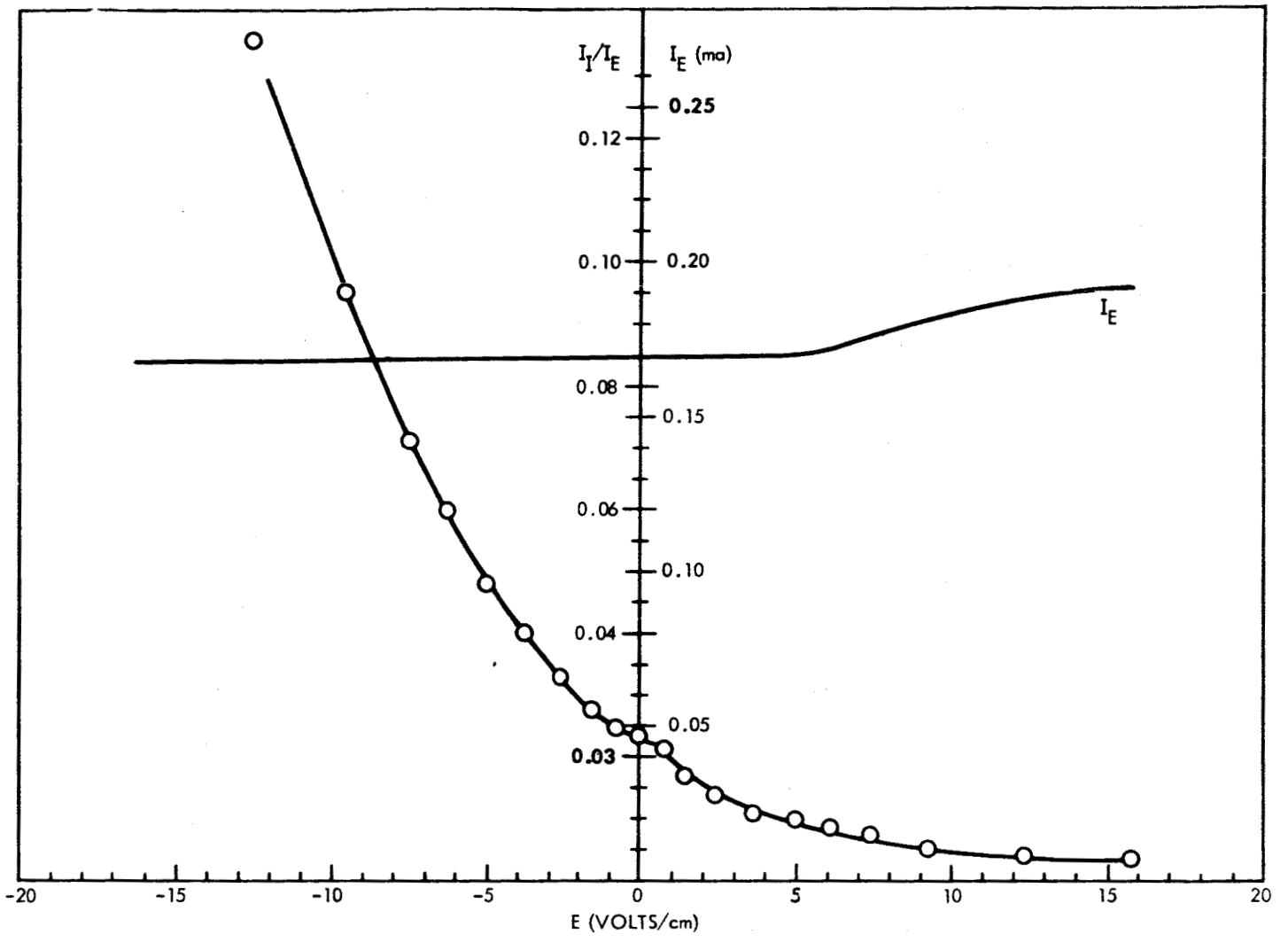

Figure 12. Response Of The Plane Collecting Plate Hooded Filament E-meter. The Ratio Of The Inner Collecting Plate Current To The Cathode Emission Current (I_I/I_E) Is Presented As A Function Of The Electric Field. The Collector Plates Are Positive With Respect To The Vehicle

a hooded filament. The current to the outer collecting plates shows a double valued relationship to the electric field. The tungsten filament power is 3 watts. The outer pair of plates is 20 volts positive. The inner pair of collecting plates is 10 volts positive. Note that the cathode emission current I_E is almost independent of the electric field. The current to the collecting plates is still sensitive to the plate potential. However, the position of the filament is not as critical to the overall meter performance.

A typical plane collector hooded filament meter is illustrated in Fig. 7. This meter was also calibrated with the collecting plates and hood at the vehicle (base plate) potential and with the filament 24 volts negative. The response of this meter to electric fields under these conditions is shown in Fig. 13. The response proved to be relatively insensitive to the filament emission and potential as long as the currents to the collecting plates were normalized to the emission current.

By placing a coarse grid over the open sides of a hooded filament E-meter the current density to the collecting plates was increased slightly. Both the hood and grid are about 1/2 inch from the filament and so do not exert a strong control over the filament emission current. The hood plus grid structure quite effectively shields the filament from external electric fields (to about one part in 200 for E fields up to 40 volts/cm). The addition of a second grid structure closer to the cathode has been shown to give a considerable enhancement of the current to the collecting plates.

The current response to electric fields of a grided hooded E-meter is given in Fig. 14. The collecting surfaces, hood, and grid are at the potential of the base plate. The cathode is 20 volts negative. Filament power is approximately 2.5 watts.

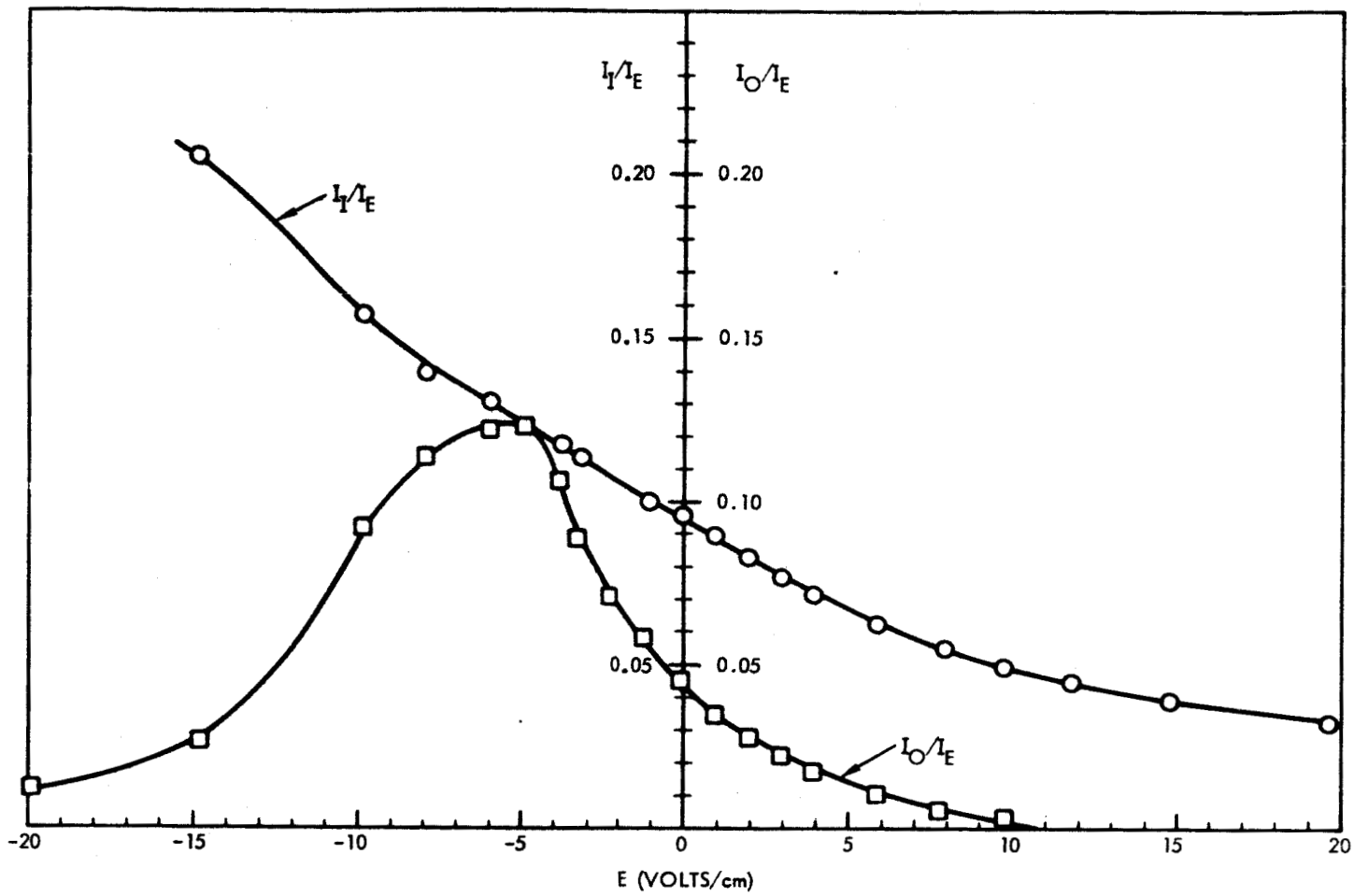

Figure 13. Response Of Plane Collecting Plate Hood Filament E-meter. The Collecting Plates Are At Vehicle Potential. The Cathode Is Negatively Biased.

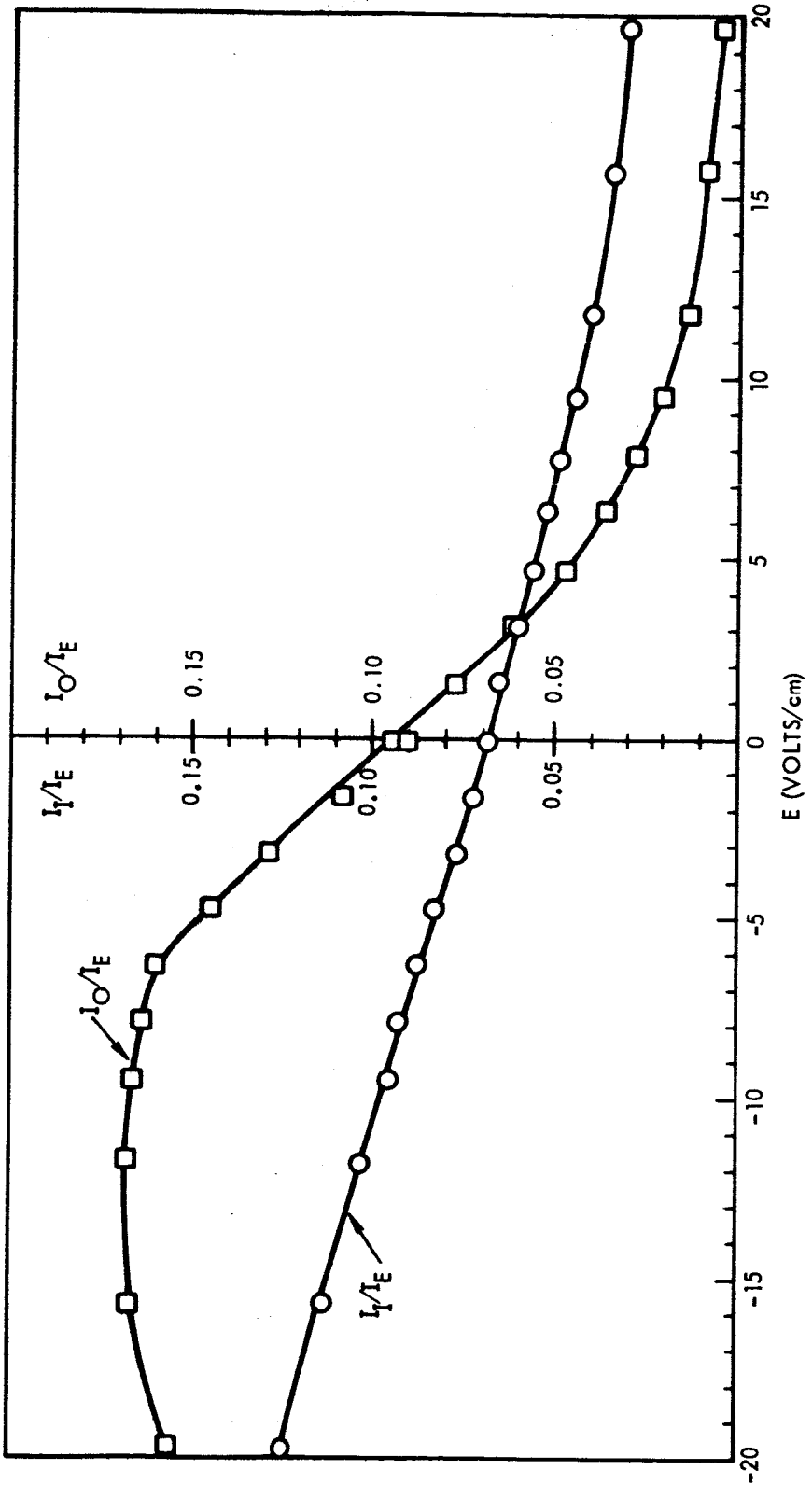

Figure 14. Response Of A Shallow Vee Collecting Plate Hooded Filament E-meter With A Grid. The Collecting Plates Hood And Grid Are At The Potential Of The Vehicle. The Cathode Is Negatively Biased

In addition to the dc operation in which the filament heating current is constant, the E-meter can be used as a pulsed instrument by periodically heating the filament with a rectified ac current. If the pulsing rate is sufficiently fast, the filament will remain hot during the non-heating part of the cycle. During this period the cathode is a unipotential source of electrons. The filament of the hooded filament, plane collector E-meter shown in Fig. 7 was heated by a 250 cycle per second pulsed voltage. The current to the collecting plates during the non-heating period was measured and the resulting response curve to electric fields was identical to that obtained with dc operation of the filament.

An E-meter with plane collecting surfaces was calibrated. Its response was then examined in the presence of a magnetic field successively applied along three mutually perpendicular directions: (1) parallel to the filament, (2) perpendicular to the filament and the plane of the collectors, and (3) perpendicular to the filament and parallel to the collecting plates. Magnetic fields as large as 2 gauss along any direction produced no measurable effect on the performance of the E-meter. A magnetic field strength of over 5 gauss parallel to the plane of the collecting plates was required before a noticeable change in the current to a symmetrical pair of collecting plates occurred. A 5 gauss magnetic field perpendicular to the collector plate produced a small decrease in the currents to the collecting surfaces.

Three different models of the E-field meter were subjected to a series of shake tests which simulate the shock of a vehicle launch. The E-meters were shaken along three mutually perpendicular axes. The tests consisted of a combination of random noise and sinusoidal vibrations with frequencies from 5 to 2000 cycles per second and amplitudes up to 5 g rms for the sinusoidal components and 0.12 g^2/cps for the random noise.

In addition, a filament holder was fabricated that permitted the simultaneous vibration testing of 12 filaments. Several of the filaments held in place by means of a simple bent wire spring were damaged by the tests. However, all filaments (0.002 inch tungsten and 0.002 inch tungsten + 26% rhenium) held in place by means of the clamp coil spring assembly survived these tests when the filament tension equaled or exceeded 50 grams. Several 0.002 inch tungsten-rhenium filaments were heated under normal operating conditions for two hours and then subjected to a shake test. All of these filaments survived the tests undamaged. In summary, an emissive E-meter using a 0.002 inch filament can survive the vibration encountered during a vehicle launch.

The transit time of 20 eV electrons from the filament to the outermost plates is about 10^{-7} seconds. This suggests that an upper limit to the frequency response of E-meters of the sizes described would be about 1 megacycle per second. This is borne out by tests using time-dependent E-fields.

The possible impairment of the E-meter performance by the solar radiation and plasmas encountered in space was also investigated. The photoelectric current induced by the solar uv should be less than 10^{-9} amps per square centimeter from a clean surface and is negligibly small in comparison to typical collecting plate currents of 10 to 100 μamps per square centimeter. The currents from the plasma will depend upon plasma density, vehicle potential relative to the plasma, and the local properties of the plasma-vehicle sheath. For the most dense space plasmas, those at the peak of the F2 layer,[5] the particle current densities to the spacecraft are of the order of 1 $\mu A/cm^2$. Thus, the ratios of the signal current to the noise currents are $\sim$ 50, at the least, with still higher ratios prevailing at higher altitudes above the earth.

The effects of the presence of the plasma cannot be totally neglected in surface field measurements, however. Since surface fields are interpreted, in turn, in terms of the vehicle potential relative to the space plasma, the complicated relationships between this potential increment, the surface field, and the various plasma parameters must be taken into account. Estimates of the "field enhancement factor" due to the presence of the plasma are given in Ref. 6, and would be utilized independently of the particular method by which the surface field might be determined. In the application of an E-field meter to a particular spacecraft which will operate in some known region of the space plasma, a pre-calibration in the laboratory would be undertaken. The plasma wind tunnel techniques described in Ref. 7 have been applied to the emissive E-meter shown in Fig. 7. Enhancement of the electric field in approximate agreement with the expected enhancement has been observed.

A second important consideration introduced by the presence of the plasma is the thickness of the plasma sheath over the vehicle. Since the electric field ranges from its maximum at the surface of the vehicle to an essentially zero field at the boundary between the plasma and the sheath, the effect upon electron trajectories would be complicated if the trajectories ranged through substantial portions of this sheath. The thickness of the sheath is of the order of the Debye length. For typical plasma parameters in space, this length is >1 centimeter, being at its minimum value for those regions in the peak of the F2 layer. For the meters discussed in the previous sections, the electron trajectories of interest are confined, in general, within distances which are small compared to the sheath thickness. These considerations do act to place some restrictions upon the allowable size of the meter. An upward scaling of the meter dimensions to enhance the meter sensitivity would not be allowable if the excursion of the electron trajectories away

from the vehicle surface were to become comparable to the plasma sheath thickness.

V. VEHICLE CHARGING EFFECTS

The electron currents in the E-meters terminate for the greater part upon the meter sensing elements. However, a fraction of the emitted current can escape from the vehicle. This condition is enhanced, moreover, if the vehicle is at a negative potential with respect to the space plasma. The extent to which this current flow away from the spacecraft affects the vehicle potential will be determined by the magnitude of the various particle currents to and from the spacecraft. If an electric propulsion unit is on the spacecraft, the currents from the thrustor are at least four orders of magnitude greater than the E-meter currents and, hence, totally dominate the conditions of the vehicle potential. For a "passive" spacecraft, the particle currents are derived from the space plasma, the solar uv and the E-meter. Since the spacecraft current from the plasma depends upon the total area of the spacecraft, a current density of the order of 1 $\mu amp/cm^2$ over the spacecraft may produce currents considerably in excess of the E-meter currents and yet preserve a favorable signal-to-noise ratio in the E-meter operation. Thus, the condition

$$\frac{j_- \big|_{\text{E-meter}}}{j \big|_{\text{plasma}}} >>> 1$$

at the current sensing elements of the E-meter is possible, even though $j\big|_{\text{plasma}} A_{\text{veh}} > j_- \big|_{\text{E-meter}} A_{\text{E-meter}}$, where A_{veh} is an effective area of the spacecraft for the collection of plasma currents and $A_{\text{E-meter}}$ is the area of the collecting

sensors of the meter. If, however, $j_{plasma} A_{veh} \simeq j_{-E\text{-meter}} A_{E\text{-meter}}$ for smaller spacecraft or in more dilute regions of the space plasma, then the E-meter design should be modified to prevent the escape of signal currents from the meter to the surrounding plasma. This modification has been made through raising the current collecting elements from the planar geometry into a shallow vee.

VI. CONCLUSIONS

Several configurations of emissive E-meters have been examined. The meters have displayed a range of sensitivities to electric fields. By suitable shielding of the filament or by a diminution in the electron trajectories, fields in the 1 to 100 V/cm range may be measured. Sensitivity to weak electric fields is obtained by increasing the length of the electron trajectories or by the use of particular geometrical configurations. For the more sensitive meters, it has been demonstrated that field strengths of 1 V/cm can be determined within 0.1 V/cm.

The frequency response of the meters has been examined and ranges from the dc to the low rf region. The meters have demonstrated that they are not affected by the presence of magnetic fields at the level of the earth's magnetic field. The signal currents in the meter are at about two orders of magnitude above the noise currents from the space plasma and are five orders of magnitude above the solar photocurrents. The meters are, thus, insensitive to background signals due to the space environment.

Ruggedness of the meter structure to shock and vibration has been demonstrated. The required power for the meter

operation is ~3 watts. Further reductions in this power are possible through a reduced filament length or by a reduced filament diameter.

No single optimum configuration of the emissive E-meter has emerged. Rather a breadth of capability has been demonstrated, and the ultimate configuration of a meter for a specific measuring task would result from the adaptation of the whole range of meter capabilities to the particular demands of the spacecraft.

REFERENCES

1. R. C. Waddel, "An Electric Field Meter For Use On Airplanes," Rev. Sci. Instr. 19, 31, January, 1948.

2. S. G. Forbes, R. F. Kemp, J. M. Sellen, Jr., H. Shelton and J. C. Slattery, "Ion Engine Testing Techniques," ARS Space Flight Report To The Nation, New York, New York. ARS 2183-61. October, 1961.

3. P. D. Tannen, "Engineering Support For Electric Propulsion Space Tests," AFSWC, Kirtland AF Base, June, 1964

4. J. Davis and A. T. Forrester, "Ion Thrustor Program," Electro-Optical Systems Report AFAPL-TR-65-87, October, 1965.

5. W. B. Hanson, "Structure Of The Ionosphere," Satellite Environment Handbook, Edited by Francis S. Johnson (Stanford University Press, Stanford, California, 1961).

6. David F. Hall, Robert F. Kemp, and J. M. Sellen, Jr., "Plasma-Vehicle Interaction In A Plasma Stream," AIAA J. 2, 1032-9, June, 1964.

7. David F. Hall, Robert F. Kemp, and J. M. Sellen, Jr., "Generation And Characteristics Of Plasma Wind-Tunnel Streams," AIAA J. 3, 1490-7, August, 1965.